The Role of Aconitase in the Regulation of Metabolism and Sporulation in *Bacillus subtilis*

A dissertation submitted by

Kieran Baxter Pechter

In partial fulfillment of the requirements for the degree of

Doctor of Philosophy

in

Molecular Microbiology

TUFTS UNIVERSITY

Sackler School of Graduate Biomedical Sciences

August 2011

Advisor: Abraham L. Sonenshein

Acknowledgements

I first want to thank my advisor and mentor, Linc Sonenshein. From a strictly science perspective, I feel so grateful to have had the opportunity to work with you, Linc. I always feel like I learn something new when we talk; your scientific knowledge is so vast, and you have the ability to explain difficult concepts with eloquence. Beyond this, I am grateful to you for your compassion, patience, and humor during what seemed like a very long journey at times. I really cannot thank you enough for all of your guidance and support during these past years. As I go forward in my career I will continue to draw on all that you have taught me as I strive to be a successful scientist and mentor.

Thank you to my thesis committee: Carol Kumamoto, Joan Mecsas, Brian Schaffhausen, and Cathy Squires. Your wisdom, creativity, and patience have been invaluable over the years, and our meetings have kept me focused. Thank you also to Sue Fisher, for serving as my outside examiner, and for generating interesting discussions during my defense and previously at conferences.

I would like to thank Hiromu Takamatsu for the generous gift of GerE antibody. In addition, I want to thank all those who helped me to learn the FPLC here at Tufts: Andrew Hempstead and Whitney Amyot in the Isberg lab; Ayman Ismail and Stephanie Mitchell in the Camilli lab; and Jared Pitts, Tirumal Chowdary, and Jessica Silverman in the Heldwein lab. Thank you also to Andrew Wright, Alison Davis, and Paola Zucchi for helpful discussions.

I have been fortunate enough to work alongside many wonderful colleagues in Linc's lab. Thank you to Alisa Serio, who introduced me to the aconitase project: your enthusiasm for science is infectious and your mentorship has helped me a great deal over the years. Thank you to Charlotte Majerczyk, my classmate, labmate and friend. I cannot possibly recount the number of times you have helped me with a problem, scientific or otherwise! I am looking forward to having our chats in person once again. Past lab members: Anu Villapakkam, Sean Dineen, Joe Sorg, and Luke Handke. You are amazing

colleagues and people, and made the lab environment enjoyable over the years. Many thanks to my current labmates: Shaun Brinsmade, Shonna McBride, Agnès Roux, Laurent Bouillant, Kathy O'Day Kerstein and Boris Belitsky. Your input and opinions have been invaluable, and they shaped my project and myself as a scientist. Thank you in particular to Kathy and Laurent, for answering many of my random questions through the years and listening to many stories, and also for your wonderful senses of humor. Thank you to Boris, not only for being a fantastic scientific resource, but for your interest in other projects going on in the lab that has led to many interesting discussions.

I would like to thank the Molecular Biology and Microbiology department staff past and present: Verna, Lauralyn, Evyan, Lyn, Christine, Jaime, Teri, Tom, and Gloria. Thank you so much for making my experience here go so smoothly. In addition, I must thank Perry and the media kitchen staff for pouring innumerable plates over the years.

I have been lucky to have wonderful friends at Tufts. Thank you to Enrique, my classmate, for being such a force of positivity. Thank you to Ivona, I will miss our chats while walking home from the lab, you always cheered me up when things were going tough. Thank you to Erin: it has been so fun getting to know you and sharing insights about our favorite shows. The hilarity of Monday nights has been the perfect antidote for stressful times. Thank you to Irvin, Ravi and Jared: you all have been such good friends to me, and I will miss my role as occasional contributor to our trivia wins. Thank you to the entire softball team for many wonderful seasons, I have enjoyed them immensely, win or lose. Thank you to Robbie for being an excellent listener, and for challenging me to think about things differently. Thank you to Brian, not only for being an excellent source of scientific advice, but for being supportive in stressful times and for curing my anxiety with humor. Thank you to Katie, who has been my loyal friend and confidant, and is an amazing scientist and person. I will sincerely miss you, but I also look forward to catching up in the future and seeing what exciting things you do.

Thank you to my bandmates, Jean, John, Basil, and Nick, for giving me such a amazing outlet during my last year at Tufts. Thank you to Lindsay, for being such a wonderful, loyal friend. Thank you to my roommate and friend, Emily, and to my friends Eric, Greer, and Jon, for many years of support and friendship. Thank you to Liz and Sarah Forrest: I am so grateful for your unwavering friendship over the years. Your support in good times and in bad is priceless. Thank you also to Sarah Steward, my wise and hilarious friend since the sixth grade, for nearly twenty years of friendship.

I want to thank the wonderful teachers and mentors who have guided me through the years: Donna Steinmetz, Patricia Elvington, Donald Barnett, Howell Detofsky, Wesley Womelsdorf, Richard Spano, Merle Citron, Cathy Bitner, Diane Gittleman, Richard Sutton, Dennis Smith, and Natalie Kuldell. In particular, I want to thank Jennifer Hood-Degrenier, whose mentorship and support was invaluable as I made the decision to go to graduate school.

Finally, I want to thank my family. My siblings, Rhea and Mike, and my brother-in-law, Pete, have been so supportive during this long process. Rhea, thank you for being such an amazing listener through the years, I would be lost without your advice. Pete, thank you for taking an interest in what I do and being so supportive of me. Mike, thank you for your compassion and support and for being inquisitive about my work, philosophy, and life. Thank you to my extended family of grandparents, cousins, aunts and uncles: you have been been a wellspring of positive energy and faith in me throughout this process. To my parents, Jean and Dave, the support you have given me goes far beyond anything I could possibly have asked for or expected. I am so grateful for your love and support throughout my life, and for all of the opportunities you have given me. The work contained within these pages would not be possible without your unending faith in me, thank you.

Table of Contents

List of Figures

List of Tables

Abstract

Previously, it was shown that an aconitase (*citB*) null mutation results in a vast over-accumulation of citrate in the culture supernatant of growing *Bacillus subtilis* cells, a phenotype that causes secondary effects, including the hyper-expression of the *citB* promoter. The first chapter of this thesis, in part, reveals the mechanism of this hyper-expression: CcpC, which acts as a repressor in the absence of citrate, was shown to act through a binding site at the -66 position on the *citB* promoter to activate expression of aconitase in high levels of citrate. In addition, the mechanism behind the accumulation of citrate in a *citB* null was elucidated. Two different aconitase point mutants were created: an enzymatically dead aconitase (C450S; *citB2*), and a mutant aconitase defective in RNA binding (R741E; *citB7*). The *citB2* mutant (Enz-) was a glutamate auxotroph while the *citB7* mutant (RNA-) was a glutamate prototroph; unexpectedly, the *citB7* strain accumulated citrate in the culture supernatant. Both *citB2* and *citB7* cells exhibited overexpression of the *citB* promoter and high levels of aconitase protein. These strains exhibited higher levels of citrate synthase protein and activity in cell extracts compared to wild-type. The same is true for a *citB* null mutant strain. Indeed, the major citrate synthase gene (*citZ*) was overexpressed in *citB* null cells independent of CcpC. Wild-type Acn bound to an *in vitro* transcribed *citZ* leader RNA by filter binding assay, but the mutant proteins (C450S, R741E) did not. In addition, the R741E mutant was ~4-fold less enzymatically active than the wild-type aconitase.

The second chapter of the thesis describes an analysis of the aconitase-dependent regulation of *gerE* gene expression, a previously described target of aconitase. A delay in the appearance of GerE protein in the *citB5* strain was demonstrated, and a sequence in the 3' UTR of the *gerE* message was necessary for proper GerE protein accumulation.

The third chapter of the thesis describes a new purification scheme for aconitase. Wild-type and mutant (C450S, R741E) forms of aconitase were purified from *B. subtilis* without overexpression using a four-step purification scheme.

Introduction

1 *Bacillus subtilis*

Bacillus subtilis is a Gram-positive soil bacterium that was originally described in 1835 in a publication that referred to it as *Vibrio subtilis* (Ehrenberg). Forty years later, it was reclassified under its current name by Cohn (1872). Even in this early age of bacteriology, *B. subtilis* had the potential to be a model organism; it is easily grown in the laboratory and is not pathogenic. Indeed, it is often consumed by humans; soybeans fermented with *B. subtilis* are used to make the Japanese and Korean foods natto and cheonggukjang, respectively (Cutting 2011, Soh *et al.,* 2008). However, it was not until the mid-20th century that a series of experiments made the use of *B. subtilis* as a model organism attractive.

In 1947, Burkholder and Giles (1947) exposed wild-type *B. subtilis* cultures to heavy doses of UV light and X-rays, producing a series of auxotrophic mutants. The auxotrophic mutants allowed researchers to unravel many biosynthetic pathways. In addition, one of these mutants, number 168, was a tryptophan auxotroph that was also extremely genetically competent. Spizizen (1958) demonstrated that strain 168 could be transformed to prototrophy by incubation with wild-type DNA. Anagnostopoulos and Spizizen (1961) then went on to define a protocol for the efficient transformation of *B. subtilis*. This protocol, and strain 168, have led to the creation of nearly all lab strains in existence; a recent report examining the genomes of *B. subtilis* legacy strains offers a look at this "domestication" process from a post-genomics era perspective (Ziegler *et al.,* 2008).

Genetic competence is not the only aspect of *B. subtilis* physiology that has made it an attractive model organism; the *Bacillus* genus is one of very few groups of bacteria that produce dormant spores (Priest 1993). Sporulation in *B. subtilis* follows a genetic program that is analogous to developmental processes found in higher organisms, and thus is an intriguing avenue of study.

Overall, the knowledge microbiologists have gained over the past 60 years regarding *B. subtilis* metabolic and gene regulatory networks has made this organism the best studied Gram-positive bacterium in nature, and the second most well-studied bacterium behind *Escherichia coli*. As a result, *B. subtilis* continues to be an incredible tool for basic science research at the biochemical and molecular genetics level.

2 *B. subtilis* central metabolism

My primary interest is to understand how metabolism and gene regulation intersect within the cell, each exerting pressure on the other to achieve the greatest efficiency. The word metabolism is Greek in origin, and means "the chemical changes in living cells by which energy is provided for vital processes and activities and new material is assimilated" (Merriam-Webster 2011). In other words, metabolism is the sum of all the reactions within the cell that deal with energy production and biosynthesis. For the purposes of this thesis, I will focus on the central metabolic pathways and some metabolic branch points important to the themes of this thesis.

The central metabolic pathways in *B. subtilis* catalyze the complete oxidation of glucose to carbon dioxide (CO_2), along the way releasing energy that fuels all cellular processes. The released energy is stored via substrate-level phosphorylation and through the charging of the redox cofactors nicotinamide adenine dinucleotide (NAD^+), nicotinamide adenine dinucleotide phosphate ($NADP^+$) and flavin adenine dinucleotide (FAD^+). The reduced forms of these cofactors (NADH, NADPH, and $FADH_2$) can donate electrons to fuel biosynthesis or can be fed into the electron transport chain (ETC) to produce the high-energy storage molecule adenosine triphosphate (ATP) via oxidative phosphorylation (Voet *et al.,* 2004). When grown aerobically, *B. subtilis* uses O_2 as its terminal electron acceptor; however, anaerobically-grown *B. subtilis* can utilize nitrate or nitrite for respiration (Nakano *et al.,* 1998).

The energetic and biosynthetic fate of glucose as it passes through the central metabolic pathways in *B. subtilis* is diagrammed in Figure 1. Glucose is processed by the

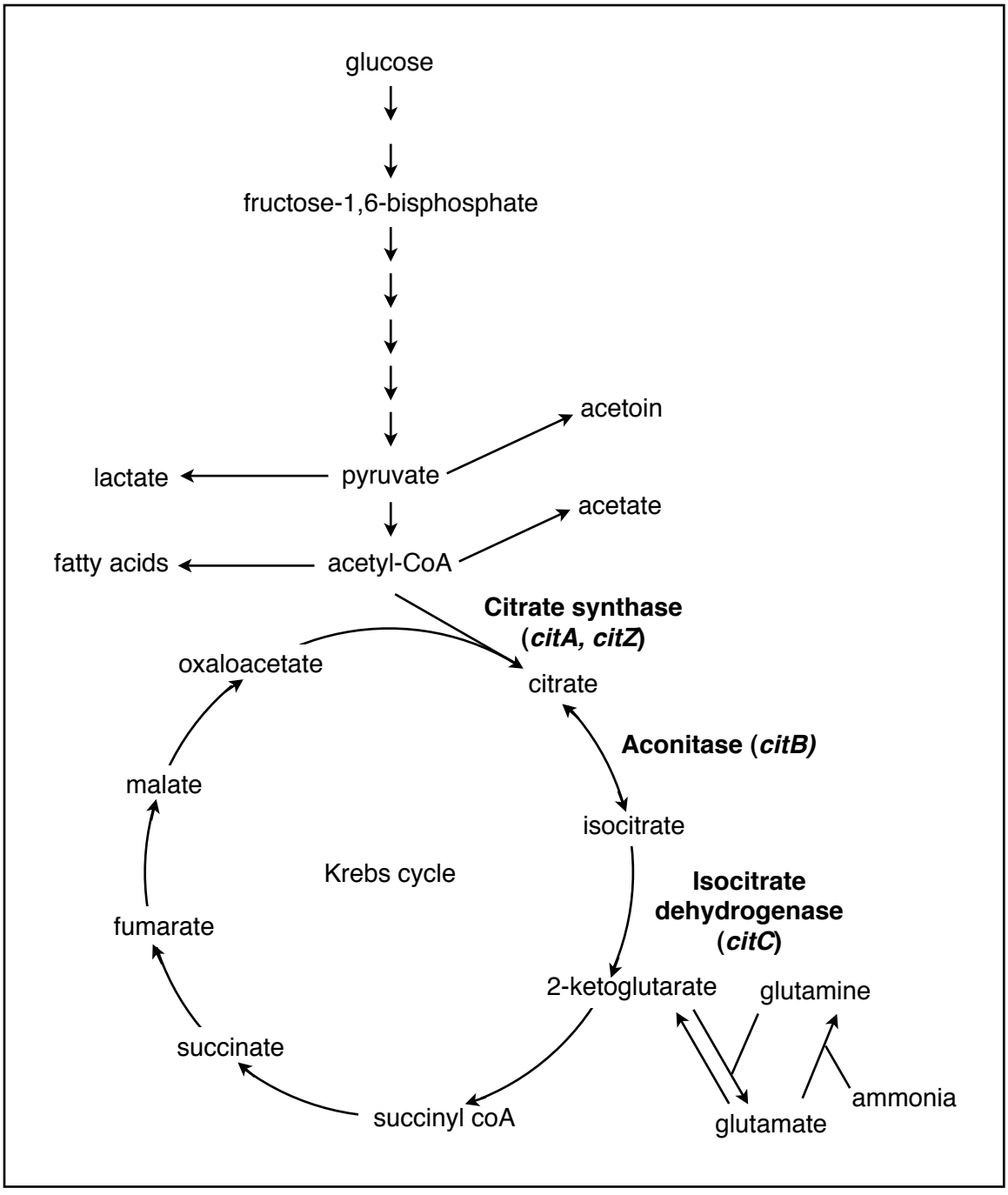

Figure 1. Central metabolism and the Krebs cycle in *B. subtilis*. The fate of glucose as it travels through central metabolism to the Krebs cycle is shown. Carbon overflow pathways relevant to this thesis are depicted. The TCA branch enzymes and their corresponding genes are highlighted.

glycolytic enzymes to pyruvate during fermentation (Voet *et al.,* 2004). Pyruvate can be converted to fatty acids, lactate, acetoin, and acetate, which can be used for biosynthesis of different cellular components or act as carbon overflow products when glucose is plentiful (Sonenshein 2002). Ultimately, pyruvate and any carbon overflow products can be converted to acetyl-CoA, the entry point for the Krebs cycle.

3 The Krebs cycle

The Krebs (or citric acid or TCA) cycle is a series of reactions catalyzed by eight enzymes (see Figure 1). It begins with the addition of the 2-carbon acetyl group from acetyl-CoA to a 4-carbon molecule of oxaloacetate to produce a 6-carbon citrate molecule. In the course of the cycle, the acetyl group is completely oxidized to 2 molecules of CO_2, regenerating oxaloacetate (Voet *et al.,* 2004). However, rather than being a futile cycle, this process has two major functions. First, it allows the cell to extract the maximum amount of energy from glucose. During glycolysis, each 6-carbon molecule of glucose is oxidized to two 3-carbon molecules of pyruvate, producing a net two molecules of ATP along with 2 equivalents of NADH; each pyruvate is further oxidized to acetyl-CoA, releasing CO_2 and producing one NADH (Voet *et al.,* 2004). The acetyl-CoA molecule is fed into the Krebs cycle, producing a single molecule of GTP, from substrate-level phosphorylation, along with 2 NADH, 1 NADPH, and 1 $FADH_2$ (Voet *et al.,* 2004). Thus, for each 6-carbon molecule of glucose, 2 ATP or GTP, 4 NADH, 2 NADPH, and 2 FADH2 molecules are produced beyond those garnered from the oxidation of glucose to acetyl-CoA.

The second function of the Krebs cycle involves the production of biosynthetic intermediates. As citrate is converted to oxaloacetate, certain products of the Krebs cycle reactions are extracted and used as precursors for important metabolites in the cell. These reactions are referred to as cataplerotic (Owen *et al.,* 2002). In particular, 2-ketoglutarate (or α-ketoglutarate, 2-oxoglutarate), the product of the isocitrate dehydrogenase enzyme, is an important cataplerotic reaction substrate; it is utilized by

B. subtilis for the synthesis of glutamate (Sonenshein 2007). This reaction, catalyzed by glutamate synthase (also glutamate-oxoglutarate amidotransferase, or GOGAT), is the only *de novo* source of glutamate in *B. subtilis* (Sonenshein 2007). Glutamate itself is a precursor for proline and arginine (Belitsky 2002); it is also the starting point for heme biosynthesis (von Wachenfeldt *et al.,* 2002). In addition, glutamine is synthesized from glutamate and ammonium by glutamine synthase (GS); these two amino acids are the source of nearly all nitrogen-containing groups in *B. subtilis* metabolites (Belitsky 2002). Beyond glutamate, the other main Krebs cycle intermediate in *B. subtilis* is oxaloacetate, which is the precursor of aspartate and its derivative metabolites (Belitsky 2002).

It is important to note that the Krebs cycle alone cannot serve to add cellular biomass; as mentioned above, the acetyl-CoA molecule that enters the cycle is completely oxidated to CO2, resulting in the regeneration of oxaloacetate and no net increase in carbon skeletons. However, the Krebs cycle does not exist in isolation; the cataplerotic reactions discussed above clearly siphon intermediates away from the cycle to produce biomass. Therefore, in order to retain Krebs cycle function, the intermediates are replenished by another set of reactions, referred to as anaplerotic (Owen *et al.,* 2002). For example, the conversion of glutamate to 2-ketoglutarate, via the glutamate dehydrogenase enzyme (*rocG*) (Belitsky *et al.,* 1998), is an anaplerotic reaction that allows *B. subtilis* to introduce glutamate and other amino acids into the Krebs cycle and convert them to oxaloacetate, which can then be used to maintain cycle function or as a biosynthetic intermediate.

B. subtilis lacks one of the more notable anaplerotic reactions in nature, however: the glyoxylate shunt. The glyoxylate shunt allows for the conversion of isocitrate to succinate and malate via a glyoxylate intermediate; instead of being converted to 2-ketoglutarate, isocitrate is cleaved to succinate and glyoxylate by isocitrate lyase (Cozzone 1998). The malate synthase enzyme then catalyzes the formation of malate from one molecule each of glyoxylate and acetyl-CoA, producing a 4-carbon skeleton

from two 2-carbon molecules (Cozzone 1998). The *B. subtilis* genome encodes neither an isocitrate lyase nor a malate synthase enzyme, therefore, it cannot utilize the Krebs cycle to form biomass if acetate (which is converted to acetyl-CoA inside the cell) is provided as the sole carbon source (Sonenshein 2002); *E. coli*, however, is capable of growth on acetate (Cozzone 1998).

So far, it is clear that the Krebs cycle is a vital part of metabolism in *B. subtilis*. The ability of the Krebs cycle to perform its two biological functions relies heavily on the maintenance of a balance between the cycle itself and cataplerонic and anaplerонic reactions. Part of this thesis will explore a situation in which that balance is perturbed by a mutation. One cycle intermediate, citrate, accumulates far beyond normal cellular levels when one member of the Krebs cycle, aconitase, is removed (Craig *et al.,* 1997). To understand the physiology of this particular situation, we will consider the aconitase protein and the two other enzymes that comprise the first three steps of the Krebs cycle, i.e., the TCA branch enzymes.

3.1 The TCA branch enzymes

The tri-carboxylic acid (TCA) branch of the citric acid cycle is comprised of three enzymes: citrate synthase (CS), aconitase (Acn), and isocitrate dehydrogenase (ICDH). Together, these enzymes catalyze the conversion of acetyl-CoA and oxaloacetate to citrate, isocitrate, and finally 2-ketoglutarate (see Figure 2). As discussed above, 2-ketoglutarate is the direct precursor for glutamate biosynthesis in *B. subtilis*; therefore, the loss of any one of the TCA branch enzyme functions results in glutamate auxotrophy. In *B. subtilis*, the TCA branch enzymes are encoded by the *cit* genes: citrate synthase (*citA, citZ*), aconitase (*citB*) and isocitrate dehydrogenase (*citC*). The architecture of these genetic loci is shown in Figure 3.

3.1.1 Citrate synthase

The citrate synthase enzyme catalyzes the first reaction of the citrate acid cycle, the production of citrate via a condensation reaction between acetyl-CoA and

oxaloacetate (Figure 2). This reaction is the only one in the Krebs cycle to form a carbon-carbon bond (Wiegand *et al.,* 1986). The citrate synthase reaction is catalyzed by three active site residues: two histidines and an aspartate (Remington 1992). Binding of oxaloacetate occurs first and induces a conformational change that creates the acetyl-CoA binding site and concomitantly prevents oxaloacetate from escaping from the active site (Wiegand *et al.,* 1986). Following acetyl-CoA binding, the active site residues catalyze the formation of an intermediate citryl-CoA molecule, which is then hydrolyzed to yield citrate and release CoA (Voet *et al.,* 2004). Importantly, this reaction is irreversible, and as the *B. subtilis* genome does not encode a citrate lyase, the citrate synthase reaction acts as the commitment step towards the production of 2-ketoglutarate.

There are two classes of citrate synthase enzymes found in nature: a hexameric complex is present in Gram-negative bacteria, while Gram-positive bacteria and higher organisms possess a dimeric CS (Wiegand *et al.,* 1986). The *B. subtilis* genome encodes two CS isozymes. The major citrate synthase (CS II) is encoded by the *citZ* gene in an operon with isocitrate dehydrogenase (*citC*) and malate dehydrogenase (*citH*); *citA*, the gene for the minor citrate synthase (CS I) is found at a separate chromosomal locus and is transcribed as a monocistronic RNA (Jin *et al.,* 1994a, b). The *citA* and *citZ* genes are homologs, with 59% DNA sequence identity and 42% identity at the amino acid level (Jin *et al.,* 1994a). Both genes encode 41 kilodalton (kDa) proteins. Purification of citrate synthase (CS II or CitZ) revealed that the CitZ protein is dimeric in nature, while the oligomeric nature of CitA is unknown (Jin *et al.,* 1996).

The two citrate synthase proteins of *B. subtilis* appear to have different roles *in vivo*. While deletion of the *citA* isozyme has little effect, deletion of the *citZ* gene causes a growth defect in the absence of glutamate (Jin *et al.,* 1994a). This difference in phenotype is not surprising when one considers that the *citA* gene lacks one of the active site residues (aspartate-375 in the canonical porcine CS sequence) and instead has a

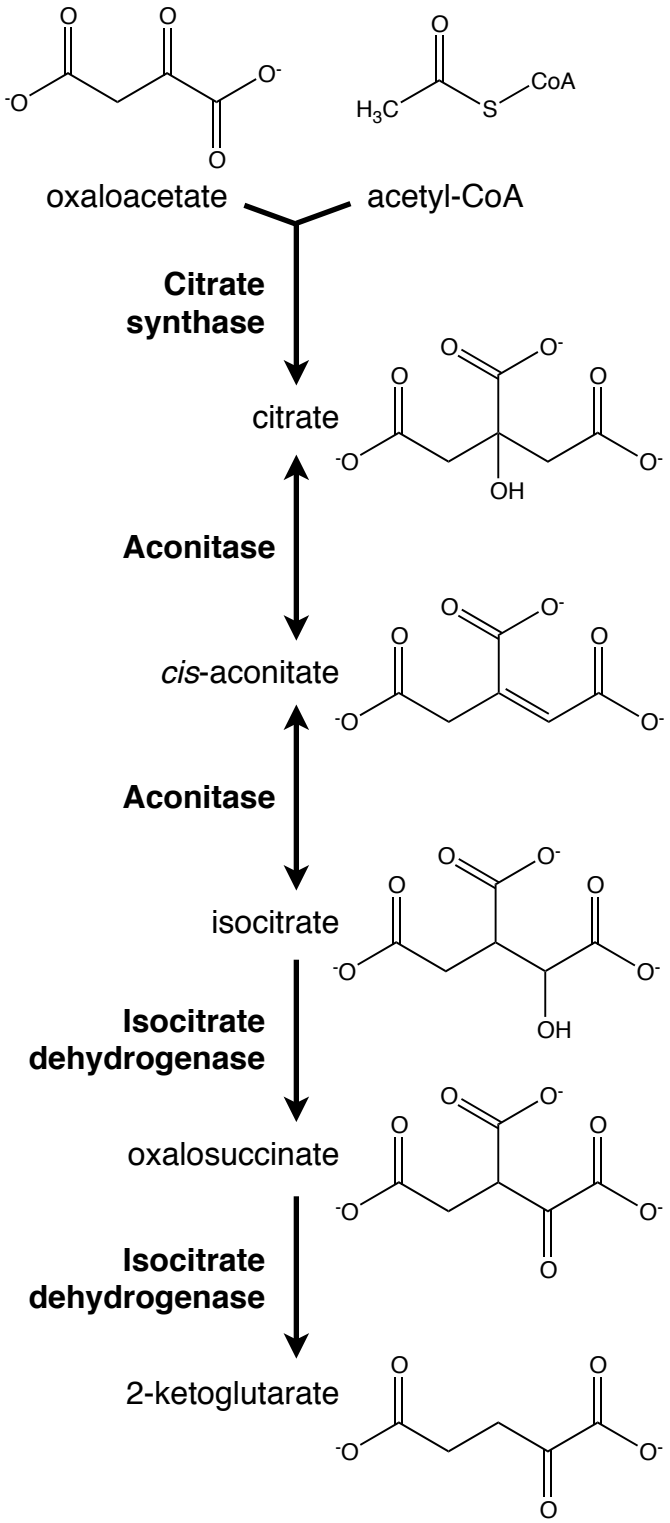

Figure 2. Reactions of the TCA branch of the Krebs cycle. The substrates and products of the enzymatic reactions of the TCA branch of the Krebs cycle are shown, along with the intermediate products *cis*-aconitate and oxalosuccinate. The enzyme that catalyzes each reaction is noted. The reversible nature of the aconitase reactions is indicated by a double arrow.

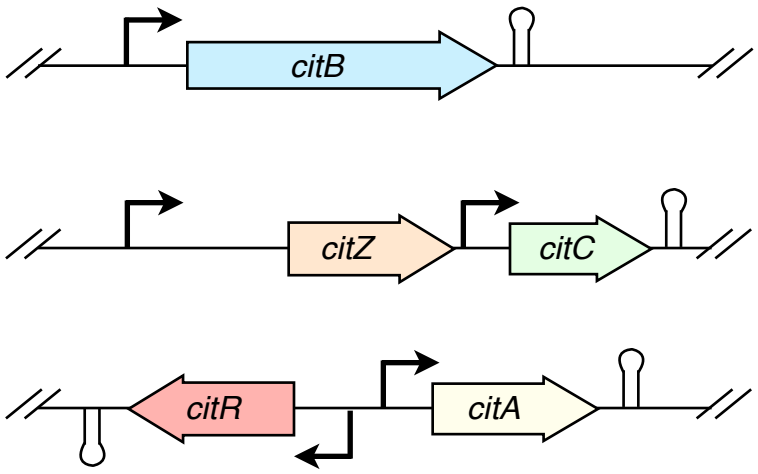

Figure 3. Genetic loci encoding the TCA branch enzymes in *B. subtilis*. The separate operons encoding citrate synthase (*citZ*, *citZ*), aconitase (*citB*) and isocitrate dehydrogenase (*citC*) are shown. The *citR* gene, encoding a repressor of *citA* and transcribed in the opposite orientation, is also depicted.

glutamate at this position (Glu-307). Mutation of this residue to an aspartate increases enzymatic activity five-fold (Jin *et al.,* 1994a).

3.1.2 Aconitase

Aconitase catalyzes the second reaction of the TCA branch of the citric acid cycle, the interconversion of citrate and isocitrate via a *cis*-aconitate intermediate (Voet *et al.,* 2004), as shown in Figure 2. In a 1937 paper, Martius and Knoop first observed a catalytic basis for the reversible hydration of *cis*-aconitate. Citric acid incubated with extracts of mammalian tissue was converted to *cis*-aconitate and isocitrate and an equilibrium between these three metabolites was maintained (Martius *et al.,* 1937). Later that same year, the enzyme catalyzing this activity was named aconitase (Breusch 1937).

There are five major types of aconitases in nature: mitochondrial aconitase (mAcn); cytoplasmic aconitase/iron regulatory protein (cAcn/IRP) and bacterial aconitase A; bacterial aconitase B; isopropylmalate isomerase (an enzyme of leucine biosynthesis); and homoaconitase (Gruer *et al.,* 1997). Of these five types, the cAcn/IRP/ AcnA and AcnB proteins are bifunctional; they are capable of post-translational regulation of RNA in addition to their enzymatic function (Alén *et al.,* 1999, Beinert *et al.,* 1996, Tang *et al.,* 1999). A more detailed examination of the bifunctional nature of cAcn/IRP and bacterial aconitases can be found below.

B. subtilis possesses a single bacterial AcnA-type aconitase protein, encoded by the *citB* gene in a single-gene operon (Dingman *et al.,* 1987, Rosenkrantz *et al.,* 1985). Like nearly all aconitases in nature (Gruer *et al.,* 1997), save *E. coli* AcnB (Tang *et al.,* 2005), discussed below, *B. subtilis* Acn is a monomeric protein consisting of 909 amino acids and has a molecular weight of ~99 kDa (Dingman *et al.,* 1987).

For all members of the aconitase family, the catalytic function is dependent on the presence of a covalently-bound iron-sulfur (4Fe-4S) cluster. The cluster is ligated to the protein by three cysteine residues that interact directly with the iron residues in the cluster. The fourth iron atom, Fe_a, is exposed to solvent and is coordinated by the oxygen

of a loosely bound water molecule when substrate is absent (Lauble *et al.,* 1994). When substrate is bound, three oxygen atoms coordinate the Fe_a iron atom: two provided by the substrate (a carboxyl group and a hydroxyl group) and one by the water molecule (Lauble *et al.,* 1994).

The aconitase mechanism of action involves several catalytic residues that work together with the 4Fe-4S cluster (Voet *et al.,* 2004). For the forward enzymatic reaction, the Fe_a atom acts with a histidine residue on the protein backbone to cause dehydration, while a nearby serine residue deprotonates an adjacent carbon atom, resulting in the loss of a water molecule and the formation of the *cis*-aconitate intermediate (Beinert *et al.,* 1996). This *cis*-aconitate molecule is released from the enzyme and another, in the opposite orientation, takes its place (Lauble *et al.,* 1994, Lloyd *et al.,* 1999). The final step is a reverse of the first, and results in the hydration of *cis*-aconitate to form isocitrate. This mirror-image mechanism is why the aconitase reaction is referred to as the reversible isomerization of citrate and isocitrate.

3.1.3 Isocitrate dehydrogenase

Isocitrate dehydrogenase catalyzes the third reaction of the Krebs cycle, the oxidative decarboxylation of isocitrate to 2-ketoglutarate (Figure 2). The ICDH reaction also produces the first CO_2 and reduced cofactor of the cycle (Voet *et al.,* 2004). Both NAD^+ and $NADP^+$-dependent isocitrate dehydrogenases are found in nature, and both require a divalent cation (Mn^{2+} or Mg^{2+}) cofactor for catalytic function (Gálvez *et al.,* 1995); *B. subtilis* encodes a single $NADP^+$-dependent isoform at the *citC* (sometimes referred to as *idh*) locus on the chromosome, in a transcriptional unit with the major citrate synthase (*citZ*) gene (Jin *et al.,* 1994a). In Figure 3, the two promoters that drive *citC* expression are shown: *citC* has its own promoter and is also transcribed by read-through transcription from the *citZ* promoter (Jin *et al.,* 1994b). The *citC*-encoded ICDH protein is active as a dimer (K. Matsuno, unpublished), much like the *E. coli* enzyme (Gálvez *et al.,* 1995).

The isocitrate dehydrogenase reaction proceeds in three steps. First, in the $NADP^+$-dependent step, isocitrate is deprotonated to oxalosuccinate. The Mn^{2+} or Mg^{2+} cofactor interacts with oxalosuccinate to result in the release of a CO_2 molecule (Voet *et al.,* 2004). This reaction, like that catalyzed by citrate synthase, is irreversible. These two irreversible steps have broad implications for the flow of carbon in *B. subtilis*; carbon sources entering the Krebs cycle through 2-ketoglutarate (for example, glutamate) must be converted first to succinyl-CoA and then undergo four more reactions to produce oxaloacetate.

4 Regulation of the TCA branch enzymes in *B. subtilis*

Although the TCA branch of the Krebs cycle plays a dual role as both a biosynthetic and energy-producing pathway, these functions are not always needed by the growing *B. subtilis* cell. When growing with an excess of a rapidly metabolizable carbon source (glucose) and a good source of nitrogen (glutamine), the cell has no reason to completely oxidize glucose to CO_2. Instead, it is energetically favorable to produce energy through glycolysis and acetate production until the glucose runs out, and only then commence Krebs cycle function via uptake of the carbon overflow products (see above). Adding to the energy equation, citrate synthase, aconitase, and isocitrate dehydrogenase are large, energy-expensive proteins to produce. For example, aconitase is 99 kDa and requires a 4Fe-4S cluster for function. Therefore, the cell has every reason to prevent the expression of the TCA branch enzymes when they are not required. In *B. subtilis*, there is a series of regulatory mechanisms in place that accomplishes this goal. I will discuss each in turn, beginning with a mechanism that is common in the microbiological world and is referred to as carbon catabolite repression.

4.1 Repression of the *citB*, *citZ,* and *ccpC* promoters by CcpC

The concept of carbon catabolite repression (CCR) refers to regulation that prevents the expression of genes necessary for the use of secondary carbon sources when a preferred carbon source is provided (Görke *et al.,* 2008). CCR was discovered nearly

seventy years ago by Monod when he observed that *E. coli* growing on medium containing glucose and lactose exhibited a biphasic growth pattern (Monod 1942). This pattern, termed diauxie, occurs due to sequential use of these two carbon sources; all glucose is exhausted from the medium before lactose is utilized. Since Monod's discovery, it has become clear that many bacteria exhibit CCR. Although the mechanisms of regulation differ, studies of *E. coli* and *B. subtilis* reveal that both bacteria utilize both global and operon-specific regulatory proteins to accomplish CCR (Görke *et al.,* 2008).

Catabolite control of TCA branch genes in *B. subtilis* was identified nearly half a century ago by Hanson *et al.* (1964) during studies on aconitase gene expression and was described in a series of publications (Hanson *et al.,* 1967, Ohne 1974). These studies were corroborated by data from our own laboratory demonstrating that transcription of *citB* is repressed when *B. subtilis* cells are grown in minimal medium containing glucose and a source of 2-ketoglutarate (glutamate or glutamine), and derepressed during growth on citrate as the sole carbon course (Rosenkrantz *et al.,* 1985). Using *citB-lacZ* fusion constructs, a 121 bp region within the *citB* regulatory region (positions -84 to +36 relative to the transcriptional start site) was identified that contains all *cis*-acting elements that are necessary for this regulation (Fouet *et al.,* 1990). A 30-kDa protein was purified from cell extracts using a purification scheme that relied on a positive gel shift of this 121 bp region as an indicator of activity; this protein as identified by peptide sequencing and named CcpC (Jourlin-Castelli *et al.,* 2000).

CcpC is a LysR-family transcriptional regulator that responds to citrate and binds as a dimer to the promoters for *citB, citZ* and the *ccpC* gene itself (Jourlin-Castelli *et al.,* 2000). The mechanism for CcpC-dependent regulation is best characterized at the *citB* promoter, where it binds to two sites, a dyad symmetry element centered at the -66 position and a half-dyad at -27, relative to the transcriptional start site (Figure 4). A CcpC dimer binds to each of these sites and the dimers interact, producing a tetramer; this interaction stabilizes the binding to the -27 site, which is inherently weak

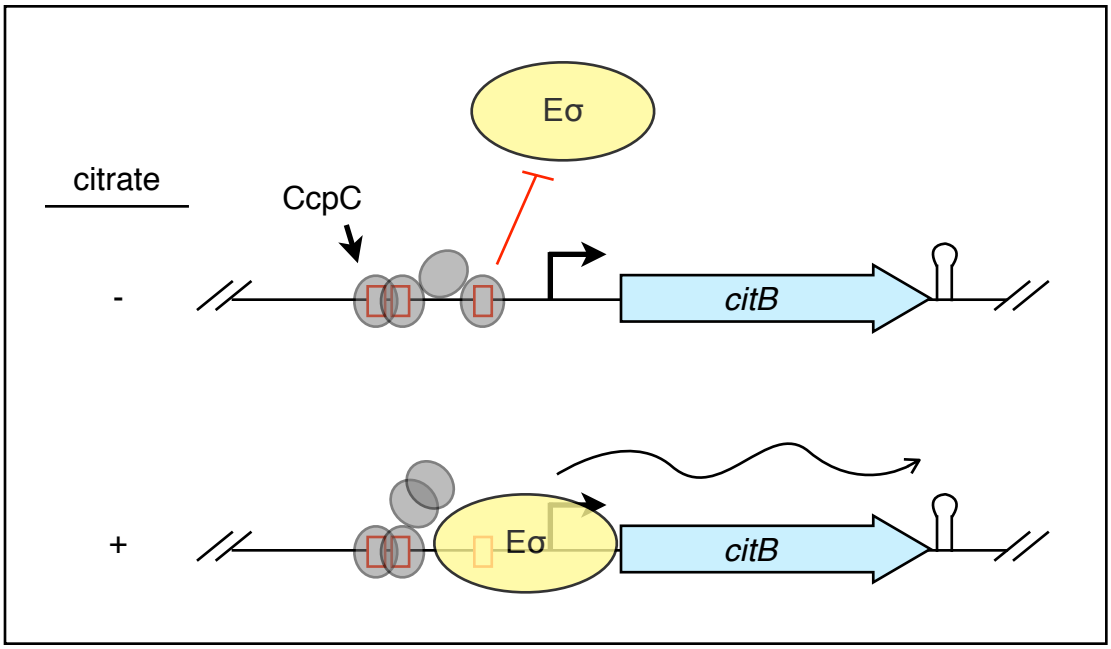

Figure 4. Current model for the regulation of the *citB* promoter by CcpC. There are two CcpC binding sites (red boxes) in the *citB* promoter. Both are occupied by CcpC (grey circles) when citrate is low (- citrate); this binding prevents *citB* transcription. When citrate levels rise (+ citrate), citrate antagonizes CcpC binding to the half-site, resulting in derepression of *citB*.

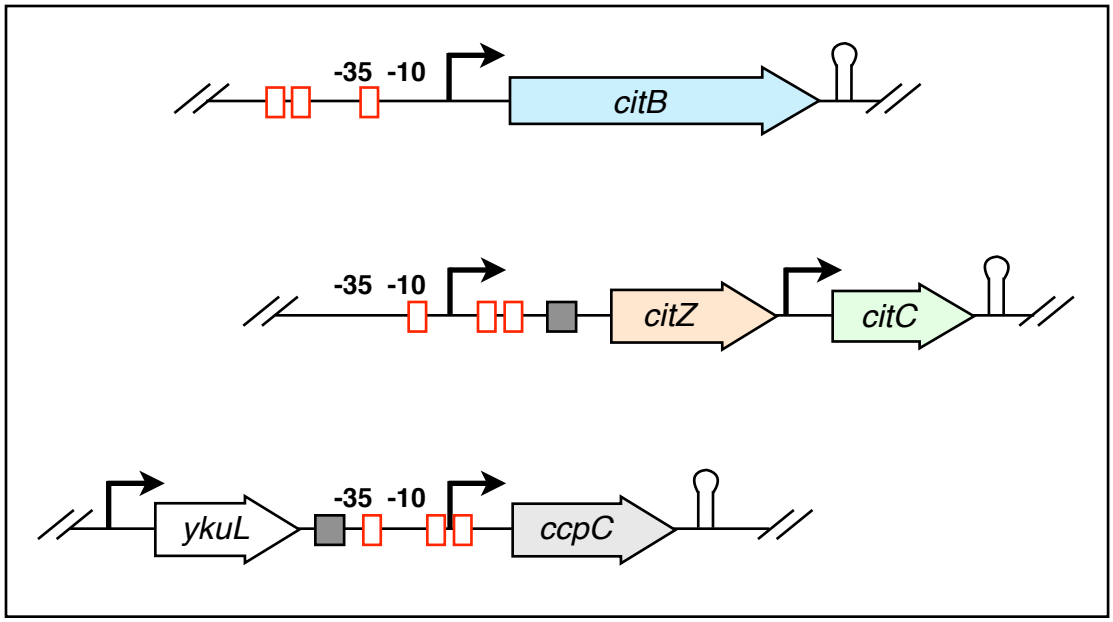

Figure 5. Architecture of CcpC and CcpA binding sites at the *citB*, *citZ* and *ccpC* loci. The locations of CcpC (red-lined white boxes) and CcpA (grey boxes) binding sites are indicated on the *citB, citZ*, and *ccpC* promoters.

(Jourlin-Castelli *et al.,* 2000). However, when citrate is present, CcpC vacates the -27 site (Jourlin-Castelli *et al.,* 2000). The CcpC tetramer, however, stays intact, and remains bound to the -66 element despite the presence of citrate. However, binding at the -66 element does not prevent RNA polymerase from interacting with the promoter (S.I. Kim *et al.,* 2003). Therefore, when citrate levels rise within the cell, *citB* is derepressed due to the loss of CcpC binding at the -27 half-dyad site. In this model, the CcpC tetramer is bound to the -66 full dyad symmetry element in all conditions, and binding to the -27 site is modulated by citrate levels to control *citB* expression.

CcpC repression has also been described for the *citZ* locus. Interestingly, while there are also two CcpC binding sites present at the *citZ* promoter, the orientation of the two binding sites is inverted compared to *citB*; a half-dyad symmetry element is present from positions -11 to +6 and a full dyad centered at +30 (Jourlin-Castelli *et al.,* 2000). A comparison of these two sites is shown in Figure 5. The location of these sites implies a different model for CcpC-dependent repression of *citZ* than for *citB*; binding to the half-dyad would obscure the -10 region of the promoter, and binding to the +30 region would act as a roadblock for RNA polymerase. In addition, the binding of CcpC to these sites is reduced equally in the presence of citrate (Jourlin-Castelli *et al.,* 2000). Therefore, at the *citZ* promoter, CcpC completely disassociates from the DNA in the presence of citrate, resulting in a simple on-off model of repression in response to an effector.

The regulation of *citZ* and *citB* by CcpC in response to citrate is an elegant example of an inducer in action. Expression of these two genes, encoding citrate synthase and aconitase, is repressed by CcpC when carbon is not entering the TCA cycle via citrate. Citrate acts as the inducer (produced either through leaky expression of *citZ* or through *citA* expression, discussed briefly below), causing derepression of *citZ* and citrate synthase production, producing more citrate. In turn, this citrate causes derepression of *citB*, which converts the citrate to isocitrate. Moreover, the expression of isocitrate dehydrogenase (*citC*) via read-through expression from the *citZ* promoter

completes the TCA branch pathway. In this model, the CcpC-citrate interaction allow for the complete induction of the TCA branch of the Krebs cycle in the presence of citrate, resulting in its conversion to 2-ketoglutarate. This model is much like that of the *lac* operon, in which allolactose (an analog of lactose produced by β-galactosidase) acts as the inducer; binding of allolactose to the LacI repressor causes its disassociation from the DNA and derepression of the *lac* genes (Lewis 2005). Again, as in the CcpC model, leaky expression of the *lac* operon is required for the presence of the inducer. That is, *lacY*, which encodes lactose permease, must be expressed at low levels to allow for the transport of lactose into the cell; β-galactosidase (*lacZ*) is required for the production of allolactose (Lewis 2005).

In addition, regulation by CcpC is complicated by regulation at the *ccpC* locus itself. The *ccpC* locus on the *B. subtilis* chromosome has two promoters, a *ccpC*-specific promoter (P1) located immediately upstream of the *ccpC* transcriptional unit, and the P2 promoter, located upstream of the hypothetical open reading frame adjacent to *ccpC*, *ykuL* (Kim *et al.,* 2002a). Similarly to its other target loci, the P1 promoter has two CcpC binding sites, the familiar half dyad and full dyad symmetry elements. In this case, the half dyad symmetry element overlaps the -35 region and the full dyad overlaps the transcriptional start site (Kim *et al.,* 2002a). This architecture most closely resembles that of the *citZ* promoter (Figure 5), and dictates a similar model of repression; CcpC binds to the *ccpC* promoter and represses transcription when citrate levels are low, but the interaction is perturbed in the presence of citrate, leading to derepression. It is interesting to consider that citrate itself causes the production of more CcpC, but the excess CcpC protein would be unable to repress transcription of *citZ* and *citB* due to antagonism by citrate. Kim *et al.* hypothesized that this mechanism allows the cell to prepare for the eventual need to shut off TCA branch enzyme production in the event of an influx of glucose; the large pool of CcpC would allow for a fast response to falling citrate levels (2002a).

This regulatory picture is further complicated by an interesting unpublished observation: in *citB* null cells, the expression of a *citB-lacZ* fusion at an exogenous locus is highly overexpressed (H.J. Kim, unpublished). This effect is both citrate-dependent and CcpC dependent, indicating that CcpC may act as a positive regulator of *citB* in conditions of high citrate. I will explore this possibility, along with implications for the CcpC regulatory model, in Chapter 1 of this thesis.

In addition to the carbon catabolite repression of *citB*, *citZ*, and *citC* by CcpC, which interacts with a TCA branch-specific metabolite, these genes (and many others) are subject to CCR by catabolite control protein A (CcpA), a transcriptional regulator that senses glucose levels within the cell.

4.2 Repression of *citZ* and *ccpC* by CcpA

The CcpA protein is a dimeric LacI/GalR-family transcription regulator that was discovered in a hunt for mutations that derepress expression of a secondary carbon source utilization gene (alpha-amylase; *amyE*) in the presence of glucose (Henkin *et al.,* 1991). When active, CcpA binds to 15-bp palindromic sequences, called catabolite response element (*cre*) sites, found in at least 50 loci in *B. subtilis* (Fujita 2009). Most of these targets are repressed by CcpA, but, in a few cases, CcpA activates gene expression (Görke *et al.,* 2008). Like many transcription factors that respond to nutrient availability, CcpA is activated by binding to a cofactor, or effector, molecule that indicates nutritional status. In this case, CcpA has a protein cofactor, the histidine protein (HPr). The CcpA-HPr complex can only form when HPr is phosphorylated on a specific serine residue (Fujita 2009). [HPr is best known for its role in the phosphorelay that activates sugar transport through the phosphoenolpyruvate (PEP)-dependent phosphotransferase system. In this role, HPr is phosphorylated on a histidine residue (Görke *et al.,* 2008).] Moreover, HPr is serine-phosphorylated only when there is ample fructose-1,6-bisphosphate and ATP present within the cell, indicating the presence of glucose or another rapidly metabolizable carbon source (Görke *et al.,* 2008). In addition,

the CcpA-HPr complex is stabilized by direct binding of fructose-1,6-bisphosphate and glucose-6-phosphate (Schumacher *et al.,* 2007), ensuring that the transcriptional activity of CcpA is limited to conditions in which specific nutrients are plentiful.

CcpA regulates the *citZ* and *ccpC* promoters. The *citZ* locus contains a *cre* site between positions +80 and +97 relative to the transcriptional start site, shown in Figure 5 (Kim *et al.,* 2002b). Despite being nearly 100 bp downstream of the start site, this element is not within the *citZ* open reading frame; the *citZ* mRNA has a 195 base leader region before the start codon (Jin *et al.,* 1994b). Given the position of the *cre* site so far downstream of the start site, CcpA is hypothesized to act as a roadblock for RNA polymerase, resulting in *citZ* repression (Kim *et al.,* 2002b). The model for CcpA-dependent regulation at the *ccpC* locus also invokes a roadblock mechanism of repression (Kim *et al.,* 2002a). As described above, the *ccpC* locus has two promoters, P1 and P2. A *cre* site is present upstream of the P1 promoter -35 element (Figure 5), and CcpA binds to this site *in vitro* (Kim *et al.,* 2002a). Expression from the P2 promoter is subject to CcpA-dependent glucose repression, suggesting that CcpA binding to the *cre* site prevents read-through transcription from a promoter ~330 bp upstream (Kim *et al.,* 2002a).

In binding to the *citZ* promoter, CcpA controls the expression of citrate synthase in response to glucose availability. When glucose is high, *citZ* is repressed by CcpA and citrate levels remain low within the cell. Low citrate levels mean that CcpC is active, further repressing *citZ*. In addition, the regulation of *ccpC* by CcpC and CcpA results in repression of this regulator when glucose is high and citrate is low. However, when glucose levels fall and citrate levels rise, these regulators are deactivated and both *citZ* and *ccpC* are expressed. In this manner, CcpA indirectly regulates the *citB* locus (and the *ccpC* locus for that matter) by repressing the production of citrate, the inducer of *citB* (and *ccpC*) expression.

4.3 Regulation of *citB* by CodY, AbrB, and TnrA

In addition to the regulation by CcpA and CcpC described above, the expression of the TCA branch genes is regulated by three more transcriptional regulators that respond to nutritional conditions in the cell: CodY, AbrB, and TnrA.

The *codY* gene was described in 1995 as a member of an operon responsible for the control of *dpp*, the dipeptide permease transport operon (Slack *et al.,* 1995). Since that time, CodY has been shown to be a global regulatory protein that binds to DNA to either repress or activate gene expression (Sonenshein 2007). CodY activity is modulated by two classes of effectors that are present in high concentrations during the exponential growth phase: GTP (Ratnayake-Lecamwasam *et al.,* 2001), and branched-chain amino acids (Shivers *et al.,* 2004). The branched-chain amino acids (BCAAs; isoleucine, leucine, and valine) cause a conformational change in CodY that is evident in the crystal structure (Levdikov *et al.,* 2006), but the GTP binding site remains unknown. Through the interaction with these two types of effectors, CodY activity is linked to the nutritional content of the cell from several points of view. GTP levels provide a snapshot of the energy content of the cell, but they also offer information concerning amino acid pools. During the stringent response, the presence of uncharged tRNAs, which indicates a lack of amino acids, stimulates GTP conversion to ppGpp, a signalling molecule that acts to reduce overall RNA and protein synthesis (Condon *et al.,* 1995). In addition, BCAA levels provide another, more direct indicator of amino acid availability. The end result of this linkage to GTP and BCAA levels is that CodY-regulated genes are repressed during exponential growth but are derepressed at the entry to stationary phase, when the levels of the effectors drop. CodY targets in *B. subtilis* include many genes involved in the adaptation to nutrient limitation, including genetic competence and sporulation (Sonenshein 2007). In addition, in Gram-positive pathogens such as *Clostridium difficile* and *Staphylococcus aureus*, CodY is responsible for the repression of virulence factors (Dineen *et al.,* 2007, Majerczyk *et al.,* 2008).

Like CodY, AbrB is a pleiotropic transcriptional regulator involved in stationary phase gene expression in *B. subtilis*; however, unlike CodY, AbrB activity is controlled at the transcriptional level (Strauch *et al.,* 1990). During exponential phase, AbrB is transcribed and acts as a negative regulator of stationary phase-specific genes. In addition, AbrB acts as a repressor of its own synthesis (*abrB*) (Strauch *et al.,* 1993). The induction of AbrB-regulated genes occurs when Spo0A, the master regulator of *B. subtilis* sporulation, is activated by phosphorylation. Spo0A~P binds to and represses *abrB* expression, resulting in a rapid decrease in the amount of AbrB in the cell (Fürbaß *et al.,* 1991). AbrB therefore acts in direct response to the Spo0A phosphorelay that initiates sporulation, discussed in more detail below.

The final protein involved in *citB* regulation is TnrA, a global transcription factor that regulates nitrogen metabolism genes (Fisher 1999). TnrA is active as a DNA-binding protein during conditions of nitrogen limitation. In the presence of the preferred nitrogen source, glutamine, TnrA is inactivated by a unique mechanism; it interacts with the glutamine synthase (GS) protein and glutamine to form a complex that is unable to bind DNA (Wray *et al.,* 2001). Since GS is feedback-inhibited when bound to glutamine (Deuel *et al.,* 1974), both proteins of this complex are inactive.

The combined activities of these three transcriptional regulators at the *citB* promoter results in a complex orchestration of aconitase expression. When active, CodY regulates TCA branch enzyme gene expression by directly binding to sequences in the *citB* promoter region and represses aconitase expression. CodY interacts with two sites in the *citB* promoter region: the first from positions -83 to -43, and the second from positions -6 to +27, relative to the transcriptional start site (H.J. Kim *et al.,* 2003). The first of these two sites overlaps the CcpC dyad symmetry element centered at the -66 position, and DNase I footprinting of the *citB* promoter in the presence of both CodY and CcpC indicates that the two proteins compete for binding in this region (H.J. Kim *et al.,* 2003). Complicating matters, AbrB also binds to this region. DNase I footprinting of the

citB promoter in the presence of AbrB revealed a protected region from positions -35 to +14 (H.J. Kim *et al.,* 2003). However, an *abrB* null mutant has lower levels of *citB-lacZ* activity than wild-type, leading to the current hypothesis that AbrB acts as a positive regulator by competing with CodY and CcpC for binding to the *citB* promoter (H.J. Kim *et al.,* 2003). Finally, while both CodY and AbrB act directly to regulate gene expression by binding to the *citB* promoter, TnrA may have an indirect effect. In a *tnrA* null strain, *citB* expression in the presence of glutamate and glucose was significantly lower than in the wild-type, suggesting that TnrA plays a role in the regulation of *citB* under these conditions (Blencke *et al.,* 2006).

4.4 Regulation of *citA* and *citC*

While the *citC* gene is subject to read-through transcription from the *citZ* promoter, and thus regulation by CcpC and CcpA, it is also expressed from a *citC*-specific promoter immediately upstream of the open reading frame (Jin *et al.,* 1994b). Like the *citZ* promoter, expression from the *citC* promoter is subject to catabolite repression, although the mechanism of this regulation is unknown (Jin *et al.,* 1994b).

The *citA* gene is located at a separate chromosomal locus from *citZ* and *citC,* just upstream of *citR*, a gene on the opposite strand that encodes a putative LysR-family regulatory protein (Jin *et al.,* 1994a). The expression of *citA* is induced as cells enter stationary phase, but the level of induction is not as dramatic as with *citZ.* Alleviation of repression by the CitR protein is likely responsible for the increase of *citA* expression; *citR* null mutants overexpress a *citA-lacZ* fusion (Jin *et al.,* 1994b). However, the mechanism of CitR regulation and the means of derepression are unknown.

There is little if any evidence for cross regulation of *citA* and *citZ* (Jin *et al.,* 1994b). It seems likely that the regulatory networks governing these two enzymes are separate.

4.5 Inhibition of CitZ (CS II) by 2-ketoglutarate and ATP

As described above, full repression of *citB* requires glucose and a source of 2-ketoglutarate. In unpublished work, Hyun-Jin Kim observed that 2-ketoglutarate inhibits CitZ by competing with oxaloacetate for binding (Sonenshein 2007). This result is consistent with work in other organisms; feedback-inhibition of citrate synthases by 2-ketoglutarate has been described in the literature for nearly 50 years (Wright *et al.,* 1967). This feedback inhibition explains the repression of *citB* in medium containing glucose and glutamine (Rosenkrantz *et al.,* 1985). The provided glutamine is converted to glutamate by glutamate synthase, glutamate is converted to 2-ketoglutarate by glutamate dehydrogenase, and 2-ketoglutarate inhibits CitZ. The inactivated CitZ results in lower levels of citrate, causing CcpC to be active as a repressor, leading to repression of *citB*.

In addition to this 2-ketoglutarate effect, the CitZ protein is inhibited by ATP (Flechtner *et al.,* 1969, Jin *et al.,* 1996). However, unlike citrate synthases from Gram-negative bacteria that are inhibited by NADH (Weitzman 1981), CitZ activity is not sensitive to NADH (Jin *et al.,* 1996). The response of CitA to 2-ketoglutarate, ATP and NADH is not known.

5 Regulation of the TCA branch enzymes in other bacteria

Studies of the expression of citrate synthase, aconitase, and isocitrate dehydrogenase in bacteria other than *B. subtilis* allow us to compare and contrast the diverse approaches to metabolic regulation that have evolved to achieve the goal of efficient energy usage.

5.1 *Escherichia coli*

Escherichia coli encodes a single citrate synthase (*gltA*), two aconitase isozymes (*acnA*, *acnB*) and an isocitrate dehydrogenase (*icd*) enzyme. The aconitases of *E. coli* play different roles in cell physiology. AcnB is the major enzyme responsible for metabolism of citrate during growth, while AcnA is induced by oxidative stress and the

presence of iron (Cunningham *et al.,* 1997). In addition, residual aconitase activity, at one point termed AcnC, can be detected in an *acnA acnB* double mutant: a 2-methylcitrate dehydratase encoded by the *prpD* gene is a component of the propionate metabolism pathway and is responsible for this activity (Blank *et al.,* 2002). [*B. subtilis* also contains a predicted *prpD* homolog, the *mmgE* gene, which is expressed early in sporulation and is subject to regulation by CcpA (Bryan *et al.,* 1996, Steil *et al.,* 2005).] Like their counterparts in *B. subtilis*, the *E. coli* TCA branch genes are controlled by multiple regulatory mechanisms.

E. coli regulates the TCA branch enzymes and other genes responsible for secondary carbon source utilization by two mechanisms: inducer exclusion, and by the cyclic AMP (cAMP) receptor protein, CRP. Inducer exclusion is the primary means by which *E. coli* represses secondary carbon source utilization in the presence of glucose (Deutscher 2008). The mechanism of inducer exclusion involves the phosphorylation state of the EIIA subunit of the glucose transporter ($EIIA^{Glc}$). The $EIIA^{Glc}$ subunit is dephosphorylated in the presence of glucose due to a low ratio of phosphoenolpyruvate (PEP) to pyruvate (Görke *et al.,* 2008). The unphosphorylated form of $EIIA^{Glc}$ binds to and inactivates permeases responsible for transporting secondary carbon sources, such as lactose, maltose, and raffinose, inside the cell. This mechanism is operon specific; the interaction of $EIIA^{Glc}$ with a permease can only occur when its specific substrate is present (Görke *et al.,* 2008). Additionally, when glucose is exhausted from the medium, PEP levels rise compared to pyruvate, and $EIIA^{Glc}$ is phosphorylated, resulting in activation of adenylate cyclase. The cAMP receptor protein, CRP, then binds to cAMP to activate or repress a wide range of targets in response to carbon source availability (Görke *et al.,* 2008). In particular, expression of the *E. coli* citrate synthase gene (*gltA*) is activated by the CRP-cAMP complex (Gosset *et al.,* 2004). In addition, the *acnA* and *acnB* genes are both activated by CRP-cAMP (Cunningham *et al.,* 1997).

The *E. coli* TCA branch enzymes are also regulated in response to oxygen levels by two mechanisms. The ArcAB system is activated during the transition from aerobic to anaerobic growth; it represses TCA cycle gene expression under anaerobic conditions (Gunsalus *et al.,* 1994). Direct evidence for regulation by ArcA (the response regulator) has been demonstrated for the *gltA* gene (Lynch *et al.,* 1996), although the effects of repression are evident for aconitase and isocitrate dehydrogenase (*icd*) genes, as well (Iuchi *et al.,* 1988, Shalel-Levanon *et al.,* 2005). Fnr (fumarate and nitrate reduction) is a global oxygen-sensing transcription factor that is active as a dimer. Dimerization of Fnr is dependent on the presence of a 4Fe-4S cluster that is sensitive to oxygen (Green *et al.,* 2009). Fnr represses the expression of *acnA* in *E. coli* (Cunningham *et al.,* 1997).

5.2 *Corynebacterium glutamicum*

Another example of TCA branch enzyme regulation can be found in *Corynebacterium glutamicum*, a Gram-positive soil bacterium that is utilized in industry for the production of L-glutamate, used as monosodium glutamate as a flavor enhancer, and L-lysine, an animal feed additive (Bott 2007). Thus far, three separate transcription factors, AcnR, RipA, and RamA, have been identified that target the TCA branch enzymes in *C. glutamicum* and all regulate aconitase (*acn*) expression. AcnR is a TetR-type repressor that binds directly to the *acn* promoter, but the signal that AcnR responds to is unknown (Krug *et al.,* 2005). RipA responds to iron levels and represses *acn* under iron limitation; the *ripA* gene is a target of the DtxR master iron regulator in *C. glutamicum* (Bott 2007). Finally, RamA is responsible for activating *acn* expression in the presence of acetate (Bott 2007).

5.3 *Staphylococcus aureus* and *Streptococcus mutans*

Recently, there has been interest in the regulation of the TCA cycle genes in the Gram-positive pathogens *Staphylococcus aureus* and *Streptococcus mutans*. *S. aureus*, a colonizer of the skin and mucous membranes, causes a host of diseases ranging from minor skin infections to serious conditions such as pneumonia and endocarditis (Tang *et*

al., 2010). In *S. aureus*, as in *B. subtilis*, the TCA cycle is activated at the exit from the exponential phase (Chatterjee *et al.,* 2005). One regulator implicated in this activation is the ClpC ATPase, which has been identified as a global regulator of metabolic genes, including aconitase (Chatterjee *et al.,* 2005, Chatterjee *et al.,* 2009). While the mechanism of this regulation is still being elucidated, it is clear that ClpC is an important regulator that mediates the response to nutrient limitation during stationary phase (Chatterjee *et al.,* 2009).

S. mutans, which is the principal causative agent of dental caries in humans (Lemos *et al.,* 2008), encodes genes for aconitase (*acn*), citrate synthase *(citZ*) and isocitrate dehydrogenase (*icd*) clustered together at a single locus. Expression of these genes in *S. mutans* is repressed by acid as well as high osmolarity and temperature (Chia *et al.,* 2001), although the mechanism of transcriptional regulation of these genes has not been established.

6 TCA branch enzyme mutant phenotypes

I have described the regulatory mechanisms that govern the expression of the TCA branch enzymes in *B. subtilis*. In order to understand why these proteins are so well regulated, it is useful to consider their physiological relevance. If one considers only the enzymatic activities of the TCA branch enzymes, a discrete metabolic effect, in the form of glutamate auxotrophy, would be seen if any of the enzymes were deleted. However, the effect of deleting the *citB* or *citZ* or *citC* genes is anything but discrete. Deletion in any one of these TCA cycle enzymes has profound effects on cell physiology, and in particular, on sporulation.

6.1 Sporulation in *B. subtilis*

In the laboratory, *B. subtilis* cells sporulate in response to nutrient exhaustion or when resuspended in a defined medium with a poor carbon source. On a molecular level, this process begins when one of five different kinases senses an environmental signal

and transmits that signal to a phosphorelay, which activates by phosphorylation Spo0A, the master transcriptional regulator of sporulation (Burbulys *et al.,* 1991).

Spo0A~P is responsible for starting a transcriptional program that involves four different sporulation-specific sigma factors: mother-cell specific factors σ^E and σ^K and forespore-specific factors σ^F and σ^G. To begin this program, Spo0A~P activates and represses a large number of genes controlled by the vegetative cell-specific sigma factors σ^A and σ^H (Strauch *et al.,* 1990), resulting in two early morphological changes, the formation of the axial filament and the subsequent asymmetric cell division that produces the forespore (Bylund *et al.,* 1993). Prior to asymmetric division, σ^A and σ^H, along with activated Spo0A, drive the expression of pro-σ^E and σ^F (Haldenwang 1995). The σ^F protein is bound and held inactive by an anti-sigma factor, SpoIIAB (Duncan *et al.,* 1993). After septation, two unequal compartments are formed. In the smaller forespore compartment, inactivation of σ^F by SpoIIAB is alleviated by SpoIIAA, an anti-anti-sigma factor (Duncan *et al.,* 1996). Once active, σ^F directs the expression and activation of a membrane-bound proteolysis complex that cleaves pro-σ^E specifically in the mother cell compartment (Hilbert *et al.,* 2004). Active σ^F also drives the expression of *spoIIIG*, which encodes the σ^G protein, the latest-acting forespore-specific sigma factor. Mature σ^G is held inactive by overlapping mechanisms that involve SpoIIAB (Kellner *et al.,* 1996, Serrano *et al.,* 2004) and SpoIIGA (Chary *et al.,* 2005). Similarly, in the mother cell, activated σ^E drives the expression of many genes, including *sigK*, which encodes the latest-acting mother cell-specific sigma factor. The *sigK* gene product is synthesized as an inactive precursor, pro-σ^K (Haldenwang 1995).

Before the cell may activate σ^G and σ^K, the mother cell must engulf the forespore. Engulfment is directed by σ^E-specific gene products (Eichenberger *et al.,* 2004). Complete engulfment, along with the expression of the *spoIIIA* locus in the mother cell, and the presence of SpoIIIJ protein in the forespore, results in the activation of σ^G (Serrano *et al.,* 2003, Serrano *et al.,* 2004). σ^G then activates a signaling cascade to

trigger the cleavage of pro-σ^K to σ^K in the mother cell (Campo *et al.,* 2006, Resnekov *et al.,* 1998, Rudner *et al.,* 2002). Once active, σ^K directs the overall maturation of the spore, including spore coat synthesis, before release into the environment.

6.2 Mutations in TCA branch enzymes

As mentioned above, mutations in the TCA branch enzymes exhibit altered sporulation phenotypes. In fact, early work on citrate synthase, aconitase, and isocitrate dehydrogenase null mutants focused on their sporulation phenotypes (Fortnagel *et al.,* 1968).

A *citZ* null strain produces 10-fold fewer heat-resistant spores than does the wild-type, while the *citC* strain has a more severe phenotype, producing over 10^6-fold fewer heat-resistant spores than the wild-type strain (Jin *et al.,* 1994a). Introduction of a *citA* mutation to the *citZ* null strain resulted in a more severe phenotype that resembled the *citC* null defect (Jin *et al.,* 1994a). The *citC* mutant is able to activate Spo0A-dependent gene expression, but it is blocked at Stage I, just prior to asymmetric septation (Jin *et al.,* 1997). Further exploration of this defect concluded that a *citZ* mutation could partially suppress the *citC* phenotype, indicating that citrate accumulation was partially responsible for the *citC* Stage I block (Matsuno *et al.,* 1999). (Note that a *citC* mutant accumulates citrate rather than isocitrate because the equilibrium of the aconitase reaction strongly favors conversion of isocitrate to citrate.) In addition, the *citC citZ* double null mutant could not express σ^G and σ^K-dependent genes unless a constituitively active form of Spo0A (*sof-1*) was supplied; however, the *sof-1* allele could not suppress the *citC* null mutant phenotype in a *citZ*$^+$ strain (Matsuno *et al.,* 1999). This result is confusing, but it points towards the importance of the maintanence of citrate levels within the cell.

A *citB* null strain exhibits a block at stage 0; it cannot activate Spo0A by phosphorylation (Craig *et al.,* 1997). As described in brief above, *citB* null mutants accumulate citrate in the culture fluid of growing cells (Craig *et al.,* 1997). The

mechanism of citrate accumulation was long attributed to a metabolic roadblock; I will present an updated model to explain this phenomenon in chapter 1 of this thesis. Regardless of the mechanism, it is this accumulation of citrate that prevents the phosphorylation of Spo0A, because excess citrate lowers the extracellular pH and chelates divalent cations, which are necessary for the activation of Spo0A (Craig *et al.,* 1997, Matsuno *et al.,* 1999). The Spo0A block can be overcome by expressing the *sof-1* allele in the *citB* null background, but this strain is still blocked at a later stage (Craig *et al.,* 1997). Alternatively, citrate was eliminated by creating a citrate synthase (*citA citZ*) and aconitase triple mutant; this strain can activate Spo0A, but it is unable to activate σ^G-dependent gene expression (Craig *et al.,* 1997). Removal of the excess citrate by resuspending cells in fresh medium had a similar effect, that is, partial restoration of sporulation (Craig *et al.,* 1997).

The results concerning *citC* and *citB* null mutant sporulation phenotypes demonstrate two things. First, the presence of a functional TCA cycle is necessary to prevent the improper accumulation of metabolites (such as citrate) that can interfere with sporulation gene expression. Second, both the *citC* and *citB* null mutants exhibit sporulation defects separate from citrate accumulation. For the *citC* null mutant, the mechanism that drives the discrepancy between the *citC sof-1* and *citC citZ sof-1* phenotypes is unknown, and warrants further study. In the case of the *citB* null, however, we have ample evidence to indicate that a non-enzymatic function is responsible for the citrate-independent sporulation defect. As discussed briefly above, many aconitases in nature are bifunctional. In addition to its well characterized enzymatic function, *B. subtilis* aconitase can bind to RNA to regulate gene expression post-transcriptionally (Alén *et al.,* 1999, Serio *et al.,* 2006a).

7 The bifunctional aconitase protein

The bifunctional nature of aconitase proteins was first discovered in eukaryotes 20 years ago. Eukaryotes possess two aconitase proteins: the main Krebs cycle enzyme

(mAcn) found in the mitochondrion, and a bifunctional protein (cAcn) that localizes to the cytosol. Both enzymes contain the characteristic 4Fe-4S cluster found in all aconitase proteins. It is the cluster itself that provides the molecular switch between functions. Because of the chemistry of the 4Fe-4S cluster, the Fe_a iron atom is labile and can be lost *in vivo* following oxidation by reactive oxygen species (ROS), such as superoxide or hydrogen peroxide (Imlay 2006). Loss of the Fe_a atom results in a catalytically inactive 3Fe-4S cluster. This inactive form of the enzyme is also subject to more extensive cluster disassembly, resulting in an apoprotein that lacks the cluster entirely. In the case of cytosolic aconitase (cAcn), the apoprotein form has a second, nonenzymatic function; it binds to RNA as iron regulatory protein 1 (IRP1) (Emery-Goodman *et al.,* 1993, Haile *et al.,* 1992, Kennedy *et al.,* 1992).

7.1 The IRP1 regulation model

IRP1 binds to stem-loop structures called iron-responsive elements (IREs) in the 5' or 3' untranslated region (UTR) of messenger RNAs. IREs are found in the mRNAs of genes involved in the uptake, transport, and usage of iron (Haile 1999). When IRP1 binds to an IRE in the 5' UTR, it blocks ribosome loading and negatively regulates gene expression. Alternatively, when IRP1 binds to an IRE in the 3' UTR, it exerts positive regulation by preventing the degradation of the mRNA (Beinert 2000).

The enzymatic and RNA-binding functions of IRP1 are mutually exclusive. Recent crystal structures of both the enzymatic cAcn and IRP1 in complex with RNA have made it clear that the switch between these two functions requires major structural rearrangements (Walden *et al.,* 2006). IRP1 can be switched between the two states *in vitro* by treatment with varying concentrations of oxidizing agents, such as ferricyanide or persulfate (Haile *et al.,* 1992, Kennedy *et al.,* 1983). At low concentrations of ferricyanide, the catalytically inactive 3Fe-4S cluster form is obtained, but this form of IRP1 is still capable of binding to substrate (Kennedy *et al.,* 1992). At high concentrations of ferricyanide, the cluster is completely lost, and the apoprotein form

binds to RNA (Haile *et al.,* 1992). Reinsertion of the 4Fe-4S cluster restores catalytic activity and abolishes RNA-binding (Emery-Goodman *et al.,* 1993). Furthermore, the cysteine residues that coordinate the three iron atoms of the cluster can be individually mutated to serine to prevent cluster formation and abrogate catalytic activity, but these mutants are still capable of binding to RNA (Hirling *et al.,* 1994, Philpott *et al.,* 1993).

Biochemical studies have revealed that the RNA-binding function of apo-IRP1 requires a reduced environment. Purified apo-IRP1 treated with diamide, a thiol-oxidizing agent, loses RNA-binding activity. In the presence of diamide, it is likely that C437 forms a disulfide bond along with one of the other free cysteine residues (C503, C506) that coordinate the cluster. Substituting the cysteine residue with serine (C437S) produces a mutant that retains RNA-binding in the presence of diamide (Philpott *et al.,* 1993). These data suggest that it is imperative to use sufficient concentrations of reducing agents when preparing and utilizing wild-type apo-IRP1 *in vitro*.

7.2 Bifunctional aconitases in other prokaryotes

Since the discovery of the bifunctional IRP1 aconitase, prokaryotic aconitases have been shown to possess RNA-binding functions. The two aconitases of *E. coli*, AcnA and AcnB, enhance their own expression by binding to the 3' UTRs of the *acnA* and *acnB* transcripts (Tang *et al.,* 1999). In addition, AcnA and AcnB both bind to the superoxide dismutase (*sodA*) transcript, but they have opposite effects on its stability (Tang *et al.,* 2002). AcnB, in particular, switches between its enzymatic and RNA-binding functions by a unique mechanism; iron-dependent dimerization produces the catalytic enzyme while AcnB monomers are active as RNA-binding proteins (Tang *et al.,* 2005).

Several other, less well characterized examples of bifunctional aconitases are found in the microbial world. In *Salmonella enterica*, the AcnB aconitase protein indirectly regulates bacterial motility by destabilizing the *ftsH* transcript and lowering the levels of FtsH, a protease that negatively regulates flagellar synthesis (Tang *et al.,*

2004). The *Mycobacterium tuberculosis* aconitase binds to the thioredoxin (*trxC*) and iron-dependent repressor/activator (*ideR*) transcripts *in vitro* (Banerjee *et al.,* 2007).

7.3 *B. subtilis* aconitase is bifunctional

B. subtilis aconitase and IRP1 are 70% similar at the amino acid level, a fact that prompted an examination of the RNA binding ability of purified Acn *in vitro*. Purified aconitase was shown to bind to an exogenous target, the rabbit ferritin IRE, as well as to two potential endogenous RNA targets that possess IRE-like sequences, the *qoxD* and *feu* transcripts (Alén *et al.,* 1999). Acn can be switched to one form or another by adding exogenous iron or by including an iron chelator (Alén *et al.,* 1999), indicating that the functional switch in *B. subtilis* is very likely the same as that found in eukaryotes for IRP1.

7.3.1 Single-function mutants: C517A and *citB5*

In order to determine the contribution of each of the aconitase functions to *B. subtilis* physiology, attempts have been made to create single-function mutants; i.e., strains that express an aconitase that is only an enzyme or only an RNA-binding protein. One mutant, *citB517*, has a single amino acid substitution at one of the cluster-coordinating cysteines (C517A). This single residue abolishes enzymatic activity but retains partial *in vitro* RNA binding (Alén *et al.,* 1999). In addition, this cysteine mutant was reported to sporulate with forty-fold greater efficiency than the *citB* null mutant (Alén *et al.,* 1999). However, the *citB517* strain was unstable for reasons that at the time the authors could not explain (C. Alen, unpublished observations). Results presented in Chapter 1 will provide a likely explanation for this phenomenon.

A second mutant strain was obtained when the RNA-binding function was targeted for mutation. The mutant allele, *citB5*, contains five substitutions near the carboxyl terminus of the protein (Serio *et al.,* 2006a), two of which (R741E, Q745E) are at residues homologous to residues in IRP1 that are important in the interaction with an IRE (Kaldy *et al.,* 1999). Importantly, these mutations do not abolish enzymatic activity;

the mutant protein is an active aconitase (Serio *et al.,* 2006a), although I will explore the nuances of that issue in Chapter 1 of this thesis. The *citB5* mutant was utilized extensively to look at the contribution of aconitase to both sporulation and iron metabolism.

7.3.2 A role for aconitase in sporulation

B. subtilis cells expressing the *citB5* mutant aconitase initate sporulation like wild-type cells, but experience a temporary block at a late stage. Seven hours after the initiation of sporulation (T_7), wild-type cells have a sporulation efficiency of 60%, while the *citB5* mutant sporulation efficiency is 0.72%. By T_{20}, the mutant (76%) catches up to the wild-type (82%) (Serio *et al.,* 2006a). A time-course microarray analysis was utilized to identify differentially expressed transcripts in the *citB5* strain. While σ^E- and σ^G-dependent transcripts levels are similar in both strains, the transcript levels of many σ^K-dependent genes are less abundant in the *citB5* mutant compared to wildtype (Serio *et al.,* 2006a). Among these σ^K-dependent genes, a potential target for aconitase, *gerE,* was identified.

The *gerE* promoter is recognized by σ^K and is transcribed during the first wave of σ^K-induced genes, a group that includes spore coat genes *cotA* and *cotD* (Zheng *et al.,* 1990). The *gerE* mRNA transcript can be detected by Northern blot starting 4 hours after the induction of sporulation (Cutting *et al.,* 1986). GerE is a small, 74 amino acid protein that acts as a dimer and is similar in structure to the DNA-binding domain of the *E. coli* response regulator NarL (Ducros *et al.,* 1998, Ducros *et al.,* 2001). The GerE protein binds to a number of σ^K-dependent promoters to activate or repress transcription (Zheng *et al.,* 1992). The strict σ^K regulon consists of 111 genes, of which 36 depend strongly on GerE for transcriptional activation, and 55 are repressed by GerE (Eichenberger *et al.,* 2004). Furthermore, the *sigK* promoter is repressed by GerE (Ichikawa *et al.,* 1999, Zheng *et al.,* 1992). GerE also plays a role outside of the σ^K regulon. It activates 5 genes that are under σ^E and σ^K control (Eichenberger *et al.,* 2004). Strains with mutations in

gerE release the forespore at a slower rate than wild-type strains and cannot germinate properly (Moir 1981). As GerE is required for the expression of many spore coat genes, this germination defect is likely due to an immature spore coat structure. Electron microscopy supports this hypothesis, as spores of *gerE* null cells have an electron-diffuse coat in comparison to the densely-staining coat of wild-type spores (Moir 1981).

The *gerE* transcript levels are six-fold lower in the *citB5* mutant than in the wild-type (Serio *et al.,* 2006a). Accordingly, the transcript levels of many genes that are positively regulated by GerE are less abundant in the *citB5* strain (Serio *et al.,* 2006a). Two tagged versions of aconitase were purified and studied *in vitro*. Wild-type aconitase with a His_{10} tag at the N-terminus (His_{10}-Acn) binds to *gerE* mRNA *in vitro* with an apparent K_d of 4.4 – 8.8 nM (Serio *et al.,* 2006a). The mutant protein, with a C-terminal His_6 tag, Acn_{citB5}-His_6, binds to the same *gerE* RNA with a 4.5-fold lower affinity than the wild-type Acn-His_6 protein, and the *citB5* mutant strain exhibits a delay in the appearance of *gerE* mRNA (Serio *et al.,* 2006a).

7.3.3 A role for aconitase in iron metabolism

In addition to the linkage between aconitase and sporulation, *B. subtilis* aconitase also regulates genes involved in iron metabolism, perhaps similarly to the role IRP1 plays in eukaryotic cells. Microarray analysis of *citB*$^+$ and *citB* null strains in a *fur* null background (*citB*$^+$ Δ*fur* and *citB::spc* Δ*fur*) under iron limiting conditions led to the identification of possible targets of aconitase. The Ferric uptake repressor (Fur) protein is the chief iron response regulator in *B. subtilis*, and it was necessary to delete it to unmask any potential post-transcriptional regulatory role of aconitase (Bsat *et al.,* 1999). The microarray revealed 177 transcripts that were at least two-fold less abundant in the *citB::spc* Δ*fur* compared to the *citB*$^+$ Δ*fur* strain (Serio 2005). In addition, 18 transcripts were at least two-fold more abundant in the *citB::spc* Δ*fur* compared to the *citB*$^+$ Δ*fur* strain (Serio 2005). These results indicate that aconitase likely plays a role in the regulation of iron metabolism in *B. subtilis*.

Notably, several of the genes underexpressed in the *citB::spc* Δ*fur* mutant were motility genes (Serio 2005). Two of these genes, *fliS* and *fliT*, are members of a flagellar operon that is also a putative target of the Fur protein (Baichoo *et al.,* 2002). There are four open reading frames in the *fliDST* operon, the first of which is an unknown flagellar gene, *yvyC*. I will refer to this operon as *fliDST* for consistency with the literature. Transcribed as a single message from a σ^D-dependent promoter, the *fliDST* operon is involved in the regulation of flagellar assembly in *B. subtilis* and other motile bacteria. The *fliD* transcript encodes a homolog of *E. coli* and *S. typhimurium* FliD, the capping protein of the flagellar filament (Chen *et al.,* 1994, Chevance *et al.,* 2008). The *fliS* and *fliT* genes encode homologs of *E. coli* and *S. typhimurium* FliS and FliT. In *S. typhimurium*, FliS facilitates flagellin export, while FliT regulates flagella in an unknown manner (Yokoseki *et al.,* 1996, Yokoseki *et al.,* 1995). FliD, FliS, and FliT are thought to each indirectly regulate the activity of the flagellar-specific sigma factor, σ^D, through the regulation of its anti-sigma factor, FlgM (Yokoseki *et al.,* 1996). FlgM binds to σ^D and holds it inactive until the construction of the hook basal body (HBB) is complete; FlgM is then exported through the HBB, releasing σ^D (Yokoseki *et al.,* 1996). FliD, FliS, and FliT negatively regulate FlgM export; inactivation of *fliD, fliS*, or *fliT* by transposon insertion increases FlgM export, which in turn increases σ^D activity and leads to overexpression of a subset of the flagellar operons (Yokoseki *et al.,* 1996). Moreover, inactivation of *fliD*, *fliS*, or *fliT* results in loss in motility (Fredrick *et al.,* 1996).

Purified wild-type His_{10}-Acn binds to the 3' UTR of *fliT in vitro*, with a Kd = 8.8 – 17.5 nM by gel shift assay (Serio 2005). In addition, the antisense *fliT* 3' UTR exhibits a much higher K_d by gel shift (~280 nM), indicating that the sense *fliT* binding is specific (Serio *et al.,* 2006a). No further analysis of the Acn:*fliT* interaction has been pursued, and the physiological importance of this binding is still unknown.

7.3.4 A role for aconitase in the regulation of the TCA branch enzymes

It has generally been assumed that *citB* null cells accumulate citrate to levels 80-fold above wild-type in the culture fluid simply because of the lack of aconitase activity in this strain (Craig *et al.,* 1997). In addition, as *B. subtilis* lacks a citrate lyase enzyme (see above), these cells have no way of enzymatically removing the citrate once it is formed. Therefore, the metabolic roadblock hypothesis seemed a perfectly good explanation for the citrate accumulation in the *citB* null.

However, a surprising result with the RNA-binding defective *citB5* mutant poked a hole in this hypothesis. The *citB5* strain, which exhibits high levels of aconitase activity in cell extracts (Serio *et al.,* 2006a), accumulates citrate in the culture supernatant at levels near those generated by the *citB* null mutant strain and overexpresses a *citB-lacZ* fusion (Serio 2005). This result suggested that aconitase may play a second, non-enzymatic role in the regulation of the TCA branch enzymes.

7.4 Purification methods for the study of aconitase:RNA interactions

In order to study the role of *B. subtilis* as an RNA-binding regulatory protein, it is necessary to purify it for *in vitro* experiments. A section of this thesis will describe a new purification scheme for *B. subtilis* aconitase. To understand how I developed this scheme, it is useful to consider the history of aconitase protein purification.

The first report describing the purification of aconitase appeared 60 years ago (Buchanan *et al.,* 1949). The authors isolated aconitase from pig heart using a combination of ethanol fractionation and ammonium sulfate precipitation. At the time, it was not known that aconitase required an iron-sulfur cluster for enzymatic activity, but it was clear that enzyme activity decayed rapidly after cell extract preparation. Buchanan *et al.* reported that the addition of citrate or *cis*-aconitate to the cell extract stabilized aconitase activity (1949). By the early 1970s, a new method was developed that utilized ethanol fractionation, carboxymethylcellulose ion-exchange chromatography,

ammonium sulfate precipitation and isoelectric focusing to purify pig heart aconitase (Kennedy *et al.,* 1972).

A watershed moment for aconitase purification schemes came in 1983, when an affinity chromatography approach to aconitase purification was reported (Scholze 1983). Scholze discovered that aconitase binds strongly to Blue Dextran-Sepharose, and the interaction is not ionic in nature. Interestingly, Scholze suggested that the interaction is specific due to the similarity of Cibacron blue dye to nucleotides, and hypothesized that aconitase binds to an NTP cofactor (Scholze 1983). No such factor is known, but the aconitase:Cibacron blue interaction might be analogous to aconitase:RNA interaction. For this purification step, aconitase could not be eluted from the resin with 100 mM NaCl, but elution did occur with low ionic strength solutions of NADP (0.1 mM) or tricarballylic acid (30 mM), resulting in an extremely efficient purification (Scholze 1983). Interestingly, tricarballylic acid is an analog of citrate, one of the substrates of aconitase.

Elements of the Scholze affinity chromatography approach were adapted for the purification of *B. subtilis* aconitase in our laboratory (Dingman *et al.,* 1987). After an ammonium sulfate precipitation, followed by gel filtration using a Bio-Gel column, Dingman applied the extract to a DEAE-Sepharose column and eluted aconitase using a Tris-citrate gradient (Dingman *et al.,* 1987). The use of citrate allowed elution of a highly pure aconitase fraction with a low ionic strength buffer, similarly to the Scholze method. The final step in the purification was a gel filtration step using a Sephadex G-100 column (Dingman *et al.,* 1987).

In the past decade, our laboratory has utilized His-tagged versions of aconitase for purification purposes. Histidine tags provide quick, efficient purification with low levels of contamination. Aconitase was first tagged in our laboratory using a C-terminal hexahistidine tag (B. Belitsky, unpublished data); in later studies, an N-terminal decahistidine tag produced a more efficient aconitase purification, suggesting that the

tag was more accessible to a metal-binding resin at the N-terminus (Serio 2005). Results reported in this thesis, however, call into question the physiological relevance of N-terminally His-tagged aconitase.

8 Aims of this thesis

This thesis reports three principal experimental approaches for understanding the role of aconitase in *B. subtilis* physiology. In the first Results chapter, I explore the mechanism and consequences of citrate accumulation in a *citB* null strain. Through biochemical and genetic approaches, I will demonstrate that citrate accumulation is caused by two factors, the block in aconitase enzyme activity and aconitase-dependent regulation of the expression of citrate synthase, possibly mediated by direct binding to the *citZ* mRNA. In addition, I will describe how citrate accumulation results in *citB* overexpression through CcpC-dependent activation. In the second Results chapter, I will explore the interaction of aconitase with *gerE* in an attempt to determine a binding site for aconitase on the mRNA. In the final Results chapter, I will present data suggesting that the N-terminal His10-tag perturbs aconitase activity *in vivo*. Due to this surprising discovery, I developed a new purification scheme for the preparation of untagged aconitase expressed endogenously in *B. subtilis* without overexpression.

Materials and Methods

1 Bacterial strains and growth conditions

All *Bacillus subtilis* strains used in this work can be found in Table 1. *B. subtilis* was grown at 37°C with aeration unless otherwise noted. *Escherichia coli* strains were grown in L broth or on L agar plates (Miller 1972). *B. subtilis* strains were grown in L, or DSM [0.8% nutrient broth, 0.1% KCL, 0.025% $MgSO_4$ $7H_2O$, 1 mM $Ca(NO_3)_2$, 10 μM $MnCl_2$, 1 μM $FeSO_4$].

2 Molecular cloning, plasmid and strain construction

E. coli strain JM107 was used as a host for plasmid cloning. Oligonucleotides used for cloning can be found in Table 1. Polymerase chain reaction (PCR) products synthesized and used for *in vitro* transcription reactions can be found in Table 2. Plasmids used for cloning can be found in Table 3. *B. subtilis* strains utilized and constructed in this thesis can be found in Tables 4 and 5, respectively.

2.1 Construction of the *citB2* and *citZ340* mutants

The promoter and N-terminal portion of *citB* were amplified and mutagenized by site-directed PCR mutagenesis. Cysteine residue 450, expected to be essential for enzymatic activity, was mutated to serine, and an N-terminal histidine tag was introduced by using genomic DNA from AWS198 as a PCR template. AWS198 had been engineered to have 10 histidine codons near the start of the *citB* open reading frame. Primer citBF6 and mutagenic primer OKP37 were used to amplify the *citB* locus from 400 bp upstream to 1365 bp downstream of the start codon. Mutagenic primer OKP36 and primer OKP38 were used to amplify *citB* from 1333 bp to 1785 bp downstream of the start codon. The products of these two reactions were annealed and amplified using citBF6 and OKP38, yielding a final product of 2203 bp. The final product was purified, digested with restriction enzymes SphI and XmaI, and ligated to the *B. subtilis* integrative vector pJPM1 (Mueller *et al.,* 1992), creating pKP12. After transformation of *E. coli* and verification of the structure of pKP12, this plasmid was used to transform *B. subtilis* strain AWS96.

Table 1. Oligonucleotides used in this study.

Oligo	Nucleotide Sequence	Notes*
citBF6	GGGCATGCGAGAACCTCCTTAAAAGAGTTCGGTGTTATT	5' SphI site
citMF1	GCGTCTAGAACCGTAACTTTGAAGGACGTATTCAC	5' XbaI site
fliTR8	GGACGGTACCTCAGCACACCGCGAATCCATAATG	5' KpnI site
gerEFRT	AAACCCATTCGTTTCTGATTCGC	
gerEIN	GGACTCTAGAGGAGATTGCAAGCGAGCTATTTAT	5' XbaI site
gerER	CTCCTTCCAAAAGAAGGAATACC	
gerER6	GGACGGTACCTTGTCCATCCCTCACTCAAGG	5' KpnI site
M13 (-20)	CTGGCCGTCGTTTTAC	
OKP11	AATAAGAGCTCGATTCATCAGGACTGCTTC	5' SacI site
OKP17	GGTTATTGCTGTTTGTTTGGGTGCAAAACGTAGGC	
OKP18	GCCTACGTTTTGCACCCAAACAAACAGCAATAACC	
OKP19	AATAATCTAGACCTTGCACTATCTCG	5' XbaI site
OKP20	ATCATGAGCTCGTCATTTGTCCATCC	5' SacI site
OKP22	AATTAACCCTCACTAAAGGGGACTTGCCTACGTTTTGCAC	5' pT3 site
OKP36	GCTGCGATTACAAGCTCTACAAATACATCAAACCCATACGTG	
OKP37	GTTTGATGTATTTGTAGAGCTTGTAATCGCAGCAATGGC	
OKP38	ATACCCGGGTTGACCATCCTTGCCCACACC	5' XmaI site
OKP40	TTGTCCATCCCTCACTCAAGG	
OKP49	CCAAACAAACAGCAATAAAGGATTAAAGCTCTAGC	
OKP50	GCTAGAGCTTTAATCCTTTATTGCTGTTTGTTTGG	
OKP55	AAAGCTCTAGCTCACCCATTC	
OKP56	CAAACAGCAATAACCGGCTCC	
OKP59	GACTTGCCTACGTTTTGCAC	
OKP71	ATAGCATGCAGCGGTTGAGTTAGGGCTTAAG	5' SphI site
OKP72	ATACCCGGGATTGATTCATCAGGACTGCTTCATTTTTTCACGAAGC	5' XmaI site
OKP73	GATTTGGTTTTTGATTTCAATGTTGGCAAATGTTCCTCTC	
OKP74	ACATTTGCCAACATTGAAATCAAAAACCAAATCGCACCG	
OKP98	TAATACGACTCACTATA**G**GGGCTTAAACTTAAATAAGCTT	5' pT7
OKP99	CATATATAACATCTCCTTTTC	
rRNA16SF	GGGTGATCGGCCACAC	
rRNA16SR	CCCCAGTTTCCAATGACC	
ysmBR2	GCCGAATTCCGGAATCAATGACTCCTATTGG	

* Restriction sites or T3 and T7 promoters are underlined. T7 promoter start site (+1) is in bold.

Table 2. PCR products for *in vitro* transcription used in this study.

PCR product	Relevant characteristics and/or genotype	Template	Oligos utilized
PCR53	*gerE* 3' UTR sequence	pAWS100	M13 (-20) & OKP40
PCR54	*gerEΔSL1* 3' UTR sequence	pKP17	M13 (-20) & OKP40
PCR55	*gerE* + NO UTR sequence	pAWS100	M13 (-20) & OKP55
PCR56	*gerE* + SL1 sequence	pAWS100	M13 (-20) & OKP56
PCR57	*gerE* + SL1, SL2 sequence	pAWS100	M13 (-20) & OKP59
PCR63	5' T7 promoter, *fliT* 3' UTR sequence	pAWS100	M13 (-20) & fliTR8
PCR103	5' T7 promoter, *citZ* 3' UTR sequence	JH642 DNA	OKP98 & OKP99

Table 3. Plasmids used in this study.

Plasmid	Relevant characteristics and/or genotype	Source/Ref.
pAWS60	*gerE* + 250bp flanking regions in pBluescript SK	Serio *et al.*, 2005
pAWS100	*gerE* 3' UTR in pBluescript KS	Serio *et al.*, 2006
pAWS106	f*liT* 3' UTR in pBluescript KS	Serio *et al.*, 2006
pBluescript KS	*in vitro* transcription vector with T3/T7 promoters	Stratagene
pCR2.1 TOPO	TA cloning vector	Invitrogen
pHK23	*amyE* integrative vector for *B. subtilis*	H. J. Kim (Belitsky *et al.*, 2008)
pJPM1	single-crossover integrative vector for *B. subtilis*	Mueller *et al.*, 1992
pKP6	*gerEΔSL2* in pCR2.1 TOPO	This study
pKP7	*gerEΔSL2* in pHK23	This study
pKP9	*gerE*+ in pCR2.1 TOPO	This study
pKP11	*gerE*+ in pHK23	This study
pKP12	*citB2' (*2.2 kb SphI-XmaI N-terminal fragment with promoter, His_{10} tag and C450S mutation) in pJPM1	This study
pKP15	*gerEΔSL1* in pCR2.1 TOPO	This study
pKP16	*gerEΔSL1* in pHK23	This study
pKP17	*gerEΔSL1* 3' UTR in pBluescript KS	This study
pKP29	*'citB* (1200 bp XbaI-SacI C-terminal fragment) in pJPM1	This study

Table 4. *B. subtilis* strains used in this study.

Strain	Genotype	Source/Reference
JH642	*trpC2 pheA1*	J. Hoch
SMY	prototroph	P. Schaeffer
AF21	Δ*amyE::*Φ(*citBp21-lacZ cat*)	Fouet *et al.*, 1990
LS1003	*trpC2 pheA1 citZ::*Φ(*citZ'-lacZ cat*)	Jin *et al.*, 1994
SJB66	*trpC2 pheA1* Δ*citZ471*	Jin *et al.*, 1994
SJB67	*trpC2 pheA1* Δ*citA::neo* Δ*citZ471*	Jin *et al.*, 1994
SJB231	*trpC2 pheA1* Δ*citZC::spc*	S. Jin (Matsuno *et al.*, 1999)
MAB160	*trpC2 pheA1 Ωcit B::spc*	Craig *et al.*, 1997
CJB8	*ccpC::spc*	Jourlin-Castelli *et al.*, 2000
EUDC9901	*trpC2 pheA1* Δ*gerE::kan*	Crater *et al.*, 2002
HKB125	Δ*amyE::*Φ(*citBp23-lacZ cat*) Δ*codY::erm*	Kim *et al.*, 2003
HKB126	Δ*amyE::*Φ(*citBp24-lacZ cat*) Δ*codY::erm*	Kim *et al.*, 2003
HKB181	*trpC2 pheA1 citZ*-His_6 *erm*	H. J. Kim
HKB186	Δ*amyE::*Φ(*citBp21-lacZ cat*) Δ*ccpC::ble*	Kim *et al.*, 2006
AWS96	*trpC2 pheA1*	Serio *et al.*, 2006
AWS133	*trpC2 pheA1 citB5*-His_6::pAWS42(*cat*)	Serio *et al.*, 2006
AWS144	*trpC2 pheA1 citB*$^+$-His_6::pBB1065(*neo*)	Serio *et al.*, 2006
AWS173	*citA::neo citZ517* Δ*amyE::*Φ(*citBp21-lacZ tet*)	Serio *et al.*, 2005
AWS174	*trpC2 pheA1 Ωcit B::spc* Δ*amyE::*Φ(*citBp21-lacZ tet*)	Serio *et al.*, 2005
AWS175	*trpC2 pheA1 citB5*-His_6::pAWS42(*cat*) Δ*amyE::*Φ (*citBp21-lacZ tet*)	Serio *et al.*, 2005
AWS176	*trpC2 pheA1 citB*$^+$-His6:: pBB1065(*neo*) Δ*amyE::*Φ (*citBp21-lacZ tet*)	Serio *et al.*, 2005
AWS198	*trpC2 pheA1* His_{10}-*citB*$^+$*::*pAWS50(*cat*)	Serio *et al.*, 2006

Table 5. *B. subtilis* strains constructed in this study.

Strain	Genotype	Construction (Recipient x Donor)
KBP9	*trpC2 pheA1* Δ*gerE::kan*	AWS96 x EUDC9901
KBP10	*trpC2 pheA1 citB5*-His_6::pAWS42(*cat*) Δ*gerE::kan*	AWS133 x EUDC9901
KBP11	*trpC2 pheA1* Δ*gerE::kan* Δ*amyE::*(*gerEΔSL2 erm*)	KBP9 x pKP7
KBP15	*trpC2 pheA1* Δ*gerE::kan* Δ*amyE::*(*gerE*$^+$ *erm*)	KBP9 x pKP11
KBP17	*trpC2 pheA1* His_{10}-*citB2::*pKP12(*cat*)	AWS96 x pKP12
KBP18	*trpC2 pheA1* Δ*citA::neo* Δ*citZ471* His_{10}-*citB2::*pKP12(*cat*)	SJB67 x KBP17
KBP22	*trpC2 pheA1 citB2 citZ340*	AWS96 x KBP18
KBP24	*trpC2 pheA1* Δ*gerE::kan* Δ*amyE::*(*gerEΔSL1 erm*)	KBP9 x pKP16
KBP26	*trpC2 pheA1* Δ*amyE::*Φ(*citBp21-lacZ cat*)	AWS96 x AF21
KBP44	*trpC2 pheA1 citZ::*Φ(*citZ'-lacZ cat*)	AWS96 x LS1003
KBP45	*trpC2 pheA1* Ω*citB::spc citZ::*Φ(*citZ'-lacZ cat*)	MAB160 x LS1003
KBP46	*trpC2 pheA1 citB2 citZ340::*Φ(*citZ'-lacZ cat*)	KBP22 x LS1003
KBP48	*trpC2 pheA1 citZ::*Φ(*citZ'-lacZ cat*) Δ*ccpC::ble*	KBP44 x HKB186
KBP49	*trpC2 pheA1* Ω*citB::spc citZ::*Φ(*citZ'-lacZ cat*) Δ*ccpC::ble*	KBP45 x HKB186
KBP50	*trpC2 pheA1 citB2 citZ340::*Φ(*citZ'-lacZ cat*) Δ*ccpC::ble*	KBP46 x HKB186
KBP51	*trpC2 pheA1* Ω*citB::spc* Δ*amyE::*Φ(*citBp21-lacZ cat*)	MAB160 x AF21
KBP52	*trpC2 pheA1* Δ*amyE::*Φ(*citBp21-lacZ cat*) Δ*ccpC::ble*	KBP26 x HKB186
KBP54	*trpC2 pheA1* Ω*citB::spc* Δ*amyE::*Φ(*citBp21-lacZ cat*) Δ*ccpC::ble*	KBP51 x HKB186
KBP55	*trpC2 pheA1* His_{10}-*citB2::*pKP12(*cat*)	AWS96 x KBP18
KBP56	*trpC2 pheA1* Δ*amyE::*Φ(*citBp23-lacZ cat*)	AWS96 x HKB125
KBP57	*trpC2 pheA1* Δ*amyE::*Φ(*citBp24-lacZ cat*)	AWS96 x HKB126
KBP58	*trpc2 pheA1 citB2*-His_6::pBB1065(*neo*) *citZ340*	KBP22 x AWS144
KBP62	*trpC2 pheA1* Ω*citB::spc ΔamyE::Φ(citBp23-lacZ cat)*	MAB160 x KBP56
KBP63	*trpC2 pheA1* Ω*citB::spc ΔamyE::Φ(citBp24-lacZ cat)*	MAB160 x KBP57
KBP72	*trpC2 pheA1 citB7* Δ*amyE::*Φ(*citBp21-lacZ cat)*	AWS96 x PCR78, AF21
KBP81	*trpC2 pheA1 citB7* Δ*amyE::*Φ(*citBp21-lacZ tet)*	KBP72 x AWS173
KBP82	*trpC2 pheA1* His_{10}-*citB7::*pAWS50(*cat*) Δ*amyE::*Φ(*citBp21-lacZ tet)*	KBP81 x AWS198
KBP85	*trpC2 pheA1* Δ*amyE::*Φ(*citBp21-lacZ tet)*	JH642 x AWS173
KBP86	*trpC2 pheA1 citZ340* Δ*amyE::*Φ*(citBp23-lacZ cat)*	SJB231 x pAF23, KBP22

Table 5, continued. *B. subtilis* strains constructed in this study.

Strain	Genotype	Construction (Recipient x Donor)
KBP87	*trpC2 pheA1 citZ340* Δ*amyE::*Φ*(citBp21-lacZ tet)*	KBP86 x AWS173
KBP91	*trpC2 pheA1* His_{10}-*citB*$^{+}$*::*pAWS50(*cat*) Δ*amyE::*Φ(*citBp21-lacZ tet)*	AWS198 x AWS173
KBP92	*trpC2 pheA1* His_{10}-*citB2::*pKP12(*cat*) Δ*amyE::*Φ(*citBp21-lacZ tet)*	KBP55 x AWS173
KBP94	*trpC2 pheA1* Δ*amyE::*Φ(*citBp21-lacZ tet)*	AWS96 x AWS173
KBP96	*trpC2 pheA1 ccpC::spc* Δ*amyE::*Φ(*citBp21-lacZ tet)*	KBP85 x CJB8
KBP104	*trpC2 pheA1 ΩcitB::spc ccpC::ble* Δ*amyE::*Φ(*citBp21-lacZ tet*)	AWS174 x HKB186
KBP105	*trpC2 pheA1 citB5*-His_6::pAWS42(*cat*) *ccpC::ble* Δ*amyE::*Φ (*citBp21-lacZ tet*)	AWS175 x HKB186
KBP106	*trpC2 pheA1 citB*$^{+}$-His_6::pBB1065(*neo*) *ccpC::ble* Δ*amyE::*Φ (*citBp21-lacZ tet*)	AWS176 x HKB186
KBP118	*trpC2 pheA1 citB2* Δ*amyE::*Φ(*citBp21-lacZ tet)*	AWS96 x KBP94, KBP22
KBP125	*trpC2 pheA1 citB*$^{+}$*::*pKP29(*cat*)	AWS96 x pKP29
KBP126	*trpC2 pheA1 citB2::*pKP29(*cat*) *citZ340*	KBP22 x KBP125
KBP127	*trpC2 pheA1 citB*$^{+}$*::*pKP29(*cat*) Δ*amyE::*Φ(*citBp21-lacZ tet)*	KBP94 x KBP125
KBP128	*trpC2 pheA1 citB2::*pKP29(*cat*) Δ*amyE::*Φ(*citBp21-lacZ tet)*	KBP94 x KBP126
KBP129	*trpC2 pheA1 citB7::*pKP29(*cat*) Δ*amyE::*Φ(*citBp21-lacZ tet)*	KBP81 x KBP125
KBP135	*trpC2 pheA1 citB*$^{+}$*::*pKP29(*cat*) Δ*amyE::*Φ(*citBp21-lacZ tet)*	KBP85 x KBP127
KBP136	*trpC2 pheA1 citB2::*pKP29(*cat*) Δ*amyE::*Φ(*citBp21-lacZ tet)*	KBP85 x KBP128
KBP137	*trpC2 pheA1 citB7::*pKP29(*cat*) Δ*amyE::*Φ(*citBp21-lacZ tet)*	KBP85 x KBP129
KBP138	*trpC2 pheA1 citB*$^{+}$*::*pKP29(*cat*) *ccpC::spc* Δ*amyE::*Φ(*citBp21-lacZ tet)*	KBP96 x KBP127
KBP139	*trpC2 pheA1 citB2::*pKP29(*cat*) *ccpC::spc* Δ*amyE::*Φ(*citBp21-lacZ tet)*	KBP96 x KBP128
KBP140	*trpC2 pheA1 citB7::*pKP29(*cat*) *ccpC::spc* Δ*amyE::*Φ(*citBp21-lacZ tet)*	KBP96 x KBP129

Chloramphenicol resistance was used to select for integration of pKP12 at the *citB* locus by homologous recombination, creating strain KBP17 (His_{10}-*citB2 cat*). Genomic DNA from KBP17 was used to transform SJB67 (*citA::neo citZ471*), resulting in the strain KBP18 (His_{10}-*citB2 cat citA::neo citZ471*). Genomic DNA from KBP18 was later used to transform strain AWS96 to obtain the tagged *citB2* allele in a clean backround, resulting in strain KBP55 (His_{10}-*citB2 cat*).

The serial passage of strain KBP17 to obtain a derivative in which a second crossover had occurred resulted in the isolation of KBP22, a strain that had also acquired a suppressor mutation (*citZ340*). In a separate construction, KBP22 was transformed with genomic DNA from AWS144 (*citB*-His_6 *neo*), producing strain KBP58 (*citB2*-His_6 *neo citZ340*). Ultimately, the *citB2* mutation was separated from *citZ340* as follows: genomic DNA from KBP22 and KBP94 (*amyE::citBp21-lacZ tet*) was introduced simultaneously into the wild-type strain AWS96. Tetracycline-resistant transformants were isolated on DS medium containing X-Gal and blue colonies were selected, indicative of derepressed expression of the *citB-lacZ* fusion. The resulting strain was KBP118 (*citB2 amyE::citBp21-lacZ tet*).

To isolate the *citZ340* mutation, genomic DNA from KBP22 along with pAF23 plasmid DNA (*amyE::citBp23-lacZ cat*) was introduced into SJB231 (*citZC::spc*). Chloramphenicol-resistant transformants were isolated on DS medium and colonies were screened for spectinomycin sensitivity and glutamate auxotrophy. The resulting strain was KBP86 (*citZ340 amyE::citBp23-lacZ cat*). Genomic DNA from AWS173 was introduced into KBP86 to replace the *amyE* cassette; the resulting strain was KBP87 (*citZ340 amyE::citBp21-lacZ tet*).

2.2 Construction of the *citB7* mutant

A single amino-acid substitution expected to reduce RNA binding was introduced into the *citB* gene by transformation with a PCR product. The substitution, arginine-741 to glutamate, was engineered by site-directed mutagenesis. Primers OKP71 and

mutagenic primer OKP73 were used to amplify the *citB* locus from positions 1404 bp to 2238 bp downstream of the start codon. Mutagenic primer OKP74 and primer OKP72 were used to amplify the *citB* locus from 2206 bp downstream of the start codon to the stop codon. The products of each of these reactions were annealed and amplified with OKP71 and OKP72, yielding a final product of 1341 bp (including restriction site overhangs on the outside primers). The final product was purified and introduced into *B. subtilis* strain AWS96 by transformation along with genomic DNA from strain AF21 (*amyE::citBp21-lacZ cat*). Chloramphenicol-resistant transformants were selected on DS medium containing X-Gal, and blue colonies were purified. The *citB* locus in several transformants was amplified by PCR and sequenced to confirm the presence of the *citB* R741E mutation. The resulting strain, KBP72 (*citB7 amyE::citBp21-lacZ cat*), also had an unplanned silent mutation near the 3' end of the gene. Genomic DNA from AWS173 was introduced into KBP72 by transformation to replace the *amyE* cassette, and tetracycline-resistant clones were selected, resulting in strain KBP81 (*citB7 amyE::citBp21-lacZ tet*).

2.3 Construction of a *citB* integrative vector and derivative strains

To create a marked but untagged *citB* construct for genetic manipulations in *B. subtilis*, primers citMF1 and OKP11 were used to amplify the C-terminal 1.2 kb of the *citB* gene. The resulting PCR product was digested with XbaI and SacI and ligated to pJPM1 digested with the same enzymes, producing plasmid pKP29. This plasmid was introduced into *E. coli* by transformation and the sequence was verfied before introduction into *B. subtilis* strain AWS96 by single-crossover at the *citB* locus, producing KBP125 [*citB*$^{+}$*::*pKP29(*cat*)]. Genomic DNA from KBP125 was introduced into strain KBP94, producing strain KBP127 [*citB*$^{+}$*::*pKP29(*cat*) *amyE::citBp21-lacZ tet*). To create a marked version of the *citB2* allele, genomic DNA from KBP125 was introduced into strain KBP22, producing strain KBP126 [*citB2::*pKP29(*cat*) *citZ340*]. Genomic DNA from KBP126 was then used to transform KBP94 to chloramphenicol

resistance and transformants were selected that retained hyperexpression of the *citB-lacZ* reporter on DS medium containing X-gal were selected. The resulting strain was KBP128 [*citB2::*pKP29(*cat*) *amyE::citBp21-lacZ tet*]. To create a marked version of the *citB7* allele, genomic DNA from KBP125 was introduced into strain KBP81, producing strain KBP129 [*citB7::*pKP29(*cat*) *amyE::citBp21-lacZ tet*]. To create isogenic strains for the analysis of the effect of the *ccpC* mutation on the *citB2* and *citB7* phenotypes, genomic DNA from strains KBP127, KBP128 and KBP129 was introduced into strains KBP85 (*amyE::citBp21-lacZ tet*) and KBP96 (*ccpC amyE::citBp21-lacZ tet*), producing strains KBP135, KBP136, KBP137, KBP138, KBP139 and KBP140 (see Table 5 for genotypes).

2.4 Construction of *gerE*+, *gerEΔSL1* and *gerEΔSL2* plasmids

Three plasmids were created for the introduction of *gerE* constructs at the nonessential *amyE* locus. For each construct, a 750 bp region extending from 250 bp upstream to 250 bp downstream of the *gerE* open reading frame was amplified by overlapping PCR site-directed mutagenesis. For the *gerEΔSL1* construct, a 31 bp region just after the stop codon, referred to as SL1, was deleted. Primers OKP19 and OKP49 were used to amplify the 500 bp upstream region including the *gerE* ORF up to the SL1 sequence. Primers OKP50 and OKP20 were used to amplify the 220 bp downstream of SL1 to the start of the downstream gene, *ysmB*. For the *gerEΔSL2* construct, similar primer sets were employed to delete a 27 bp downstream of SL1, termed SL2. Primers OKP19 and OKP18 were used to amplify the ~550 bp upstream region, while primers OKP17 and OKP20 were used to amplify the 200 bp downstream region. For both *gerEΔSL1* and *gerEΔSL2* constructs, the resulting upstream and downstream PCR products were annealed separately and then full constructs were amplified using OKP19 and OK20. In addition, the wildtype region (750 bp) was amplified using OKP19 and OKP20 to produce the *gerE*+ complementing construct. The PCR constructs were each ligated to the pCR2.1 TOPO cloning vector (Invitrogen), excised with restriction enzymes

XbaI and HindIII, and ligated to pHK23 (Belitsky *et al.,* 2008) digested by the same enzymes. The resulting vectors, pKP11, pKP16, pKP7 (*gerE*$^{+}$, *gerEΔSL1*, and *gerEΔSL2*, respectively) were isolated after introduction to *E. coli* by transformation. After validating their sequences, the plasmids were introduced into *B. subtilis* strain KBP9 (*gerE::kan*) by double crossover at the *amyE* locus, creating KBP15 (*gerE::kan amyE::gerE*$^{+}$ *erm)*, KBP24 (*gerE::kan amyE::gerEΔSL1 erm*), and KPB11 (*gerE::kan amyE::gerEΔSL2 erm*).

To create a *gerEΔSL1* template for *in vitro* transcription, primers gerEIN and gerER6 were used to amplify a 340 bp fragment of pKP15 including the 3' 134 bp of the *gerE* ORF and the entire 205 bp 3' UTR. The fragment is analogous to the *gerE+* version contained in pAWS100, which includes the wild-type 246 bp 3' UTR. The PCR product was digested with restriction enzymes XbaI and KpnI and ligated to pBluescript KS digested with the same enzymes. The resulting plasmid, pKP17, was introduced to *E. coli* by transformation and the sequence was confirmed.

3 Sporulation and germination assays

I measured the efficiency of spore formation within a *B. subtilis* liquid culture by assaying for two characteristics of mature spores: heat-resistance and sodium hypochlorite (bleach) resistance.

3.1 Heat-resistant spore formation

B. subtilis strains were grown in DS medium and sampled to determine heat-resistant spore formation. Two 0.5 - 1 ml samples were removed from a culture; one was incubated at 80°C for 15 minutes, the other was incubated at room temperature. Both samples were then serially diluted and plated to obtain heat-resistant (spore) and total viable counts.

3.2 NaClO-resistant spore formation

B. subtilis strains were grown in DS medium and analyzed to determine sodium hypochlorite (NaClO)-resistant spore formation as described previously (Ghosh *et al.,*

2008). All steps after sample removal took place at ambient room temperature. Samples were removed, pelleted by centrifugation and resuspended in 50 mM potassium phosphate buffer (pH 7) with or without NaClO (at 10^{-2}, 10^{-3}, and 10^{-4} dilutions from a 5.25% commercial stock). After a 15 minute incubation, the NaClO was quenched by diluting 1:10 in sodium thiosulfate (1%) and incubating for 10 minutes. Samples were then serially diluted and plated to obtain NaClO-resistant (spore) and total viable counts.

3.3 Germination assays

B. subtilis spores were prepared from DS medium cultures grown for ~72 hours at 37°C with aeration. Cultures were harvested by centrifugation at 4°C. The resulting pellet was washed four times in cold dH_2O and stored at 4°C. To perform the assay, samples of spores were heat-activated at 70°C for 15 minutes and subsequently diluted to A_{600} ~0.7 in 10 mM Tris (pH 8.4) with or without 10 mM L-alanine, a *B. subtilis* germinant. Immediately after dilution, an initial absorbance reading was obtained. The spore suspensions were incubated at room temperature and the absorbance was measured at 20-30 minute intervals. Absorbance readings were expressed as a ratio of the initial absorbance value to allow comparison across strains.

4 Enzyme assays

4.1 Aconitase and citrate synthase activity assays

Aconitase (Acn) and citrate synthase (CS) enzyme activities were determined with purified proteins and in crude cell extracts. The preparation of cell extracts and the assays themselves are described below.

4.1.1 Preparation of cell extracts

For Acn and CS enzyme assays, strains were grown in DS medium unless otherwise indicated and cells were collected by centrifugation. Cell pellets were washed in a Tris-EDTA-glycerol buffer (20 mM Tris, pH 8; 1 mM EDTA; 20% glycerol) and stored at -20°C; our lab has shown previously that 20% glycerol is necessary for the stabilization of citrate synthase activity (Jin *et al.,* 1996). Cell pellets were thawed on ice

and resuspended in the same buffer supplemented with phenylmethylsulfonyl fluoride (0.1 mM PMSF). Cells were incubated with 0.4 mg/ml lysozyme for 30 minutes at 37°C. If necessary, the resulting lysate was gently sonicated on ice to break up genomic DNA using a Branson Sonifier (30% duty, level 2, 30 second intervals with 20 second rests, 3-4 times). Sonication was avoided, if possible, due to negative effects on aconitase enzyme activity; importantly, within a single experiment samples were treated identically. Cell extracts were clarified by centrifugation in a microfuge at maximum speed (~13,000 rpm) for 10 - 15 minutes at 4°C. Clarified extracts were kept on ice and assayed immediately for Acn and CS activity. Protein concentrations (c) of the samples were determined by the Bradford assay using the Bio-Rad reagent.

4.1.2 Aconitase activity assay

The aconitase enzyme activity was determined by established methods (Dingman *et al.,* 1987, Kennedy *et al.,* 1983). Briefly, the reaction buffer (20 mM $_{D,L}$-isocitrate, 90 mM Tris, pH 8.0) was prepared and used to blank a spectrophotometer at 240 nm. At room temperature, a 2 - 25µl sample (v_{sample}) of cell extract or purified protein was added to reaction buffer (total volume = 1 ml). The absorbance at 240 nm was measured immediately (A_i) and after a 10 minute incubation (A_f) to directly measure the formation of *cis*-aconitate (a change in A240 of 0.0033 is equivalent to 1 nmol *cis*-aconitate per ml). The following equation was then used to calculate the specific activity of aconitase:

$$\frac{(A_f - A_i)}{(t)(0.0033)(c)(v_{sample})}$$

Units of aconitase were expressed as nanomoles of *cis*-aconitate produced per minute per milligram of protein (U/mg).

4.1.3 Citrate synthase activity assay

The citrate synthase activity assay was performed using the method developed by Srere *et al* (1963). In brief, 10 µl of cell extract or purified protein was mixed with 0.1

mM 5,5'-dithiobis(2-nitrobenzoic acid) (DTNB), 0.3 mM acetyl coA in Tris-EDTA-glycerol buffer (see above). Samples were incubated for ~3 minutes and then the absorbance at 412 nm was measured to obtain a background reading (A_i). The final reagent, 1 mM oxaloacetate, was then added to each sample. Samples were incubated for 10 minutes (t) and the absorbance was measured again at 412 nm (A_f). The following equation was used to calculate the specific activity of citrate synthase:

$$\frac{(V_{total})\ (A_f - A_i)}{(t)(d)(e)(c)(v_{sample})}$$

The path length (d) was a function of the spectrophotometer: 1 cm for standard cuvette-type apparatus and a calculated value for 96-well plate readers based on the total volume of the sample. The total volume of the reaction was 1.0 ml for cuvette assays and 0.3 ml for 96-well plate assays. The corrected value for the TNB^{2-} ion extinction coefficient (e = 14.15 ml cm^{-1} μmol^{-1}) was utilized (Riddles *et al.,* 1983). Protein concentration (c) was determined using the Bradford reagent (Bio-Rad). Units of citrate synthase were expressed as micromoles of CoA produced per minute per milligram of protein (μmol/ min/mg).

4.1.4 Citrate synthase activity in the presence of exogenous Acn

Purified CitZ protein (40 nM) was combined with increasing concentrations of Acn in buffer (20 mM Tris, pH 8; 50 mM KCl; 10% glycerol; 1 mM EDTA). Reactions (25 μl) were incubated for 15 minutes at room temperature and then assayed for citrate synthase specific activity as described above. Control reactions without CitZ or Acn were included.

4.2 Determination of intracellular and extracellular citrate

To determine the intracellular and extracellular citrate concentrations, cells were grown in DS medium and harvested by centrifugation. The culture fluid was kept on ice. The cell pellet was washed in buffer (20 mM Tris, 1 mM EDTA), resuspended in 0.3 M

perchloric acid and incubated on ice for 10 minutes. The cells were removed by centrifugation and the supernatant was incubated with potassium carbonate (0.25 M K_2CO_3) for 15 minutes on ice. Any precipitate was removed by centrifugation. The resulting supernatant (intracellular) was analyzed along with aliquots of the culture fluid (extracellular) using a citric acid kit (R-Biopharm) according to the manufacturer's instructions. The kit measures citrate indirectly through a series of enzymatic reactions. First, citrate lyase is used to convert citrate in the sample to oxaloacetate and acetate. Next, oxaloacetate, and any pyruvate resulting from oxaloacetate decarboxylation, are converted to L-malate and L-lactate by malate dehydrogenase and lactate dehydrogenase, respectively. The consumption of NADH in these last two reactions can be followed spectrophotometrically at 340 nm, and is directly proportional to the amount of citrate in the initial sample.

4.3 β-galactosidase activity assays

For β-galactosidase activity assays, samples (1 ml) were removed from *B. subtilis* broth cultures during growth after determining the optical density (A_{600}) of the culture at that time point, and cell pellets were frozen on dry ice. Cells were treated as described previously to determine β-galactosidase activity (4). Briefly, cells were resuspended in phosphate buffer (0.1 M) containing 10 mM KCl and 1 mM $MgSO_4$, permeabilized with toluene and vigorous vortexing, and incubated at 37°C to allow the toluene to evaporate. Samples were then mixed with the substrate (ONPG) and incubated at 28°C until yellow color developed. Stop solution (sodium carbonate) was added and the sample was incubated on ice for at least 30 minutes. Samples were clarified by centrifugation at 4°C before A_{420} values were determined. β-galactosidase activity (Miller Units) was calculated from the following equation:

$$\frac{(A_{240})\ (1000)}{(A_{600})(t)(1.25)(v_{sample})}$$

where *t* is the time (min) at which the reaction was stopped, *v* is the volume of cell culture added to the reaction, and 1.25 is a correction fator for dilution of the samples due to addition of Na_2CO_3.

5 Western blot analysis of cell extracts

Preparation of samples for Western blot analysis of aconitase, citrate synthase, and isocitrate dehydrogenase levels is described above (4.1.1). Equivalent amounts of protein (~0.5 μg) were subjected to SDS-polyacrylamide gel electrophoresis (PAGE) on 10% polyacrylamide gels before transfer to an Immobilon polyvinylidene difluoride (PVDF) membrane (Millipore). Milk (5%) was used as a blocking agent and washes were performed in Tris-buffered saline (pH 8). Polyclonal antibodies raised in rabbits to *B. subtilis* aconitase (Serio 2005), citrate synthase (Jin *et al.,* 1996), isocitrate dehydrogenase (Matsuno and Sonenshein, unpublished), and CodY (Ratnayake-Lecamwasam *et al.,* 2001) were used.

For the preparation of samples for Western blot analysis of GerE, cells were grown in DS medium, harvested by centrifugation, and washed with ice-cold 10 mM Tris-HCl, pH 7.5 (supplemented with 1X complete protease inhibitors; Roche). For all experiments, sample volumes taken were normalized to be equal to 5 ml cells at $A_{600} = 1$.

For anti-GerE Westerns in *citB5* and *gerE-SL2* strains: cell pellets were resuspended in equal volumes (100 μl) of the same buffer, frozen on dry ice, and stored at -80°C. Frozen cell pellets were thawed and aliquots (10 μl) were mixed with an equal volume of buffer containing lysozyme (4 mg/ml) and 50 mM glucose. After 15 minutes, the extracts were mixed with an equal volume of SDS-PAGE sample buffer containing β-mercaptoethanol (5%), boiled for 5 minutes, and clarified by centrifugation. Equivalent volumes of samples were analyzed by SDS-PAGE and subsequent immunoblot.

For experiments involving GerE detection in the *gerE-SL1* strain, cells were washed in the buffer described above prior to freezing and storage at -80°C. Pellets were resuspended in 250μl of the same buffer and sonicated (90% duty, level 5, 20 second

intervals with 30 second rests, four times) on ice using a Branson sonifier to generate crude cell extracts. Extracts were clarified by centrifugation prior to determination of protein concentration using the Bradford reagent (Bio-Rad). Equivalent amounts of protein (5 μg) were analyzed by SDS-PAGE.

For all anti-GerE Western blot experiments, 15% polyacrylamide gels were used for protein separation prior to a short transfer (30 minutes) to a PVDF membrane due to the small molecular weight of the GerE protein (8 kilodaltons). Bovine serum albumin (5%) was used as a blocking agent and membranes were probed with polyclonal antibodies raised to GerE (Kuwana *et al.,* 2004). Washes were performed using Tris-buffered saline (pH 8) supplemented with 1% Tween-20.

For all blots, anti-rabbit IgG secondary antibodies conjugated to alkaline phosphatase (Bio-Rad) or horseradish peroxidase (Upstate Biotechnology, Inc.) were used, and blots were developed using either the alkaline phosphatase detection kit (Bio-Rad) or the ECL Plus western blotting kit (GE Healthcare), respectively. Quantification of blots was performed using ImagQuant TL software (GE Healthcare).

6 Purification methods

6.1 Purification of wild-type, C450S, and R741E Acn proteins

Wild-type, C450S, and R741E aconitase proteins were purified from *B. subtilis* with some modifications to previous methods described by Dingman *et al* (1987). For each strain (KBP94, KBP22, KBP81), two independent DS medium cultures were prepared and harvested at the end of exponential growth phase (OD_{600} ~ 0.8-1.0; when *citB* is the most highly expressed). While the volume of the cultures ranged from 500 ml - 2L, in each case a volume of cell extract equivalent to a 500 ml culture was used as the input for a single preparation. For all cultures, cells were harvested by centrifugation at 4°C (5,000 rpm; JA-10 rotor). Pellets were washed twice with ice-cold 20 mM Tris-citrate, pH 7.35 (20 mM Tris, 20 mM citrate, pH 7.35 adjusted with NaOH), and stored at -80°C.

Pellets were thawed and resuspended in ice-cold buffer (20 mM Tris-citrate, pH 7.35, 1 mM PMSF) before subjection to two passages through a French pressure cell (15,000 lb/in^2). The resulting lysate was sonicated (50% duty, level 5, 30 second intervals with 20 second rests, 3 times) on ice to fragment genomic DNA. The sonicated lysate was clarified by centrifugation at 4°C (13,000 rpm; JA-20 rotor).

After clarification, the soluble lysate fraction was precipitated with ammonium sulfate at 4°C in a two-step process. First, ammonium sulfate was added to 40% saturation and the sample centrifuged at 4°C (13,000 rpm; JA-20 rotor). The supernatant was then adjusted with ammonium sulfate to give 85% saturation and subjected to centrifugation as before. The pellet was resuspended in 20 mM Tris-citrate, concentrated if necessary using a spin column (Millipore), and subjected to gel filtration chromatography on a Superose 12 column equilibrated with 20 mM Tris-citrate (GE Healthcare). Fractions containing aconitase were identified by aconitase activity assay or by SDS-PAGE/Coomassie blue analysis.

The Superose 12 fractions were pooled (but not concentrated) and subjected to anion exchange chromatography using a MonoQ column (GE Healthcare) equilibrated by sequential washing with 20 mM and 100 mM Tris-citrate (pH 7.35). Protein was eluted with a linear gradient of 10 - 50 mM Tris-citrate (pH 7.35); aconitase eluted very early in the gradient. Fractions containing aconitase were identified by the aconitase enzyme activity assay (or SDS-PAGE analysis for the *citB2* mutant), pooled, and concentrated via a spin column (Millipore).

The MonoQ column concentrate was loaded onto a Superdex 200 gel filtration column (BioRad) equilibrated with 2X Storage Buffer (20 mM Tris, 70 mM KCl). Protein was eluted with 2X Storage Buffer; eluted fractions containing aconitase were identified by SDS-PAGE analysis with Coomassie blue. Fractions containing aconitase were pooled prior to concentration via a spin column (Millipore). Pure aconitase was diluted two-fold with 100% glycerol (10 mM Tris, 35 mM KCl, 50% glycerol) and was stored at -20°C.

6.2 Affinity purification of wild-type and *citB2* aconitase

Wild-type and *citB2* aconitase with N-terminal decahistidine (His_{10}) tags were purified from *B. subtilis* using previously described methods (Serio *et al.,* 2006a). Briefly, two 2L DS medium cultures were prepared for each strain (AWS198, KBP55) and harvested at the point of exit from exponential growth phase (OD_{600} ~ 0.8-1.0). Cells were harvested by centrifugation at 4°C (5,000 rpm; JA-10 rotor). Pellets were washed twice with 10 ml ice-cold 20 mM Tris-citrate (pH 7.35) and stored at -80°C.

Pellets were thawed and resuspended in cold resuspension buffer (200 mM KCl; 50mM Tris, pH 7.5; 10% glycerol; 0.5 mM dithiothreitol; 0.2 mM EDTA; 0.2 mM PMSF; 0.01% Nonidet P-40) before being subjected to 2-3 passages through a French pressure cell (15,000 lb/in^2). The resulting lysate was sonicated (50% duty, level 5, 30 second intervals with 20 second rests, 3 times) on ice. The sonicated lysate was clarified by centrifugation at 4°C (13,000 rpm; JA-20 rotor). The clarified lysate was dialyzed against the same buffer without dithiothreitol or EDTA overnight at 4°C.

The dialyzed lysate was incubated with Talon metal affinity resin (Clontech) preequilibrated in a binding buffer (200 mM KCl; 50 mM Tris, pH 7.5; 10% glycerol; 1 mM PMSF, 0.01% NP-40; 7 mM β-mercaptoethanol) by tumbling at 4°C. The resin was washed three times in the same buffer with 10 mM imidazole. Aconitase was eluted from the resin in the same buffer with 125 mM KCl and 300 mM imidazole. The eluted aconitase was dialyzed against a storage buffer (50 mM KCl, 20mM Tris (pH 7.5), 50% glycerol) overnight before storage at -20°C.

6.3 Affinity purification of citrate synthase

Wild-type citrate synthase II (CitZ) with a C-terminal hexahistidine (His_6) tag was purified from *B. subtilis* using previously described methods (H. J. Kim, unpublished). Briefly, two 2L DS medium cultures were prepared from strain HKB181 (*citZ*-His_6 *erm*) and harvested in late exponential growth (OD_{600} ~ 0.7). Cells were harvested by centrifugation at 4°C (5,000 rpm; JA-10 rotor). Pellets were washed twice

with 10 ml ice-cold Buffer 1 (100 mM KCl; 20 mM Tris, pH 8; 20% glycerol; 1 mM EDTA; 2 mM PMSF) and stored at -80°C.

Pellets were thawed and resuspended in cold Buffer 1 before being subjected to 2-3 passages through a French pressure cell (15,000 lb/in^2). The resulting lysate was sonicated (50% duty, level 5, 30 second intervals with 20 second rests, 3 times) on ice. The sonicated lysate was clarified by centrifugation at 4°C (13,000 rpm; JA-20 rotor). The clarified lysate was dialyzed against the same buffer for 1-2 hours at 4°C.

The dialyzed lysate was incubated with Talon metal affinity resin (Clontech) preequilibrated in a binding buffer (50 mM KCl; 20mM Tris, pH 8; 10% glycerol; 1 mM PMSF, 0.05% Nonidet P-40) by tumbling at 4°C. The resin was washed three times in the same buffer with 10 mM imidazole. Citrate synthase was eluted from the resin in the same buffer with 250 mM imidazole. The eluted citrate synthase was dialyzed against a storage buffer (50mM KCl; 20mM Tris, pH 7.5; 50% glycerol; 1 mM EDTA; 1 mM DTT) overnight before storage at -20°C.

7 Binding reactions with Aconitase and RNA

7.1 *In vitro* transcription templates

PCR products were generated for use as templates for *in vitro* run-off transcription. For the *gerE* 3' UTR region, the M13 (-20) Forward primer and primer OKP40 were used to amplify a ~460 bp fragment of plasmid pAWS100 (Serio *et al.,* 2006a). The same primers were used to amplify a ~430 bp fragment of pKP17 to produce a *gerEΔSL1* 3' UTR construct. A series of truncated *gerE* 3' UTR transcripts were created using the M13 (- 20) Forward primer in conjunction with primers OKP55, OKP56, and OKP59, producing constructs *gerE* + no UTR (217 bp), *gerE* + SL1 (267 bp), and *gerE* + SL1/SL2 (319 bp), respectively.

Products were also amplified for *citZ* and *fliT* RNA templates. For the *citZ* leader region, primers OKP98 and OKP99 were utilized to amplify a ~200 bp region of the *B. subtilis* chromosome extending from the *citZ* transcriptional start site (+1) to the start

codon of *citZ*. For the *fliT* 3' UTR, the M13 (-20) Forward primer and fliTR8 were used to amplify a portion of plasmid pAWS106 (4) containing the T7 promoter and *fliT* 3' UTR.

7.2 *in vitro* transcription reactions

Transcription reactions were performed using T3 or T7 RNA polymerase (Stratagene) in the presence of [α-^{32}P] UTP (Perkin-Elmer) to produce internally labeled RNA. Radioactive RNA transcripts were purified by phenol-chloroform extraction, precipitated with isopropanol and sodium acetate to remove unincorporated nucleotides, and resuspended in DEPC-treated deionized water supplemented with RNaseOut (Invitrogen) prior to storage at -20°C in small aliquots to avoid freeze-thaw damage.

7.3 Filter binding assays

For filter binding assays, labeled RNA was briefly heated to 80°C and then allowed to cool slowly to ambient room temperature. Cooled RNA was supplemented with RNAseOut and added to reactions containing different concentrations of aconitase and buffer (10 mM Tris pH 7.5, 35 mM KCl, 20% glycerol, 0.5 mM dipyridyl, 5 mM β-mercaptoethanol). Reactions were allowed to equilibrate for 30 minutes at room temperature before filtration through nitrocellulose discs (0.45 μm HAWP, Millipore; pre-soaked in reaction buffer) using a multi-sample filtration apparatus and the in-house vacuum line. Filters were washed twice with 0.5 ml reaction buffer, removed, and placed in scintillation fluid. A mock reaction was added directly to scintillation fluid to obtain a measure of the total radioactivity of the RNA.

7.4 Gel shift assays

For electrophoretic mobility shift assays, labeled RNA was briefly heated to 80°C and then allowed to cool slowly to ambient room temperature. Cooled RNA was supplemented with RNAseOut and added to reactions containing different concentrations of aconitase and buffer (10 mM Tris pH 7.5, 35 mM KCl, 10% glycerol, 5 mM β-mercaptoethanol). Reactions were allowed to equilibrate for 15 - 30 minutes prior to running on native 8% polyacrylamide gels in Tris-borate-EDTA. Gels were dried,

exposed to a phosphorimaging screen, and analyzed using a phosphorimager (Applied Biosystems).

8 Methods to approximate the *gerE* 3' terminus

8.1 RNA preparation from wild-type *B. subtilis*

Strain JH642 (wild-type) was grown in DS medium and cells were harvested by centrifugation at 4 and 5 hours after the initiation of sporulation, i.e., 4-5 hours after T_0, the time of entry into stationary phase. Cells were washed in buffer (50 mM Tris, pH 8; 1 mM EDTA) and pellets were frozen on dry ice before storage at -80.

For each sample, the cell pellet was resuspended in 400 µl of the same buffer containing 25% sucrose and lysozyme (0.4 mg/ml) and incubated at 37°C for 10 minutes. One-ml Trizol reagent (Invitrogen) was added to the sample and mixed prior to incubation at ambient room temperature for 5 minutes. Chloroform (200 µl) was then added and the solution was mixed well by shaking. After a 15 minute incubation on ice, the sample was centrifuged for 15 minutes at 4°C. The aqueous phase was transfered to a new tube and an equal volume of isopropanol was added. The sample was gently mixed and incubated at -80°C for 45 minutes. After thawing on ice, the sample was centrifuged for 20 minutes at 4°C to pellet total RNA. The supernatant was removed and the pellet gently washed with 75% ethanol. To remove all traces of ethanol, the sample was dried using a SpeedVac with no heat. The pellet was resuspended in diethylpyrocarbonate (DEPC)-treated deionized water containing RNAseOut (Invitrogen). RNA was quantified by spectroscopy and treated with Turbo DNase (Ambion) to remove contaminating genomic DNA according to the manufacturer's specifications. Successful removal of contaminating DNA was confirmed by PCR using primers (rRNA16SF and rRNA16SR) that amplify the 16s rRNA locus.

8.2 RNAse protection of *gerE*

A template for the *gerE* 3' antisense UTR was generated by digesting pAWS60 with XcmI. For molecular weight markers, the same plasmid was digested with BseRI,

NdeI, and EcoNI. The products were gel purified and *in vitro* run-off transcription was performed using T7 RNA polymerase (for the XcmI digest) or T3 RNA polymerase (for all others) (both from Ambion) in the presence of [α-^{32}P] UTP using the methods described above.

For RNAse protection reactions, 2.5 x 10^5 cpm of radiolabelled *gerE* 3' UTR antisense transcript was coprecipitated with 20 μg total cellular RNA (prepared as described above). The precipitate was resuspended in 20 μl hybridization buffer (40 mM PIPES, pH 6.4; 400 mM NaCl; 1 mM EDTA, pH 8.0; 80% formamide) and placed in a 70°C water bath. The temperature was immediately reset to 45°C and the reactions were allowed to slow-cool overnight. The tubes were removed from the water bath and 300 μl of RNAse digestion buffer (50 mM NaOAc, pH 5.2; 100 mM NaCl; 2 mM EDTA, pH 8.0) was added along with 12 units of RNAse T2 (Gibco BRL) prior to incubation at 30°C for 1 hour. The reactions were removed and incubated at 37°C for 15 minutes with 20 μl 10% SDS and 50 μg proteinase K. Samples were extracted with phenol:chloroform and precipitated with isopropanol and sodium acetate. The precipitate was resuspended in RNA loading buffer (90% formamide, 0.2% bromophenol blue, 0.2% xylene cyanol) and heated to 80°C for 3 minutes before analysis on a denaturing polyacrylamide gel.

8.3 RT-PCR on the *gerE* locus

Multiplex first-strand cDNA synthesis reactions were performed with Superscript RT II (Invitrogen) according to the manufacturer's instructions using the DNA-free RNA samples described above and primers gerER, OKP22, OKP20, ysmBR2, and rRNA16SR. cDNA was stored at -20°C. Separate PCR reactions to detect the *gerE* transcript were performed using forward primer gerEFRT and reverse primers gerER, OKP22, OKP20, and ysmBR2. In addition, reactions with rRNA16SF and rRNA16SR were performed to detect the 16S rRNA transcript. PCR products were detected by agarose gel electrophoresis.

Results

Chapter 1: Role of aconitase in the regulation of the Krebs cycle

The Introduction discussed how the expression of the TCA branch of the Krebs cycle in *B. subtilis* is controlled directly or indirectly by five major regulatory proteins: AbrB, CodY, CcpA, CcpC, and TnrA. In this section of my thesis, I explore the role of aconitase itself in the regulation of TCA branch gene expression. I will present a model in which aconitase indirectly regulates both *citB* and *citZ* through CcpC and directly regulates the *citZ* transcript through a protein-RNA interaction.

1 Role of aconitase in the regulation of *citB* expression

As discussed in the Introduction, our laboratory has focused for some time on elucidating the complicated regulatory circuit created by the interactions of CcpC with the *citZ* and *citB* promoters. For many years, we considered the CcpC-*citB* interaction to follow a simple repression model: we hypothesized that CcpC bound to the *citB* promoter in low citrate conditions, and that citrate antagonized the interaction of CcpC with the promoter so that derepression occurred. However, through the accumulated evidence of several different lab members, a more complex picture of CcpC-dependent regulation of *citB* has emerged. It began when Jane Craig first observed the unusually high levels of citrate found in the culture fluid of a *citB* null mutant strain (Craig *et al.,* 1997). Using a *citBp-lacZ* fusion integrated at a non-essential locus, Hyun-Jin Kim went further to demonstrate that the high levels of citrate in a *citB* null mutant are correlated with the hyperexpression of *citBp21-lacZ* (H.J. Kim *et al.,* 2003). Moreover, Kim showed that CcpC is required for the hyperexpression of *citBp21-lacZ* in a *citB* null background (H. J. Kim, unpublished data), suggesting that, when citrate accumulates to high levels, CcpC changes from a negative regulator to a positive regulator.

In addition, we know through DNase I footprinting experiments that CcpC binds to two sites in the *citB* promoter region, a dyad symmetry element centered at the -66 position and a half dyad at -27, and that both sites are required for repression *in vivo* (S.I. Kim *et al.,* 2003). Given the positioning of these sites, we hypothesized that binding

to the -66 element would be necessary for activation by CcpC, but that the -27 element would be dispensable.

1.1 Promoter elements necessary for CcpC-dependent activation of *citB*

To determine the mechanism behind CcpC-dependent activation of *citB,* I looked at the expression of various *citB* promoter fusions (Figure 6). The promoter fusions I utilized are *citBp23-lacZ* and *citBp24-lacZ*; they were created by Agnes Fouet and integrate at the nonessential *amyE* locus. The *citBp23-lacZ* fusion contains the *citB* promoter region from positions -84 to +36, relative to the +1 site of transcription (Fouet *et al.,* 1990). The *citBp24-lacZ* fusion contains sequences from positions -67 to +36; it is missing the left half of the -66 dyad symmetry element (Fouet *et al.,* 1990). I introduced these fusions into wild-type and *citB* null strains of *B. subtilis*, grew the strains in DSM, took samples during growth and analyzed them for β-galactosidase activity. The *citBp23-lacZ* fusion, which contains both CcpC binding sites, overexpressed *citBp-lacZ* in a *citB* null background (Figure 7). However, the *citBp24-lacZ* fusion, which lacks the full -66 binding site, was incapable of overexpression in a *citB* null. Thus, I have determined that the activation of *citB* in high citrate is dependent on the presence of an intact dyad symmetry element at the -66 position; this dyad is also essential for repression in the absence of citrate (S.I. Kim *et al.,* 2003).

1.1.1 CcpC does not activate *citZ* expression in high citrate

We next asked if this CcpC-dependent activation was unique to the *citB* locus. CcpC was known to repress the *citZ* promoter, which controls the genes encoding citrate synthase II (*citZ*) and isocitrate dehydrogenase (*citC*). Due to the CcpC-binding site architecture at the *citZ* promoter, we hypothesized that CcpC could only act as a negative regulator of *citZ*; the half-dyad element overlaps the -10 site and the full-dyad is located downstream of the transcriptional start site.

To test this hypothesis, I utilized a *citZ-lacZ* transcriptional fusion created by Shengfang Jin (Jin *et al.,* 1994b). This construct contains a 1.3 kb fragment that includes

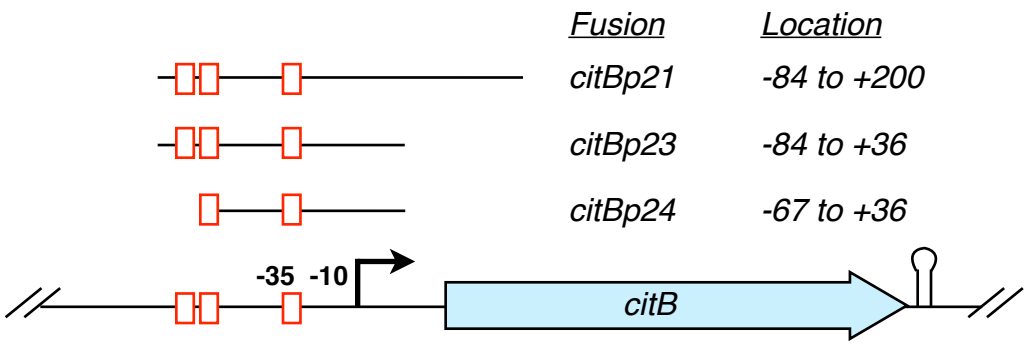

Figure 6. *citBp-lacZ* transcriptional fusions used in this study. The sequences of three *citBp-lacZ* fusions relative to the *citB* locus are shown here. Fusions *citBp23* and *citBp24* differ only in the removal of the upstream half of the -66 dyad symmetry element in the latter.

the *citZ* promoter, a 5' UTR of 195 bp, and the first 30 codons of the *citZ* gene, and it is integrated by homologous recombination at the *citZ* locus. I introduced this fusion into wild-type, *ccpC* null, *citB* null, and *ccpC citB* double null strains and assayed the production of β-galactosidase during growth in DSM (Figure 8). As expected, *citZ-lacZ* expression increased two-fold in the *ccpC* null mutant; CcpC is a repressor of *citZ* and this two-fold effect in the *ccpC* null is due to loss of repression. However, I was surprised to find that a *citB* null mutation caused *citZ-lacZ* levels to rise 5-fold after 5 hours of growth, that is, the *citB* null mutation caused a greater derepression than knocking out the repressor. If this increase in expression were due to the conversion of CcpC from a negative to a positive regulator of *citZ*, I would have expected a *ccpC* mutation to suppress the *citB* null phenotype. Instead, the two mutations had an additive effect; in a *ccpC citB* null, *citZ-lacZ* expression rose to a level approximately 10-fold higher than in the wild-type. This result suggests two possibilities: either *citZ* expression is activated by a protein other than CcpC that responds to citrate, or *citZ* expression is repressed in some way by aconitase. Testing the latter possibility is the focus of the second half of this chapter. Does aconitase play a role in the regulation of the TCA branch enzymes?

1.2 Role of the two functions of aconitase in *citB* expression

For many years, we hypothesized that the extremely high levels of citrate seen in a *citB* null mutant were due simply to a roadblock in metabolism; with no aconitase enzyme activity to convert citrate to isocitrate, citrate should build up within the cell and be excreted into the medium. However, two observations directly challenged this model. First, the finding that *citZ* is overexpressed in an aconitase null mutant suggests that increased citrate synthase levels may also contribute to citrate accumulation. Second, in an unpublished result, Alisa Serio found that the *citB5* RNA-binding mutant accumulated citrate in the culture supernatant (Serio 2005). Together, these two results raised the possibility that the metabolic roadblock model might be an incomplete

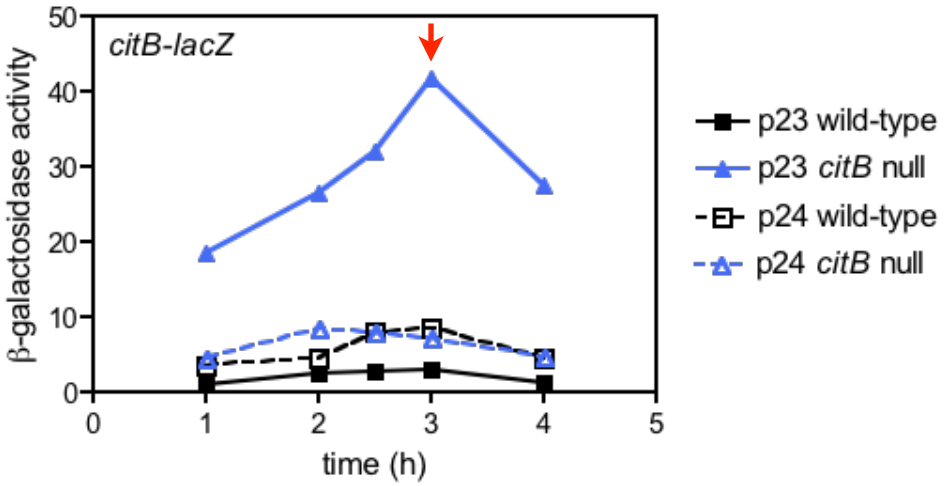

Figure 7. *citB-lacZ* hyperexpression is dependent on a full dyad symmetry element at the -66 position. Strains KBP56 (wild-type) and KBP62 (*citB* null) contain the complete *citBp23-lacZ* fusion; strains KBP57 (wild-type) and KBP63 (*citB* null) contain the *citBp24-lacZ* fusion, which lacks the upper half of the -66 dyad. The red arrow indicates T_0, the entry to stationary phase. A representative experiment of 2 is shown.

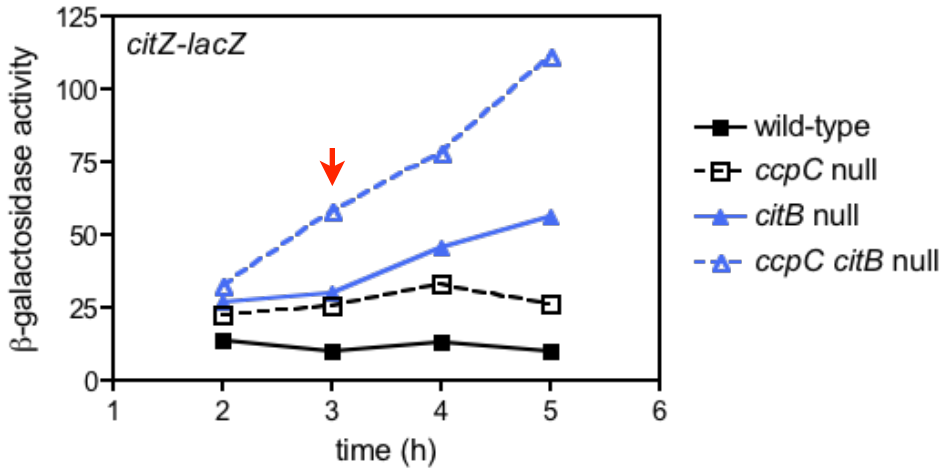

Figure 8. *citZ-lacZ* expression is activated in a *citB* null independent of CcpC. Strains KBP44 (wild-type), KBP45 (*citB* null) KBP48 (*ccpC* null) and KBP49 (*ccpC citB* null) were compared for *citZ-lacZ* expression during growth. The red arrow indicates T_0, the entry to stationary phase. A representative experiment of 2 is shown.

explanation for this phenomenon. To attempt to decipher the mechanism behind these two results, I tried to assess the contributions of the two aconitase functions to citrate accumulation.

1.2.1 Construction of an enzymatically dead mutant of aconitase (*citB2*)

To clarify the contribution of the enzymatic activity of aconitase to the maintenance of citrate levels within the cell, I sought to create an enzymatically dead mutant of aconitase that retained RNA-binding activity. An attempt to create such a mutant had been made in the past: Claudia Alen mutated one of the cysteine residues (C517A) responsible for ligating the iron-sulfur cluster to the aconitase protein. The cysteine-to-alanine (or serine) substitution approach is a well-documented method to abolish aconitase enzymatic activity (Hirling *et al.,* 1994, Philpott *et al.,* 1993). Alen's mutant, *citB517*, exhibited no aconitase activity in cell extracts; however, purified Acn_{C517A} retained some ability to bind to an exogenous RNA target (Alén *et al.,* 1999). Despite the presence of the *citB517* mutant in our strain collection, we chose not to use this strain because it was unstable. Streaking from Alen's frozen stock onto an agar plate yielded two colony types, and further attempts to purify the mutant were not successful. In retrospect, we can now explain the instability (see below), but at the time our primary concern was to avoid using an unstable strain.

My path to create a new enzymatically dead mutant of aconitase was convoluted. I began by using site-directed PCR mutagenesis to mutate to serine one of the cluster-ligating cysteine residues (C450). To do so, I amplified the 5' half of the *citB* gene with the mutation included as well as an N-terminal decahistidine (His_{10}) tag sequence. I will refer to the C450S allele as *citB2*. I ligated the *citB2'* construct to the *B. subtilis* integrative vector pJPM1 (*cat*) and introduced the resulting plasmid, pKP12, by single crossover at the *citB* locus, and selected for chloramphenicol resistance. The resulting transformants were a mixed population of both glutamate auxotrophs and prototrophs. I

purified one of the glutamate auxotrophs, producing a merodiploid strain [His_{10}-*citB2::*pKP12(*cat*)] in which the mutant allele is associated with the promoter.

The His_{10}-*citB2::*pKP12(*cat*) strain was a glutamate auxotroph, indicating that the C450S mutation abrogates enzymatic activity. I purified the His_{10}-Acn_{C450S} protein and showed that it is not an active enzyme (see Chapter 4); however, I did not test its RNA-binding ability.

To avoid the constant use of antibiotic during growth, I chose to passage the His_{10}-*citB2::*pKP12(*cat*) strain to obtain a double-crossover event and an unmarked *citB2* strain. I passaged the His_{10}-*citB2::*pKP12(*cat*) strain in rich medium without selection, plated for single colonies, and screened for one with the expected phenotype: a glutamate auxotroph with sensitivity to chloramphenicol. One clone matched this description. After purifying this strain (KBP22), I sequenced the *citB* locus and confirmed that it contained the C450S mutation, but had lost the His_{10} tag. To create an isogenic strain to compare to the existing *citB5* mutant (AWS133), which contains a C-terminal hexahistidine tag, I transformed KBP22 with genomic DNA from strain AWS144 [*citB*$^{+}$-His_6::pAWS42(*neo*)], selected for neomycin resistance and screened for glutamate auxotrophy. The resulting strain, KBP58, was used alongside KBP22 in a series of experiments.

I prepared cell extracts of KBP22 and determined that it did not possess aconitase activity (Figure 9); the same was true of KBP58. Surprisingly, however, the KBP22 strain did not accumulate citrate in the culture supernatant during growth (Table 6). To try to understand this result, I assayed citrate synthase activity in the mutant strains. Western blot analysis indicated that KBP22 and KBP58 produced a stable citrate synthase protein, but there was no enzymatic activity present. In Figure 10, I present a representative experiment from KBP58 cell extracts demonstrating a lack of CS enzyme activity despite ample CS protein (for a description of the CS activity assay, see below). I suspected that a point mutation in citrate synthase might be responsible. Sequencing of

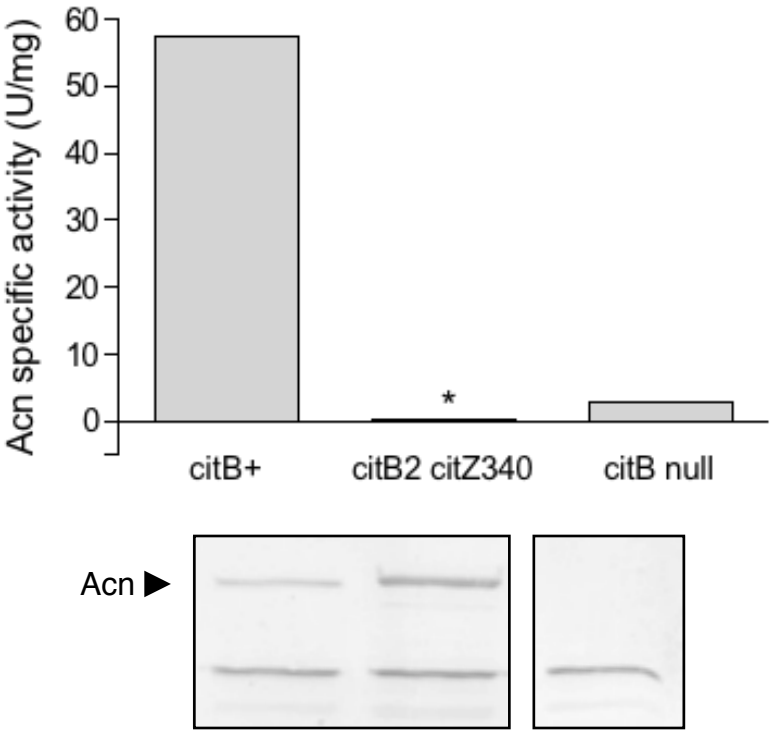

Figure 9. Specific activity of aconitase in *citB* mutant cell extracts. AWS96 (*citB*+), KBP22 (*citB2 citZ340*) and MAB160 (*citB* null) were grown in DSM and cell extracts were generated by a combination of lysozyme and gentle sonication. Protein concentration of the lysates was determined by the Bradford assay (Bio-Rad). Aliquots of cell extract were examined to determine the specific activity of aconitase. The asterisk indicates the *citB2 citZ340* activity was below the limit of detection for the assay. Aconitase protein levels were assayed using an anti-Aconitase Western blot. The arrow indicates aconitase; a cross-reacting band is visible below it.

Table 6. Citrate levels in *citB* mutants. Strains AWS96 (*citB*+), MAB160 (*citB* null) and KBP22 (*citB2 citZ340*) were grown in DSM. Cells were pelleted in late exponential phase and the culture fluid was assayed to determine the concentration of citrate.

Strain	[Citrate] mg/L
AWS96 (*citB*+)	2.3
MAB160 (*citB* null)	94.8
KBP22 (*citB2 citZ340*)	3.7

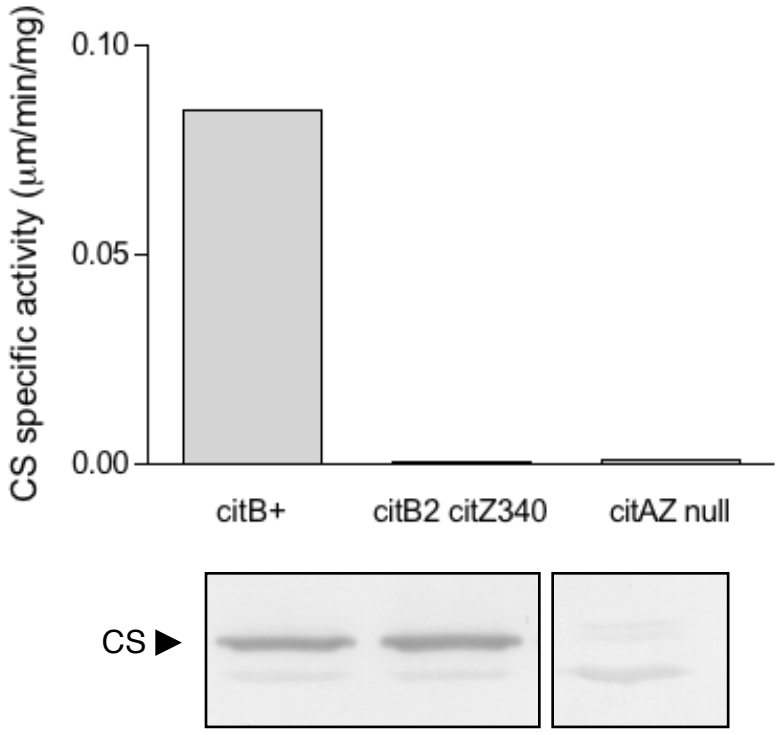

Figure 10. Specific activity of citrate synthase in *citB* mutant cell extracts. AWS144 (*citB*+ *neo*), KBP58 (*citB2 neo citZ340*) and SJB67 (*citA citZ* null) were grown in DSM and cell extracts were generated. Protein concentration of the lysates was determined by the Bradford assay (Bio-Rad). The specific activity of citrate synthase was determined and CS protein was detected by immunoblot using an anti-CS II antibody (5µg total protein loaded).

both the *citA* and *citZ* loci from KBP22 and KBP58 revealed a single point mutation leading to an H340Y substitution in the *citZ* gene. I will refer to this mutation as *citZ340*, making the true KBP22 genotype *citB2 citZ340*. I discontinued the use of KBP22, KBP58 and all their derivatives after this discovery, and set out to separate the *citB2 citZ340* mutations for independent analysis.

To separate the *citB2* mutation from the secondary *citZ340* mutation, I introduced KBP22 genomic DNA into a wild-type strain using congression. *B. subtilis* cells, if made competent, will readily take up any DNA introduced into them. If DNA is present in excess, roughly 5% of cells will take up any two pieces of DNA. In this manner, one can utilize a selectable marker to select generally for transformants and then screen for a specific phenotype conferred by integration of an unmarked mutation. I introduced KBP22 genomic DNA along with DNA containing a *citBp-lacZ tet* construct at the nonessential *amyE* locus into a wild-type strain by transformation. I selected for tetracycline resistance and then screened transformants for a blue colony phenotype (due to overexpression of the *citBp-lacZ* fusion) along with glutamate auxotrophy. The resulting strain was *citB2 amyE::citBp21-lacZ tet* (KBP118). KBP118 cannot grow on minimal medium without glutamate supplementation; I show below that this strain is defective in aconitase activity but possesses citrate synthase activity.

In addition, I separated the *citZ340* allele from the *citB2* mutation using another congression technique. I introduced KBP22 genomic DNA into a *ΔcitZC::spc* strain (SJB231) along with the integrative plasmid pAF23 (*amyE::citBp23-lacZ cat*). I selected for chloramphenicol resistance and then screened resistant clones for glutamate auxotrophy and spectinomycin sensitivity; only those strains that had lost the *ΔcitZC::spc* marker by gaining the unmarked *citZ340* point mutation would meet those criteria. The resulting strain was *citZ340 amyE::citBp23-lacZ cat* (KBP86). To confirm that the *citZ340* mutation results in a loss of citrate synthase activity, I grew up strain KBP86 along with strains JH642 (*citZ+*) and SJB66 (*ΔcitZ471*) and prepared crude cell

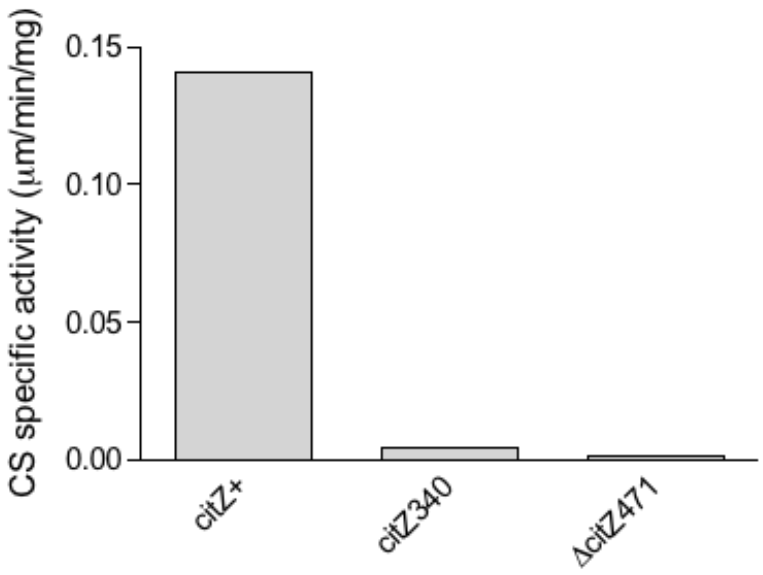

Figure 11. Specific activity of citrate synthase in *cit* mutant cell extracts. JH642 (*citZ+*), KBP86 (*citZ340*) and SJB66 (Δ*citZ471*) were grown in DSM and cell extracts were generated. Protein concentration of the lysates was determined by the Bradford assay (Bio-Rad) and the specific activity of citrate synthase was determined.

extracts by treatment with lysozyme and gentle sonication. I then tested these extracts for citrate synthase activity (Figure 11). While the *citZ*$^+$ strain exhibited CS activity in the crude cell extracts, both the *citZ340* and *ΔcitZ471* strains clearly demonstrated no activity.

1.2.2 Construction of an RNA-binding mutant of aconitase (*citB7*)

As described above, Alisa Serio established that mutations can be made in the *citB* gene that result in an RNA-binding-defective aconitase protein (Serio *et al.,* 2006a). However, the *citB5* mutant has five amino acid substitutions, making it difficult to discern which of these residues are important for RNA-binding. In addition, retaining all five mutations during strain passaging makes genetic manipulation cumbersome. To alleviate these concerns, I sought a single point mutation that would mimic the *citB5* phenotype. I suspected that only one of the five mutations, R741E, was primarily responsible for the phenotype seen in the *citB5* mutant; when I threaded the amino acid sequence of *B. subtilis* aconitase through the crystal structure of mammalian IRP1 in complex with its IRE target (Walden *et al.,* 2006), the R741 residue mapped to a part of the protein in close proximity with the RNA. To determine if this residue was solely responsible for the *citB5* phenotype, I created a single point mutant, R741E.

To create the R741E mutant, which I will refer to as *citB7*, I utilized site-directed PCR mutagenesis. I created a PCR product containing the 1.3kb C-terminal portion of the *citB* gene and the R741E-encoding point mutation. I introduced this PCR product into wild-type *B. subtilis* (AWS96) along with genomic DNA containing *amyE::citBp21-lacZ cat* (AF21). I selected for chloramphenicol resistance and screened for colonies that overexpressed *citBp-lacZ*. As mentioned in the Introduction, Alisa Serio found that *citB5* cells overexpress *citBp-lacZ*, and I assumed that the same would be true in a *citB7* mutant. I isolated a single clone (KBP72) that after sequencing was determined to have the R741E mutation along with a silent mutation due to a single nucleotide change near the 3' end of the gene. To create an isogenic strain for analysis, I introduced genomic

DNA containing the *amyE::citBp21-lacZ tet* fusion (AWS173) into this strain and selected for tetracycline resistance: the resulting strain was KBP81. KBP81 is a glutamate prototroph; it grows on minimal medium without supplementation.

1.2.3 *citB2* and *citB7* mutants accumulate citrate

Given our knowledge that the *citB2* and *citB7* strains were a glutamate auxotroph and a prototroph, respectively, I measured citrate levels in the culture supernatant of these strains. It is worth noting here that the accumulation of citrate in the culture supernatant of strains derived from JH642 (such as the strains used here) is exacerbated by a background mutation in a regulator of a citrate importer (*citS*) found during whole-genome sequencing of JH642, a strain of *B. subtilis* used commonly in our laboratory (Srivatsan *et al.,* 2008).

To assay the *citB2* and *citB7* strains for citrate accumulation in the culture fluid, I grew strains KBP94 (wild-type), AWS174 (*citB* null), KBP118 (*citB2*), and KBP81 (*citB7*) in DSM, took samples every hour during growth, and tested the culture supernatant for citrate using a citric acid assay kit (R-Biopharm). The kit works by converting citrate to oxaloacetate and acetate via the enzyme citrate lyase. The oxaloacetate and any pyruvate resulting from oxaloacetate decarboxylation are then converted to L-malate and L-lactate by malate dehydrogenase and lactate dehydrogenase, respectively. These last two reactions consume NADH, which can be measured spectrophometrically at 340 nm. I found that both *citB2* and *citB7* cells accumulated citrate, although the *citB7* citrate levels were more modest than those of the *citB2* and *citB* null strains (Figure 12).

1.2.4 *citB2* and *citB7* mutants overexpress *citB-lacZ*

To further explore this citrate accumulation phenotype, I looked at an expected side-effect of citrate accumulation: *citB* promoter overexpression. I grew the *citB2* and *citB7* strains along with the wild-type and *citB* null strains in DSM and took samples during growth to measure β-galactosidase activity. The results of this experiment can be found in Figure 13. The wild-type strain (KBP94) induced *citB* expression at the 3h time

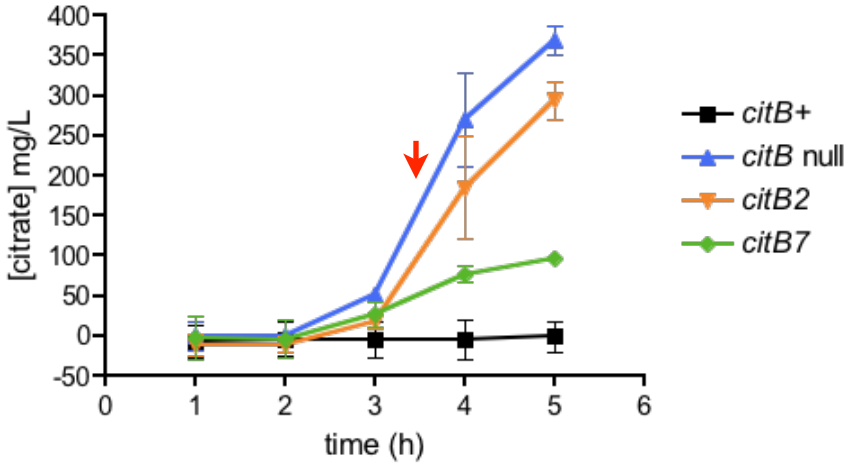

Figure 12. Citrate accumulates in the culture fluid of *citB* mutant strains. KBP94 (*citB*+), AWS174 (*citB* null), KBP118 (*citB2*), and KBP81 (*citB7*) strains were grown in DSM. Aliquots were taken at the indicated time points, cells were pelleted by centrifugation, and the concentration of citrate in the culture fluid was determined. The red arrow indicates T_0, the entry to stationary phase. The mean and standard deviation of 2 biological replicates is shown.

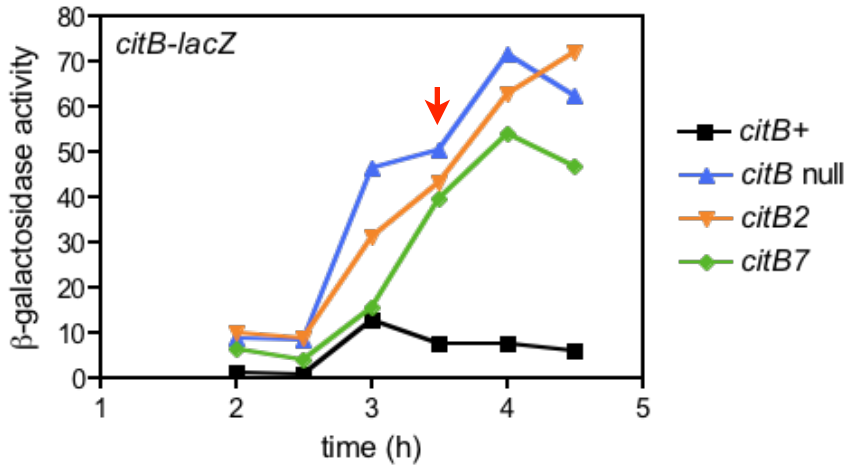

Figure 13. The *citB* promoter is hyperexpressed in *citB* mutant strains. KBP94 (*citB*+), AWS174 (*citB* null), KBP118 (*citB2*), and KBP81 (*citB7*) strains were grown in DSM. Cells were harvested by centrifugation at the indicated time points and β-galactosidase activity was determined. The red arrow indicates T_0, the entry to stationary phase. Although the experiment shown was done one time only, all strains were assayed in other experiments and gave similar results.

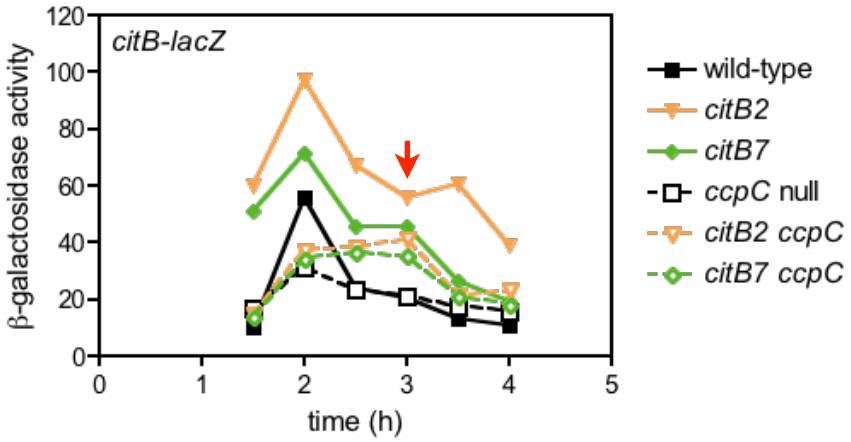

Figure 14. Hyperexpression of the *citB* promoter is dependent on CcpC in *citB2* and *citB7* strains. KBP135 (*citB*+), KBP136 (*citB2*), KBP137 (*citB7*), KBP138 (*ccpC*), KBP139 (*citB2 ccpC*), KBP140 (*citB7 ccpC*) strains were grown in DSM. Cells were harvested by centrifugation at the indicated time points and β-galactosidase activity was determined. The red arrow indicates T_0, the entry to stationary phase. A representative experiment of 2 is shown.

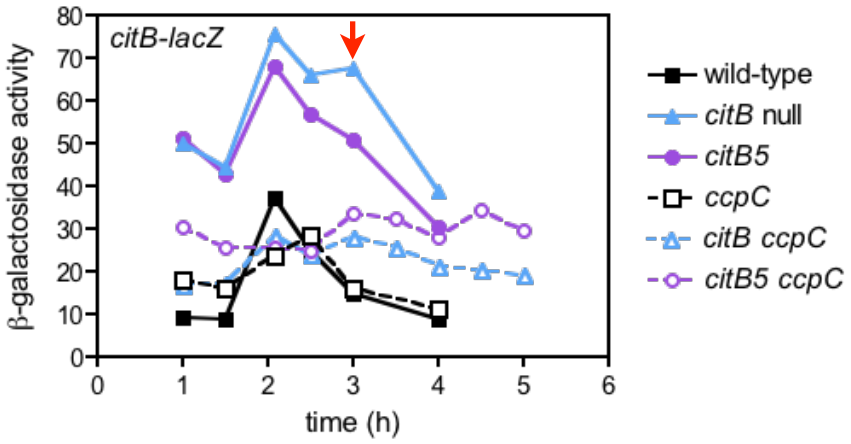

Figure 15. Hyperexpression of the *citB* promoter is dependent on CcpC in *citB* null and *citB5* strains. AWS176 (*citB*+), AWS174 (*citB* null), AWS175 (*citB5*), KBP106 (*ccpC*), KBP104 (*citB ccpC*) and KBP105 (*citB5 ccpC*) strains were grown in DSM. Cells were harvested by centrifugation at the indicated time points and β-galactosidase activity was determined. The red arrow indicates T_0, the entry to stationary phase. Although the experiment shown was done one time only, all strains were assayed in other experiments and gave similar results.

point, after which expression dropped but remained higher than the original basal level. As seen previously (H.J. Kim *et al.,* 2003), the *citB* null strain (AWS174) also induced *citBp-lacZ* at the 3h timepoint, but to levels far beyond those seen in the wild-type. As expected given the citrate levels, both the *citB2* and *citB7* strains (KBP118 and KBP81, respectively), overexpressed *citB-lacZ* to levels similar to those seen in the *citB* null strain. The *citB7* strain did not reach the same level of Miller Units as the *citB* null, but the pattern of expression was very similar. The *citB2* strain, on the other hand, reached a level of *citB-lacZ* expression similar to that of the *citB* null mutant, but expression did not drop off by the end of the experiment (4.5 h).

1.2.5 Hyperexpression of the *citB* promoter is dependent on CcpC

As discussed above, hyperexpression of *citB-lacZ* in the *citB* null mutant is dependent on CcpC (H.J. Kim, unpublished data). To test the dependence on CcpC of this hyperexpression in the *citB2* and *citB7* mutants, I introduced a *ccpC* mutation into these strains. In Figure 14, you can see that the *ccpC* mutation suppressed the overexpression phenotype of the *citB2* and *citB7* strains. This was the case in the *citB5* strain as well (Figure 15).

1.2.6 *citB2* and *citB7* strains overexpress aconitase protein

To determine the effect of *citB* promoter hyperexpression on aconitase protein levels in the *citB2* and *citB7* strains, I grew strains KBP94 (*citB*+), KBP118 (*citB2*) and KBP81 (*citB7*) in DSM and took samples at 30-60 minute intervals during growth. I prepared cell extracts as described in Materials and Methods, using a combination of lysozyme treatment and gentle sonication to break open cells followed by centrifugation to remove debris. Total protein was determined using the Bradford reagent (Bio-Rad) and equivalent amounts of total protein were analyzed by immunoblotting with polyclonal antibodies raised against Acn and CodY (Ratnayake-Lecamwasam *et al.,* 2001, Serio *et al.,* 2006b). I quantified the protein bands using ImagQuant TL software and normalized each sample to CodY to account for differences in loading. The results

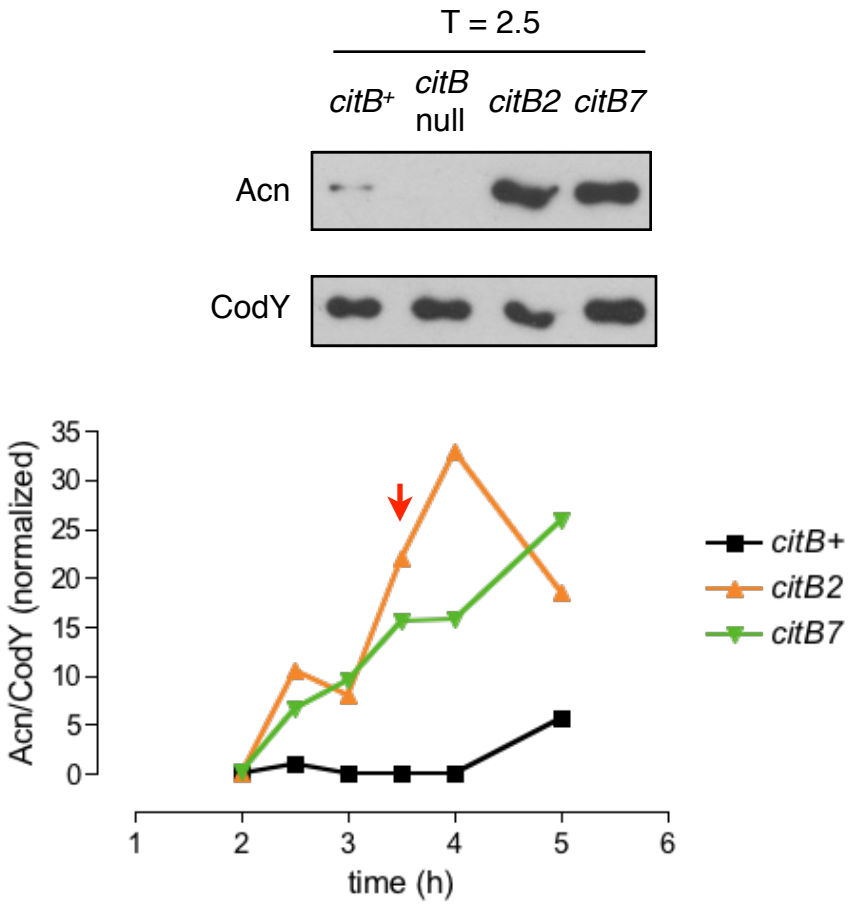

Figure 16. Aconitase protein is overexpressed in *citB* mutant strains. KBP94 (*citB*+), AWS174 (*citB* null), KBP118 (*citB2*), and KBP81 (*citB7*) strains were grown in DSM. Cells were harvested by centrifugation at the indicated time points and crude cell extracts were generated. Crude extracts (0.25 - 0.5µg) were analyzed by immunoblot using polyclonal antibodies raised to Acn. Anti-CodY antibodies were used as a loading control. In the top panel, an immunoblot for a single time point from a representative experiment is shown, with the *citB* null strain included as a control. The bands were quantitated and values are presented as a ratio of Acn relative to CodY, normalized to the ratio of the *citB*+ strain expression level at time 2.5 h. The red arrow indicates T_0, the entry to stationary phase. A representative experiment of 2 is shown; overall trends were preserved despite variability in the replicates due to differences in intensity of the CodY bands between experiments.

for each time point are shown for a representative experiment in Figure 16. It is clear that both the *citB2* and *citB7* strains overexpressed aconitase; therefore, the hyperexpression of the *citB* promoter causes higher-than-normal accumulation of the mutant proteins.

However, we still were perplexed by the citrate accumulation in the *citB7* mutant. Logically, if the *citB7* strain is a glutamate prototroph, it must have a TCA branch of the citric acid cycle that is functional enough to produce adequate 2-ketoglutarate to serve as a substrate for glutamate biosynthesis. In fact, given that glutamate is the cell's most abundant anion, with an *in vivo* concentration of ~100-200 mM (Fisher *et al.,* 1984), the rate of 2-ketoglutarate synthesis must be high to maintain those levels. Why then would a strain expressing a functional aconitase protein accumulate citrate? To know whether the R741E mutation has an effect on enzyme activity, I purified the protein and studied it *in vitro*. In addition, to confirm that glutamate auxotrophy in the *citB2* strain results from an inactive aconitase protein, I purified and studied the C450S Acn protein as well.

1.2.7 Specific activities of C450S and R741E Acn proteins

To determine how the C450S and R741E mutations affect the specific activity of aconitase, I purified both proteins from *B. subtilis*. The purification scheme is the subject of Chapter 4 of this thesis. Briefly, I purified these proteins (along with wild-type aconitase) using classical biochemical methods to avoid issues involving the use of affinity tags. I purified the wild-type from strain KBP94 (*citB*$^{+}$), and the R741E mutant directly from strain KBP81 (*citB7*). However, my attempts to obtain a large (500 ml) culture of the KBP118 (*citB2*) strain were unsuccessful. It was impossible to grow up a large volume of this strain without a significant portion of the population acquiring suppressor or revertant mutations. This was not surprising; my original isolation of the *citB2* strain was hampered by the presence of an extragenic suppressor mutation. This issue led me to isolate the C450S protein from the original KBP22 (*citB2 citZ340*) strain; the presence of the *citZ340* suppressor mutation prevented the accumulation of citrate,

the environmental condition I believe creates a strong selective pressure against the *citB2* mutant.

I purified two preparations of each of the three proteins and then determined their specific activities using the established aconitase enzyme assay. The aconitase activity assay directly measures the production of *cis*-aconitate from isocitrate over time as an increase in the absorbance at 240 nm (Henson *et al.,* 1967). The proteins were assayed both with and without prior activation by incubation with reduced iron and sulfur: Because the proteins were purified aerobically, the iron-sulfur clusters undergo some oxidative damage but can be reactivated by incubation in a ferrous ammonium sulfate ($Fe(NH_4)_2(SO_4)_2$) buffer with a strong reducing agent (Kennedy *et al.,* 1983). I tested all six protein preparations under these two conditions; the results can be seen in Figure 17. As expected, the C450S mutation abolished essentially all enzyme activity; a small level of activity was detected after incubation with Fe and S. Surprisingly, the R741E mutation also caused a defect in specific activity, but not nearly as severe as the C450S mutation. The R741E preparations were approximately 4-fold less active than their wild-type counterparts. This result raised the possibility that citrate accumulation in *citB7* cells was due to a partial enzymatic defect. However, given that *citB7* cells overexpress aconitase (Figure 16), overproduction of a form of aconitase with reduced enzyme activity might compensate for any defect in individual molecules.

1.2.8 *citB7* strain exhibits high aconitase activity levels in cell extracts

To test the combined effects of hyperexpression of aconitase protein and reduced specific activity, I analyzed crude cell extracts of strains KBP94 (*citB*+), AWS174 (*citB::spc*), KBP118 (*citB2*) and KBP81 (*citB7*) for aconitase activity. As expected, the *citB2* and *citB* null strains had very low levels of activity throughout growth (Figure 18). There was, however, an increase in *citB2* aconitase activity levels beyond background at the 5 hour time point; I attribute this to the increased presence of revertants in the population. In fact, when similar cultures were plated hourly between 2 and 5 hours, the

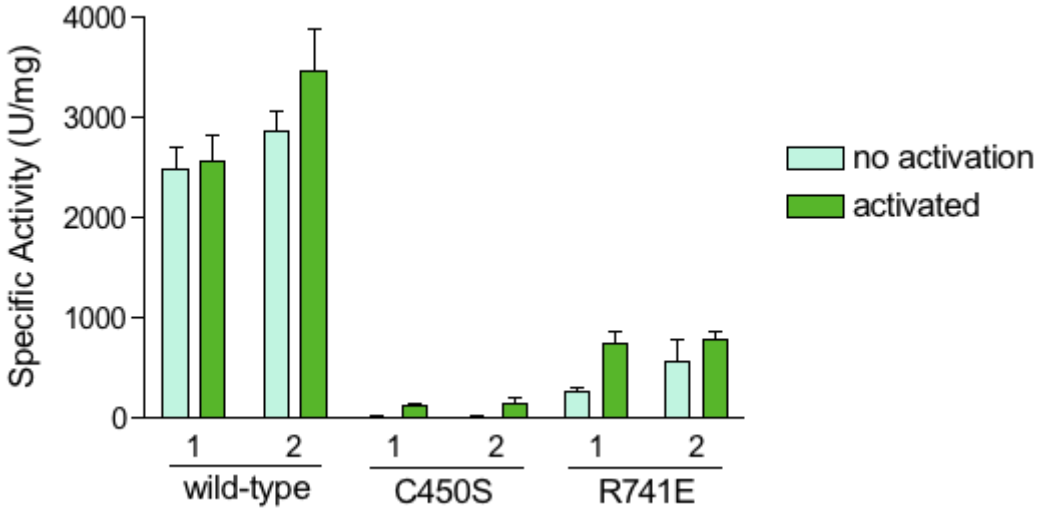

Figure 17. Specific activity of purified aconitase. The wild-type, C450S and R741E mutant aconitase proteins were prepared to ~95% purity from *B. subtilis* using a classical approach described in the Material and Methods. Two preparations of each protein were purified from independent cultures, producing six total preparations. The protein concentration of the purified proteins was determined by the Bradford assay (Bio-Rad). The specific activity of the wild-type and mutant aconitase proteins was determined before and after activation by incubation with exogenous Fe and S. The individual preparations are presented separately. Values shown are the mean and standard deviation of 2 replicates.

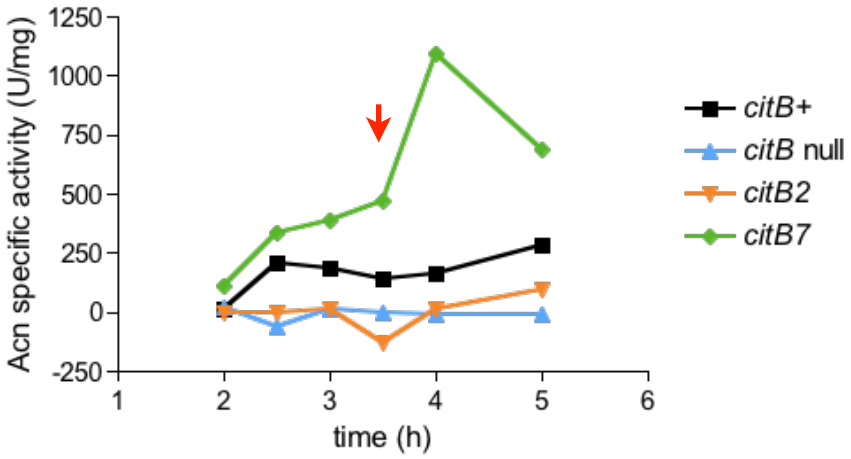

Figure 18. The *citB7* strain exhibits high Acn activity in cell extracts. KBP94 (*citB*+), AWS174 (*citB* null), KBP118 (*citB2*), and KBP81 (*citB7*) strains were grown in DSM. Cells were harvested by centrifugation at the indicated time points and crude cell extracts were generated. Crude extracts were analyzed for aconitase specific activity. Protein concentration was determined by the Bradford assay (Bio-rad). The red arrow indicates T_0, the entry to stationary phase. A representative experiment of 2 is shown; overall trends were preserved despite variability in the replicates due to differences in sonication, which negatively impacts Acn enzyme activity.

proportion of *citB*+ revertants increased from approximately 0.1% to 10% of the population over time. Importantly, the *citB7* strain showed very high levels of aconitase activity in cell extracts. At this point, we had no logical explanation for why cells containing a vast excess of aconitase (i.e., the capacity to convert citrate to isocitrate) would be left with a backlog of citrate. In our attempt to solve this mystery, we began to look at the phenomenon from a different point of view.

2 Role of aconitase in the expression of citrate synthase

In the first half of this chapter, I established that the high citrate accumulation phenotype observed in *citB* null cells also occurs in *citB2* and *citB7* cells. In addition, from Alisa Serio's data we know that this is the case for the *citB5* strain as well. As discussed above, the presence of high citrate in the *citB7* and *citB5* cells was perplexing given that these strains are glutamate prototrophs. But given the overexpression of *citZ-lacZ* in a *citB* null strain, we suspected that the high citrate phenotype in the *citB* mutant strains could be due to overexpression of the *citZ*-encoded citrate synthase (CS II). In addition, the overexpression of *citZ-lacZ* in *citB* null cells does not require CcpC. Therefore, I considered two hypotheses. First, a regulatory protein other than CcpC might activate *citZ* transcription in response to the high citrate levels present in a *citB* null. Second, aconitase itself might regulate *citZ* at the mRNA level. The second half of this chapter presents my work in support of the second of these two hypotheses.

2.1 *citB* mutations cause changes in citrate synthase levels

In order to test my hypothesis that aconitase regulates *citZ* at the mRNA level, it was first necessary to determine if *citB* mutations affect the levels of citrate synthase protein in the cell. I did this through a combination of activity assays and quantitative Western blots described below.

2.1.1 Increased CS activity in cell extracts of *citB* mutants

The CS enzyme activity assay indirectly measures the conversion of acetyl-CoA and oxaloacetate to citrate via an indicator molecule, the reagent 5,5'-dithiobis(2-nitrobenzoic acid) (DTNB), commonly called Ellman's reagent. Upon acetyl-CoA cleavage by the CS enzyme, the free thiol group of SH-CoA attacks the disulfide bond of DTNB (Ellman 1959). This reaction produces one 2-nitro-5-thiobenzoate (TNB^{2-}) ion for every molecule of SH-CoA; the ion has a characteristic yellow color that can be detected at 412 nm (Riddles *et al.,* 1983). This measurement of the consumption of acetyl-CoA can then be used to generate a specific activity for citrate synthase.

Figure 19 shows that crude extracts of the *citB* null and *citB5* strains prepared from cells in early stationary phase had approximately two-fold higher citrate synthase specific activity than did the wild-type. To determine if this increased citrate synthase activity occurs in the *citB2* and *citB7* strains as well, and to more closely examine the kinetics of the appearance of citrate synthase activity, I grew KBP94 (wild-type), AWS174 (*citB* null), KBP118 (*citB2*), and KBP81 (*citB7*) in DSM and took samples at 30-60 minute intervals during growth and stationary phase. I found that each of the *citB* mutant strains exhibited higher levels of citrate synthase activity than did wild-type (Figure 20). All of the strains exhibited an initial spike in citrate synthase activity at the 2.5 hour time point. This observation suggests that the initial induction event is triggered by the same regulatory mechanism in all four strains: likely the derepression of *citZ* by citrate-dependent antagonization of CcpC. However, after this time point, the three mutant strains begin to diverge from the wild-type, although the *citB* null and *citB2* mutants did so the most dramatically. This is likely due to the lack of aconitase enzyme activity in these cells; the citrate levels continue to rise, preventing CcpC from regaining activity. In the wild-type and *citB7* strains, the citrate can be metabolized and thus CcpC repression can be reinstated. At later time points, between 4 and 5 h, the citrate synthase

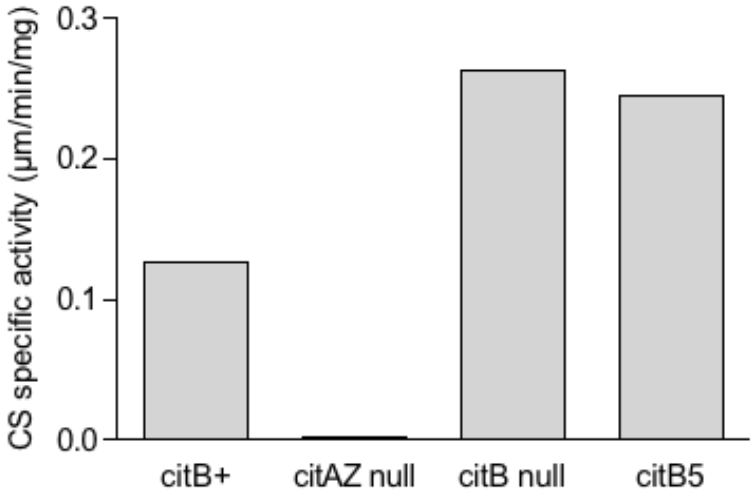

Figure 19. Specific activity of citrate synthase in *citB* mutant cell extracts. AWS144 (*citB+ neo*), SJB67 (*citA citZ* null), MAB160 (*citB* null) and AWS133 (*citB5*) were grown in DSM and cell extracts were generated. Protein concentration of the lysates was determined by the Bradford assay (Bio-Rad). The specific activity of citrate synthase was determined. Although the data shown are from a single experiment, all of the strains were assayed in other experiments and gave similar results.

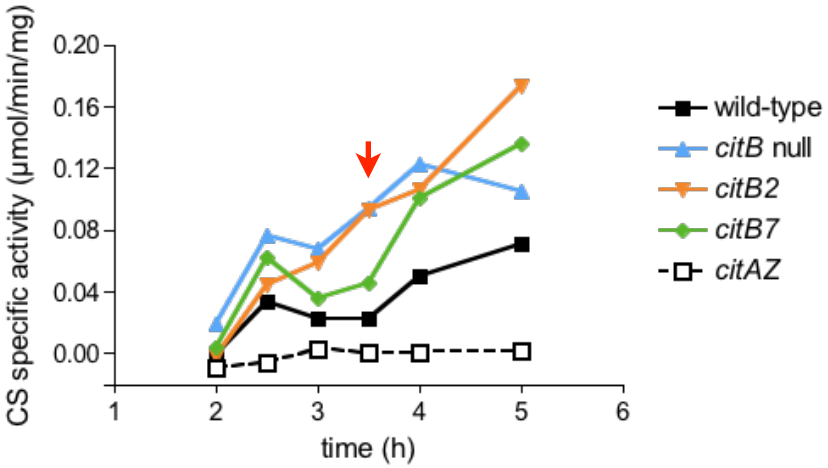

Figure 20. *citB* mutant strains exhibit high citrate synthase activity in cell extracts. KBP94 (wild-type), AWS174 (*citB* null), KBP118 (*citB2*), KBP81 (*citB7*), and SJB67 (*citAZ* null) strains were grown in DSM. Cells were harvested by centrifugation at the indicated time points and crude cell extracts were generated. Crude extracts were analyzed for citrate synthase specific activity. Protein concentration was determined by the Bradford assay (Bio-rad). The red arrow indicates T_0, the entry to stationary phase. A representative experiment of 2 is shown; overall trends were preserved despite variability in the calculated specific activity values between experiments.

activity in all four strains rose beyond the levels of the initial spike at 2.5 hours, indicating that a different regulatory mechanism may come into play at this time.

2.1.2 Citrate synthase protein is overexpressed in *citB* mutants

Given the *citZ-lacZ* results discussed above, we anticipated that citrate synthase protein would be overexpressed in the *citB* mutant strains. I therefore analyzed the cell extracts described above by Western blot using antibodies to CS and CodY. The immunoblots were quantified using ImagQuant TL (GE Healthcare) and CS levels were normalized to the CodY loading control, with wild-type levels in the 2.5 hour sample set to 1. The results of this experiment can be found in Figure 21. As with specific activity levels, citrate synthase protein levels of all strains increased between 2 and 2.5 hours of growth. However, the *citB* null, *citB2* and *citB7* strains had higher CS levels than wild-type for the remainder of the experiment.

2.1.3 Overexpression of CS in *citB* mutant strains is not dependent on CcpC

To know whether the increase in citrate synthase levels in the *citB* mutants was due to a CcpC-dependent effect, I first introduced a *ccpC* mutation into the *citB* null mutant strain and examined the wild-type (KBP26), *citB* null (KBP51), *ccpC* null (KBP52), and *citB ccpC* null (KBP54) mutant strains for citrate synthase protein levels and activity in crude cell extracts. I grew these strains in DSM, took samples at 3 and 4 hours of growth, generated crude cell extracts as described above, and analyzed them to determine the specific activity of citrate synthase in each strain. The results of this experiment are shown in Figure 22. At both time points, there was more citrate synthase activity present in the *citB* null than the wild-type strain. In addition, while there was more citrate synthase activity in the *ccpC* null than in the wild-type, the *citB* null strain outpaced the *ccpC* null in citrate synthase activity. This result alone indicates that the citrate synthase activity in the *citB* null cannot be caused merely by inactivation of CcpC-dependent repression of the *citZ* promoter in response to high citrate levels caused by the aconitase null mutation. Finally, the *citB ccpC* null mutant strain exhibited higher

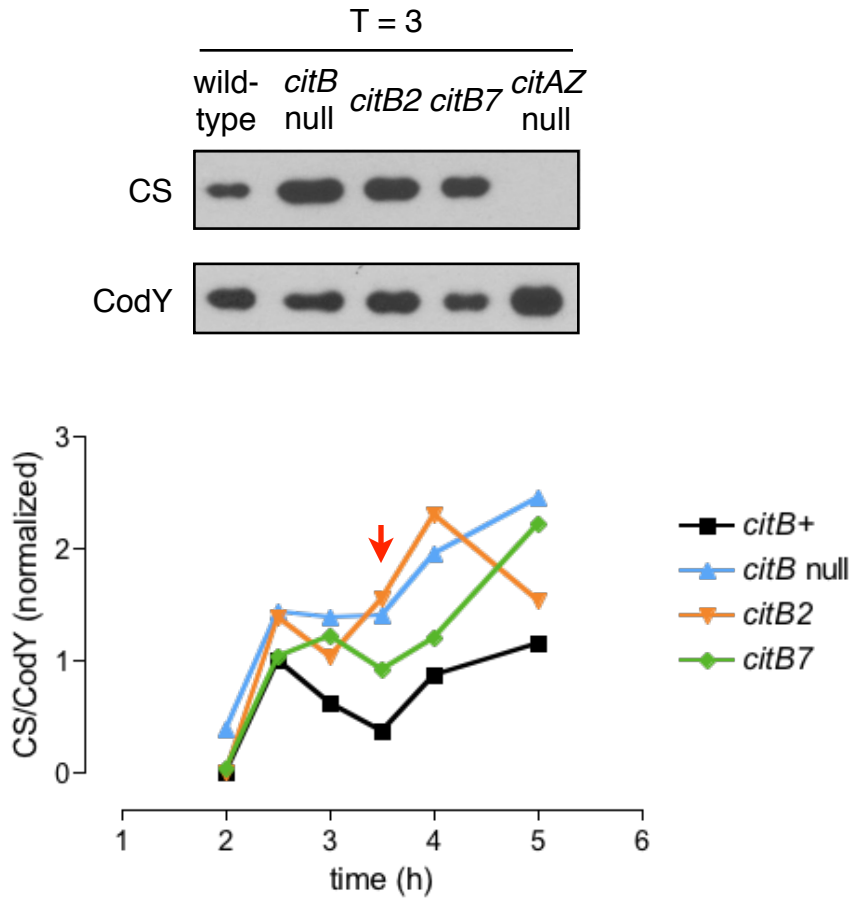

Figure 21. Citrate synthase protein is overexpressed in *citB* mutant strains. KBP94 (wild-type), AWS174 (*citB* null), KBP118 (*citB2*), KBP81 (*citB7*) and SJB67 (*citAZ* null) strains were grown in DSM. Cells were harvested by centrifugation at the indicated time points and crude cell extracts were generated. Crude extracts (0.25 - 0.5µg) were analyzed by immunoblot using polyclonal antibodies raised to CS II. Anti-CodY antibodies were used as a loading control. In the top panel, an immunoblot of a single time point in a representative experiment is shown. The bands were quantitated, and values are presented in the bottom panel as a ratio of CS relative to CodY, normalized to the ratio of the wild-type strain expression level at time 2.5 h. The red arrow indicates T_0, the entry to stationary phase. A representative experiment of 2 is shown; overall trends were preserved despite variability in the replicates due to differences in intensity of the CodY bands between experiments.

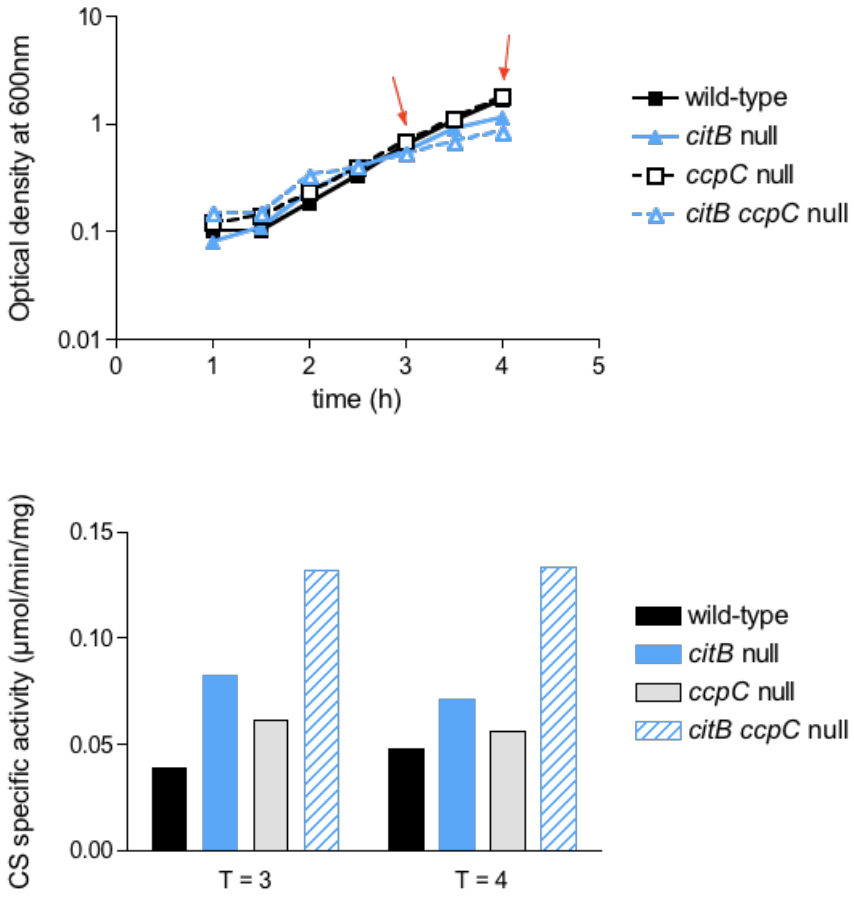

Figure 22. The overactive citrate synthase phenotype in a *citB* null mutant strain is not suppressed by a *ccpC* mutation. Strains KBP26 (*citB* +), KBP51 (*citB* null), KBP52 (*ccpC* null) and KBP54 (*citB ccpC* null) were grown in DSM (top). Cells were harvested by centrifugation at the time points indicated by the red arrows. Crude cell extracts were generated and analyzed for citrate synthase specific activity (bottom). Protein concentration was determined by the Bradford assay (Bio-rad). A representative experiment of 2 is shown.

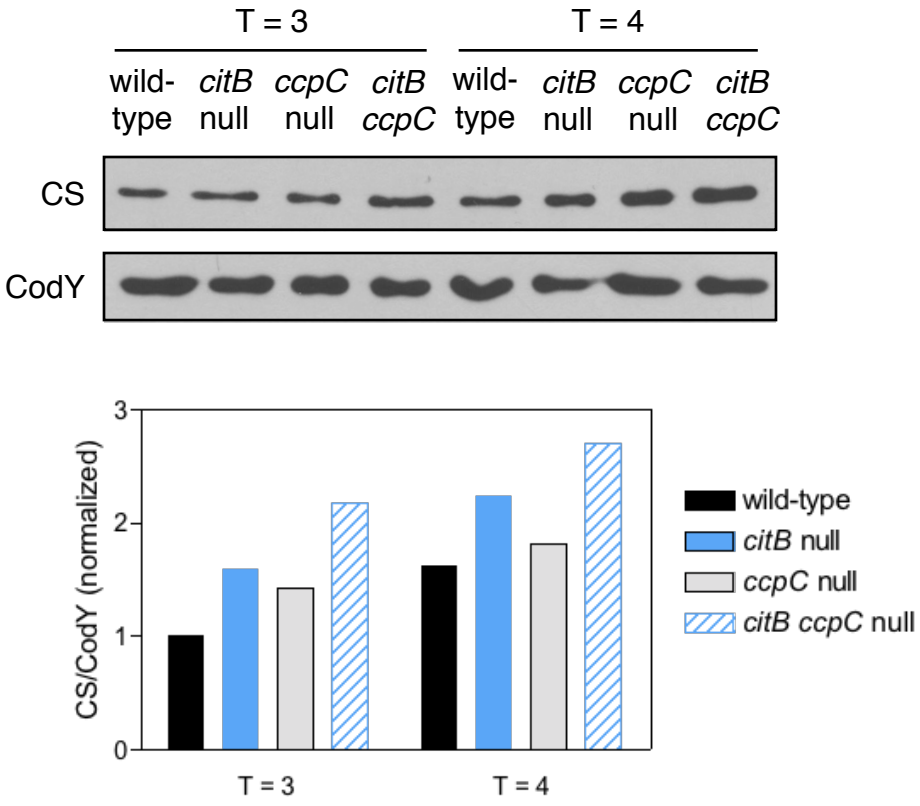

Figure 23. The overexpression of citrate synthase in *citB* mutant strains is not suppressed by a *ccpC* null mutation. KBP26 (wild-type), KBP51 (*citB* null), KBP52 (*ccpC* null), KBP54 (*citB ccpC* null) strains were grown in DSM. Cells were harvested by centrifugation at the indicated time points and crude cell extracts were generated. Crude extracts (0.25 - 0.5µg) were analyzed by immunoblot using polyclonal antibodies raised to CS II. Anti-CodY antibodies were used as a loading control. In the top panel, the immunoblot from a representative experiment is shown. The bands were quantitated, and values are presented as a ratio of CS relative to CodY, normalized to the ratio of the wild-type strain expression level at time 3 h. Sample times correspond to those in Figure 22. A representative experiment of 2 is shown; overall trends were preserved despite variability in the replicates due to differences in intensity of the CodY bands between experiments.

citrate synthase activity than either of the single mutant strains, again suggesting that these two effects act independently; they are additive.

In addition to the activity level results, I tested the aforementioned crude cell extracts in an immunoblot with antibodies raised to CS II and CodY (as a loading control). The results can be found in Figure 23. The levels of citrate synthase protein were higher in the *citB* null and *ccpC* null strains than in the wild-type. Moreover, the level was higher still in the *citB ccpC* double mutant strain. This result, like the activity result above, is inconsistent with the hypothesis that the overexpression of CS in a *citB* null mutant is due only to inactivation by CcpC and instead argues that aconitase acts in some manner independently of CcpC to control CS levels.

To determine if this is also the case in the *citB2* and *citB7* strains, I repeated the above experiment using wild-type (KBP135), *citB2* (KBP136), *citB7* (KBP137), *ccpC* (KBP138) *citB2 ccpC* (KBP139) and *citB7 ccpC* (KBP140) strains. In Figure 24, the levels of citrate synthase protein in the *citB2* and *citB7* cells were higher than in the wild-type, as expected. In the *citB7* strain, the CS levels were identical to the levels in the *ccpC* single mutant for each time point. However, the introduction of a *ccpC* null mutation had a similar effect as in the *citB* null strain; the CS levels in a *citB7 ccpC* strain were higher than in either of the single mutant strains. Results for the *citB2* strain were more surprising. A *citB2* mutation alone resulted in very high levels of CS protein in the cell, and the introduction of a *ccpC* mutation partially suppressed the *citB2* phenotype. Importantly, the levels of citrate synthase in the *citB2 ccpC* strain were higher than in a *ccpC* null strain, indicating that the *citB2* mutation has an effect independent of CcpC. This result suggests that there is an aconitase-dependent, CcpC-independent effect on citrate synthase expression in both the *citB2* and *citB7* mutant strains.

These experiments have shown us that the mutations in *citB* affect expression of citrate synthase by a mechanism that is independent of CcpC. The second half of this

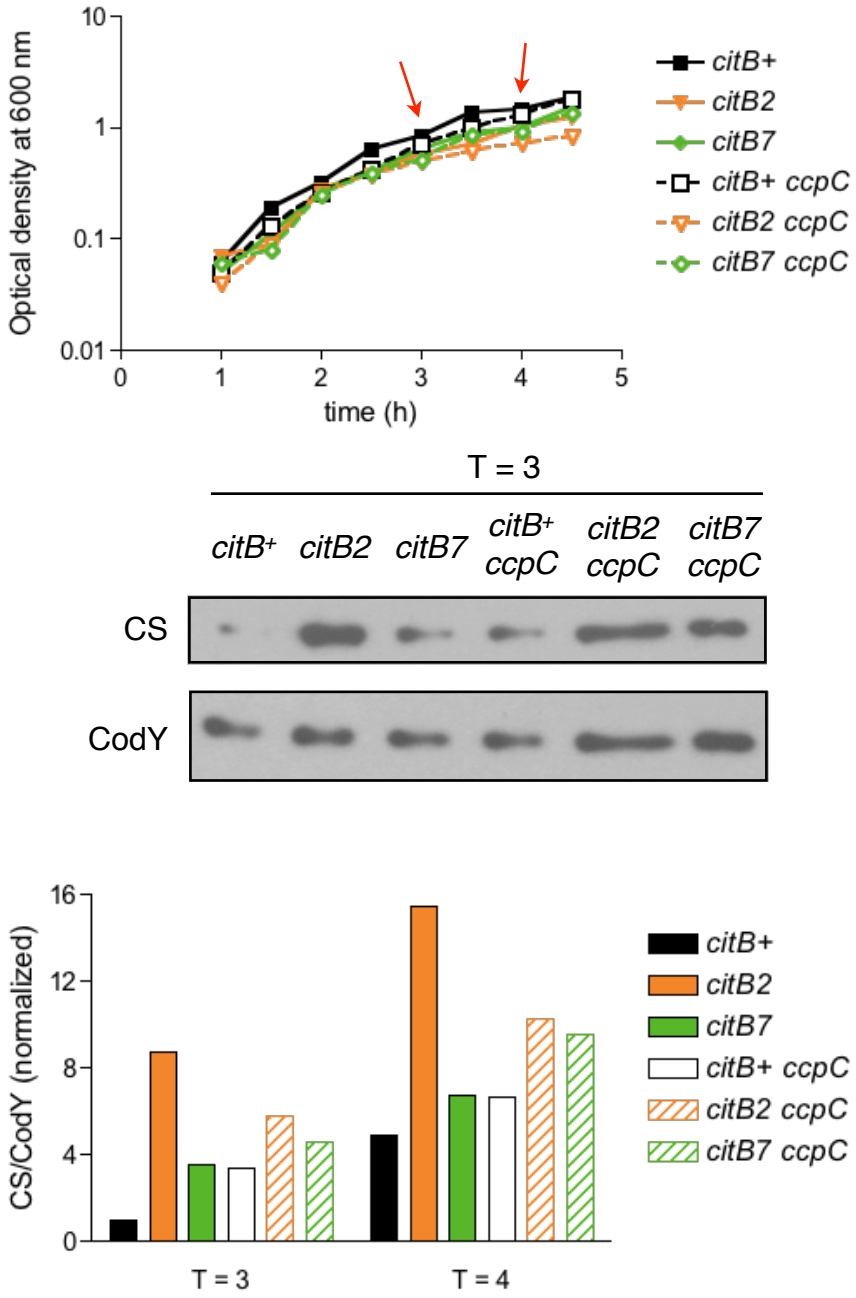

Figure 24. The effect of a *ccpC* null mutation on the overexpression of citrate synthase in *citB* mutant strains. Strains KBP135 (*citB*⁺), KBP136 (*citB2*), KBP137 (*citB7*), KBP138 (*citB*⁺ *ccpC*), KBP139 (*citB2 ccpC*) and KBP140 (*citB7 ccpC*) were grown in DSM (top). Cells were harvested by centrifugation at the indicated time points (red arrows) and crude cell extracts were generated. Crude extracts (0.25 - 0.5µg) were analyzed by immunoblot using polyclonal antibodies raised to CS II. Anti-CodY antibodies were used as a loading control. Bands were quantitated. Values are presented as a ratio of CS relative to CodY, normalized to the ratio of the *citB*+ strain expression level at time 3 h. This experiment was done one time only.

chapter tests the hypothesis that aconitase regulates citrate synthase levels by directly interacting with *citZ* mRNA.

2.2 Acn directly interacts with the *citZ* 5' leader RNA *in vitro*

I established above that citrate synthase expression levels are altered in *citB* mutants, and presented evidence that the *citZ* gene or gene product is the target of this regulation. As discussed in the Introduction, *citZ* mRNA possesses a 195 n untranslated leader region at its 5' end. I hypothesized that aconitase regulates *citZ* mRNA translation or stability by binding to the 5' leader region. The loss of this binding (for example, in the *citB7* strain) would result in more translation of *citZ* mRNA and thus more citrate synthase protein in the cell, as seen above. To test this hypothesis, I performed a series of *in vitro* binding assays using purified wild-type and mutant aconitase proteins and the *citZ* mRNA 5' leader region.

2.2.1 Wild-type Acn binds to *citZ* RNA *in vitro*; C450S and R741E do not

To demonstrate binding of the wild-type Acn protein to the *citZ* 5' leader RNA, and to show that the *in vivo* effect in the *citB2* and *citB7* strains could be caused by differences in binding to the *citZ* mRNA, I tested binding of all six wild-type and mutant Acn preps to *citZ*. To do this, I amplified a PCR product containing the *citZ* 5' leader region downstream of the T7 promoter for use in *in vitro* transcription assays. The construct contains the 195 bp *citZ* 5' leader and includes the start codon of *citZ*. I synthesized the *citZ* 5' leader RNA by *in vitro* transcription with the T7 RNA polymerase and determined the specific activity of the probe. I then incubated increasing concentrations of purified Acn (in the nanomolar range) with a constant, very low concentration of radiolabelled probe (83 pM) in buffer containing 0.5 mM dipyridyl, an iron-chelator that forces aconitase into the apoprotein, RNA-binding form (Alén *et al.,* 1999). The reactions were allowed to equilibrate for 30 minutes at room temperature. I then filtered these reactions through nitrocellulose discs and followed with two washes before I measured the radioactivity retained on the filter. (The filter binding assay is

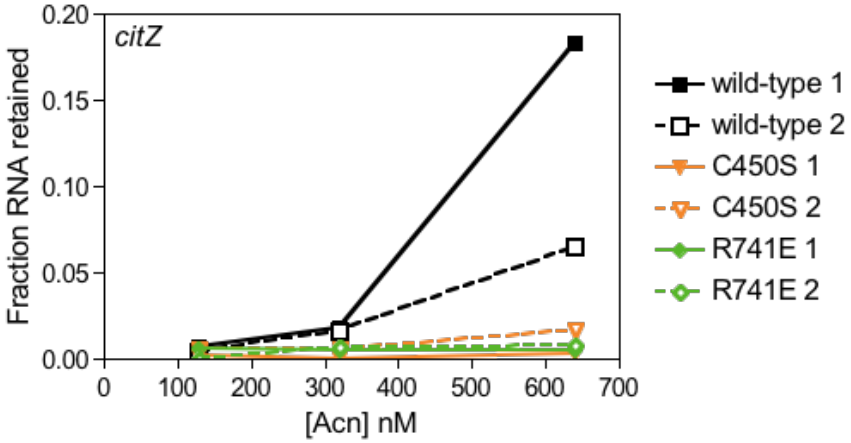

Figure 25. Differential binding of wild-type and mutant Acn proteins to *citZ 5'* leader RNA *in vitro*. Each of six Acn protein preparations were mixed separately with radiolabelled *citZ* 5' leader RNA synthesized *in vitro* at the indicated concentrations and allowed to equilibrate and allowed to equilibrate in buffer containing RNAseOut, 0.5 mM dipyridyl and 5 mM β-mercaptoethanol. The reactions were passed through a nitrocellulose membrane and the RNA present on the filter was detected by scintillation counting. The fraction RNA retained is calculated, after background subtration, as a percentage of the input RNA. Although the data shown are from a single experiment, wild-type 2, C450S1, and R741E 1 were assayed in other experiments and gave similar results.

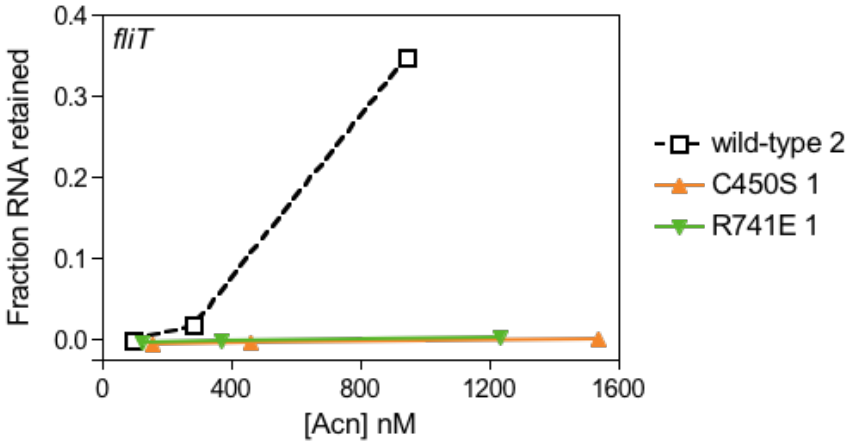

Figure 26. Differential binding of wild-type and mutant Acn proteins to *fliT* RNA *in vitro*. Wild-type, C450S, and R741E mutant Acn protein preparations were mixed separately with radiolabelled *fliT* RNA synthesized *in vitro* at the indicated concentrations and allowed to equilibrate in buffer containing RNAseOut, 0.5 mM dipyridyl and 5 mM β-mercaptoethanol. The reactions were passed through a nitrocellulose membrane and the RNA present on the filter was detected by scintillation counting. The fraction RNA retained is calculated, after background subtration, as a percentage of the input RNA. This experiment was done one time only.

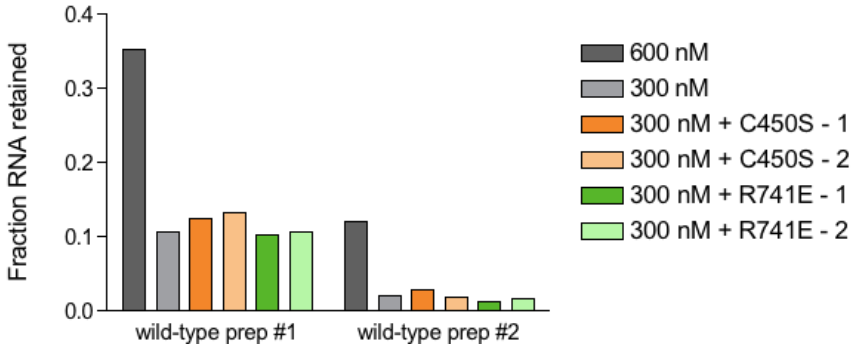

Figure 27. The C450S and R741E Acn mutants do not inhibit wild-type Acn binding to *fliT* RNA. Each of the two wild-type Acn preparations were combined at 600 nM or 300 nM with radiolabelled *fliT* RNA synthesized *in vitro*. An equal concentration (300 nM) of the C450S and R741E mutant Acn proteins were combined with wild-type Acn and the *fliT* RNA in buffer containing RNAseOut (, 0.5 mM dipyridyl and 5 mM β-mercaptoethanol. Reactions were allowed to equilibrate prior to passage through a nitrocellulose membrane. The RNA retained on the membrane was detected by scintillation counting, the background counts subtracted, and the fraction of the input RNA calculated. Although the data shown are from a single experiment, wild-type prep #2 was assayed in other experiments and gave similar results.

based on the different abilities of RNA and protein to pass through nitrocellulose pores. Unbound RNA will pass easily with very little background (~1% of total); however, proteins cannot pass through the pores due to their large size.)

The results of this experiment can be found in Figure 25, and are plotted as the fraction of RNA retained on the filter versus the concentration of Acn. Notice that the two different wild-type Acn preps had different RNA-binding activities. Indeed, the enzyme activities of the preps were also different (see above), indicating wild-type preparation #1 is a better RNA-binding protein but a less active enzyme than preparation #2. These results suggest that the two preparations are at different equilibria between the two forms of aconitase. Moreover, the C450S and R741E Acn preparations did not bind to RNA at the concentrations tested. It is possible that the C450S and R741E mutants would bind to RNA at higher concentrations but binding at concentrations above 1 μM is unlikely to be physiologically relevant.

Additionally, I found the same differential binding to *fliT*, an RNA that Alisa Serio demonstrated is a target of wild-type Acn (Serio 2005). In Figure 26, it is clear that the wild-type preparation of aconitase binds to *fliT*, but no binding is evident for either of the two mutant proteins.

2.2.2 Purified C450S and R741E Acn do not contain an inhibitory molecule

To ensure that the lack of binding of the mutant proteins to RNA was not due to an inhibitory molecule present in the protein preparations. I mixed the wild-type and mutant proteins and looked at binding to *fliT*. I incubated two different amounts of wild-type Acn (600 and 300 nM) with the RNA. In addition, I incubated the *fliT* RNA with 300 nM of wild-type Acn and 300 nM of each of the mutants. In Figure 27, one can see that the cpm bound changed slightly with the addition of the mutant proteins but not to a significant level. This experiment demonstrates that the mutant preparations do not contain any inhibitory molecule that prevents Acn:RNA binding; instead, it supports the

conclusion that the C450S and R741E mutants are inherently incapable of binding to RNA at the concentrations of protein tested.

2.3 Investigation of a direct Acn-CS interaction regulatory model

Prior to my work describing an interaction between aconitase and the *citZ* mRNA, I considered the possibility that the overaccumulation of citrate in the *citB* null strain was due to the perturbation of a physical interaction between aconitase and citrate synthase. There is evidence for an interaction between the TCA cycle enzymes citrate synthase, aconitase, isocitrate dehydrogenase, succinate thiokinase, fumarase, and malate dehydrogenase in both *E. coli* and *B. subtilis* (Barnes *et al.,* 1986). Recently, Meyer *et al.* (2011) demonstrated an interaction between *B. subtilis* citrate synthase, isocitrate dehydrogenase, and malate dehydrogenase, in addition to an interaction of aconitase with malate dehydrogenase. Our results would be explainable if the interaction of aconitase with citrate synthase slows the rate of the latter enzyme, and that the absence of aconitase results in a hyperactive citrate synthase, leading to high citrate levels. To explore this hypothesis, I utilized the His_{10}-tagged versions of the wild-type and C450S Acn proteins described in Chapter 3 to perform a series of assays with cell extracts and purified citrate synthase.

2.3.1 Exogenous aconitase does not affect CS activity in cell extracts

As described above, both *citB* null and *citB5* cell extracts demonstrate high levels of citrate synthase activity. To determine if the addition of purified Acn to *citB* null or *citB5* cell extracts affects citrate synthase activity, I grew strains AWS144 (*citB*+), AWS133 (*citB5*) and MAB160 (*citB* null) in DSM to late exponential phase and harvested cells by centrifugation. I generated cell extracts by treatment with lysozyme and sonication and looked at citrate synthase activity with and without a 15 minute pre-incubation with 400 nM wild-type or C450S mutant His_{10}-Acn (Figure 28). As seen previously, the *citB* null and *citB5* cell extracts had a higher level of citrate synthase

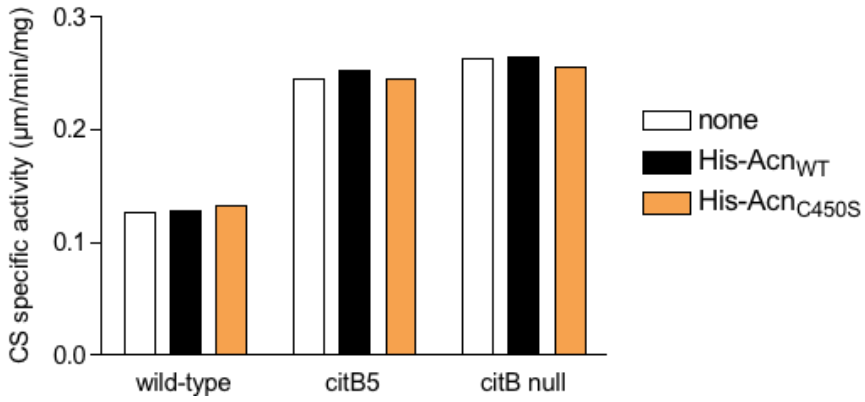

Figure 28. Pure aconitase does not reduce citrate synthase activity in *citB5* and *citB* null cell extracts. AWS144 (*citB*+), AWS133 (*citB5*) and AWS174 (*citB* null) were grown in DSM and cell extracts were generated from late-exponential phase cells. Protein concentration of the lysates was determined by the Bradford assay (Bio-Rad). Cell extracts were incubated with 450 nM pure wild-type or C450S His_{10}-Acn and incubated at room temperature for 15 minutes. The specific activity of citrate synthase was determine by established methods. In each case, it was calculated as a function of the total protein in the extract without consideration of the addition of purified aconitase. This experiment was done one time only.

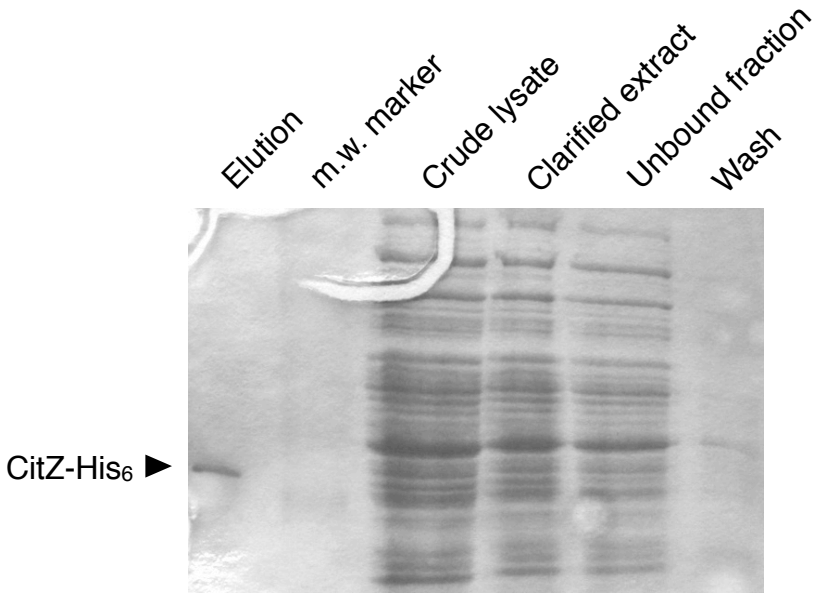

Figure 29. Purification of CitZ-His_6. Strain HKB181 (*citZ*-His6 erm) was grown in DSM to late exponential phase and harvested by centrifugation. Cells were lysed by French pressure and sonication, generating a crude lysate. The lysate was clarified by centrifugation prior to binding to metal-affinity resin. CitZ-His6 was eluted with 250 mM imidazole. Samples at the indicated points in the purification process were analyzed by SDS-PAGE and stained with Coomassie blue to detect protein.

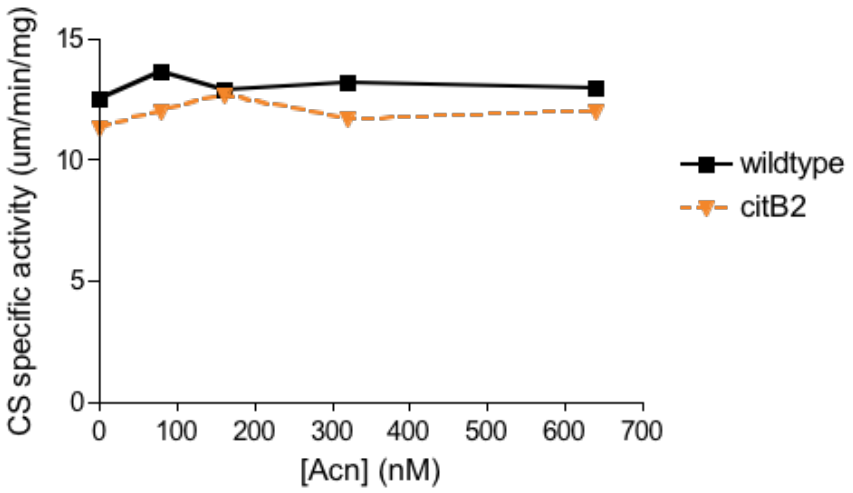

Figure 30. Aconitase does not inhibit CitZ activity *in vitro*. Pure CitZ-His_6 (40 nM) was combined with increasing concentrations of pure wild-type or C450S His_{10}-Acn and incubated at room temperature for 15 minutes. The specific activity of citrate synthase was determine by established methods. For all reactions, the protein concentration used to calculate specific activity did not include the purified aconitase. A representative experiment of 2 is shown.

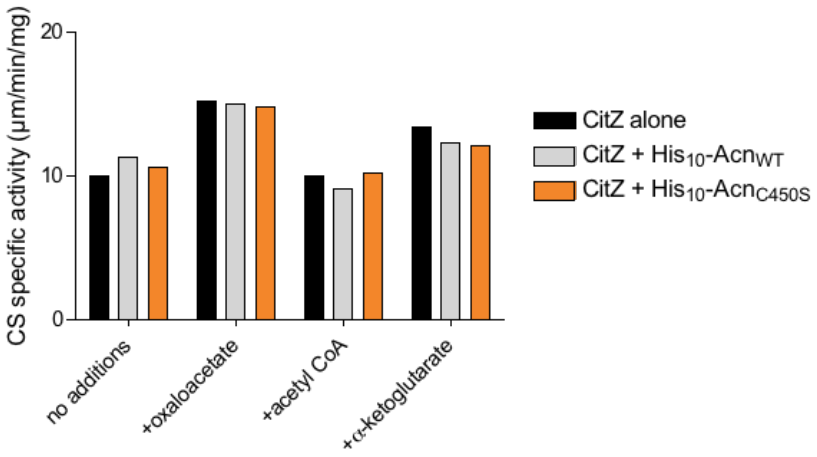

Figure 31. Aconitase does not inhibit CitZ activity in the presence of metabolites. Pure CitZ-His_6 protein (40 nM) was combined with 0.5 mM oxaloacetate, 0.25 mM acetyl-CoA, or 0.5 mM α-ketoglutarate. His_{10}-Acn_{wt} or $His_{10}Acn_{citB2}$ were added to 320 nM and the reaction was incubated at room temperature for 15 minutes and then assayed for citrate synthase activity by established methods. For all reactions, the protein concentration used to calculate specific activity did not include the purified aconitase. This experiment was done one time only.

specific activity than wild-type. However, incubation of cell extracts with aconitase protein had no effect on total citrate synthase activity levels.

2.3.2 Purification of CitZ-His$_6$ from *B. subtilis*

In order to more rigorously examine a possible interaction between aconitase and citrate synthase, I purified CitZ from *B. subtilis* so that I could study the two proteins in isolation. To prepare pure CitZ protein, I used a method developed by Hyun-Jin Kim (unpublished). I grew strain HKB181 (*citZ*-His$_6$ *erm*) in 2L DSM to early stationary phase and harvested cells by centrifugation. I resuspended the cells in a buffer containing 20% glycerol, lysed them using the combination of a French press and sonication, and clarified the extract by centrifugation. The extract was dialyzed against buffer before incubation with metal-affinity resin. CitZ-His$_6$ protein was eluted from the resin in buffer containing imidazole and dialyzed against a buffer containing 50% glycerol. In Figure 29, the purification of CitZ-His6 from crude extract to pure protein is depicted through SDS-PAGE/Coomassie blue analysis of samples taken at each step. The resulting protein was greater than 95% pure as determined by Coomassie blue staining and suitable for *in vitro* assays with pure Acn.

2.3.3 Pure aconitase does not affect pure CitZ activity

To determine if aconitase has an affect on the activity of citrate synthase *in vitro*, I combined 40 nM CitZ protein with increasing concentrations of pure Acn protein. Both wild-type and C450S His$_{10}$-tagged versions of Acn were tested. The proteins were incubated for 15 minutes at room temperature. Figure 30 shows that neither wild-type nor C450S His$_{10}$-Acn had any effect on the citrate synthase activity of the CitZ protein, even with greater than 10-fold excess of Acn. In order to determine if the presence of citrate synthase substrates was necessary to obtain the correct CitZ protein conformation for a CitZ-Acn interaction, I performed a similar experiment in the presence of various metabolites: oxaloacetate, acetyl CoA, and 2-ketoglutarate. Previous evidence suggested that 2-ketoglutarate is an inhibitor of citrate synthase (H. J. Kim, unpublished) and we

hypothesized it might be necessary to induce a conformational change in CitZ. I incubated 40 nM CitZ protein with 320 nM Acn with and without the metabolites at physiologically relevant concentrations: 0.5 mM oxaloacetate and 2-ketoglutarate, 0.25 mM acetyl CoA. As seen in Figure 31, the presence of metabolites did not reveal any effect of Acn on CitZ. One caveat for this experiment: I was unable to reproduce the inhibition of citrate synthase by 2-ketoglutarate.

3 Discussion

In this chapter, I explored the contribution of the two functions of aconitase to the regulation of the TCA branch enzymes in *B. subtilis*. In the first section of this chapter, I described the role aconitase plays in the regulation of *citB* expression. First, I demonstrated that CcpC acts as a positive regulator of *citB* in the high levels of citrate present in a *citB* null (and *citB2*, *citB7* strains) through an interaction with the -66 dyad symmetry element in the *citB* promoter region. I went on to show that this CcpC-dependent activation of aconitase manifests at the protein level in *citB2* and *citB7* strains, resulting in high levels of aconitase expression, and, in the *citB7* strain, aconitase enzyme activity. In the second half of this chapter, I explored the contribution of aconitase to citrate synthase regulation. I demonstrated that citrate synthase is overexpressed in *citB* mutants in a CcpC-independent manner, leading to increased levels of citrate synthase protein and enzyme activity. Furthermore, I presented evidence indicating that wild-type aconitase, but neither the C450S nor R741E mutants, binds to a region of *citZ* RNA containing the 195 n 5' leader region *in vitro*.

3.1 CcpC is both a repressor and an activator of *citB* expression

Through the accumulated results obtained in this chapter and results from other members of the laboratory (H.J. Kim, unpublished), I can conclude that CcpC plays a dual role in regulating *citB* expression in high citrate levels. The model for this dual

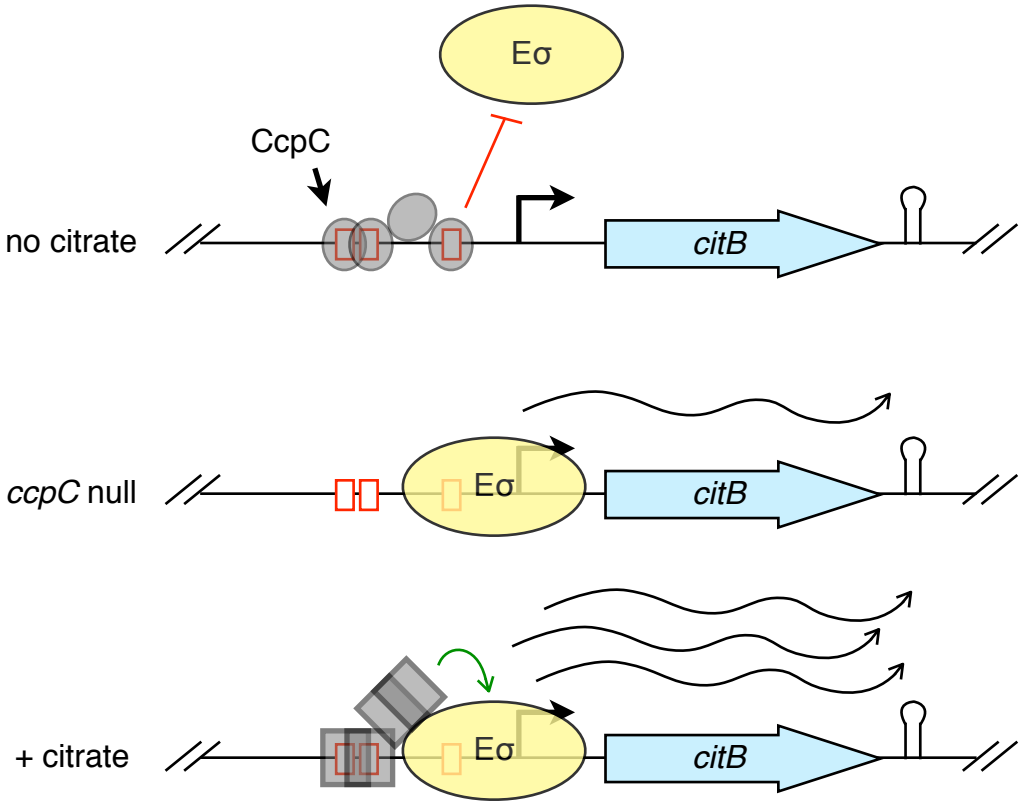

Figure 32. An updated model for the regulation of the *citB* promoter by CcpC. There are two CcpC binding sites (red boxes) in the *citB* promoter region. Both are occupied by CcpC (grey circles) when citrate levels are very low ("none") in the cell; this binding prevents *citB* transcription. When citrate levels rise (+citrate), citrate alters the conformation of CcpC. The conformational changes has two effects: first, CcpC vacates the -27 position half-dyad symmetry element (single red box); second, the altered CcpC conformation recruits RNA polymerase to the promoter and causes activation of *citB* transcription. An intermediate phenotype between these two extremes can be seen in a *ccpC* null mutant; this strain exhibits derepression of *citB* due to the absence of CcpC-dependent repression.

regulation is depicted in Figure 32. When intracellular citrate levels are low, CcpC represses *citB* expression; this repression can be removed genetically by the introduction of a *ccpC* null mutation (H.J. Kim *et al.,* 2003). Increased synthesis of citrate causes a loss of repression and conversion of CcpC to an activator of *citB* expression. This new model represents a major shift from the initial view of CcpC as strictly a negative regulator.

One implication of this new model is the need to revise a hypothesis concerning the role of CcpC autoregulation. Recall that the *ccpC* gene is repressed by CcpC, and that this repression is relieved by rising citrate levels, resulting in higher levels of CcpC in conditions when it is not active as a repressor (Kim *et al.,* 2002a). The authors of this study hypothesized that this regulatory mechanism would allow *B. subtilis* to respond quickly if glucose becomes available; ample CcpC protein would be present when citrate levels drop to reinstate repression. However, given our new model, it seems likely that the derepression of CcpC in the presence of citrate produces a pool of CcpC that can respond rapidly both to drops and increases in citrate levels. In the case of citrate accumulation, CcpC would activate aconitase synthesis, leading to conversion of citrate to isocitrate. This effect would be important for two reasons. As mentioned above, *B. subtilis* can only metabolize citrate to isocitrate via the aconitase enzymatic reaction. Therefore, in order to use citrate as an energy source, *B. subtilis* must activate aconitase in order to progress through the TCA cycle. In addition, citrate has several negative effects on cell physiology; it alters the pH of the cell and also acts to chelate divalent cations, as described above. Thus, in order to remove citrate from the cell, *B. subtilis* has no choice but to activate aconitase. Alternatively, in this revised model of CcpC autoregulation, if citrate levels drop, the large pool of CcpC would be readily available to turn off aconitase (and citrate synthase) expression, preventing the production of these expensive enzymes when they are not required.

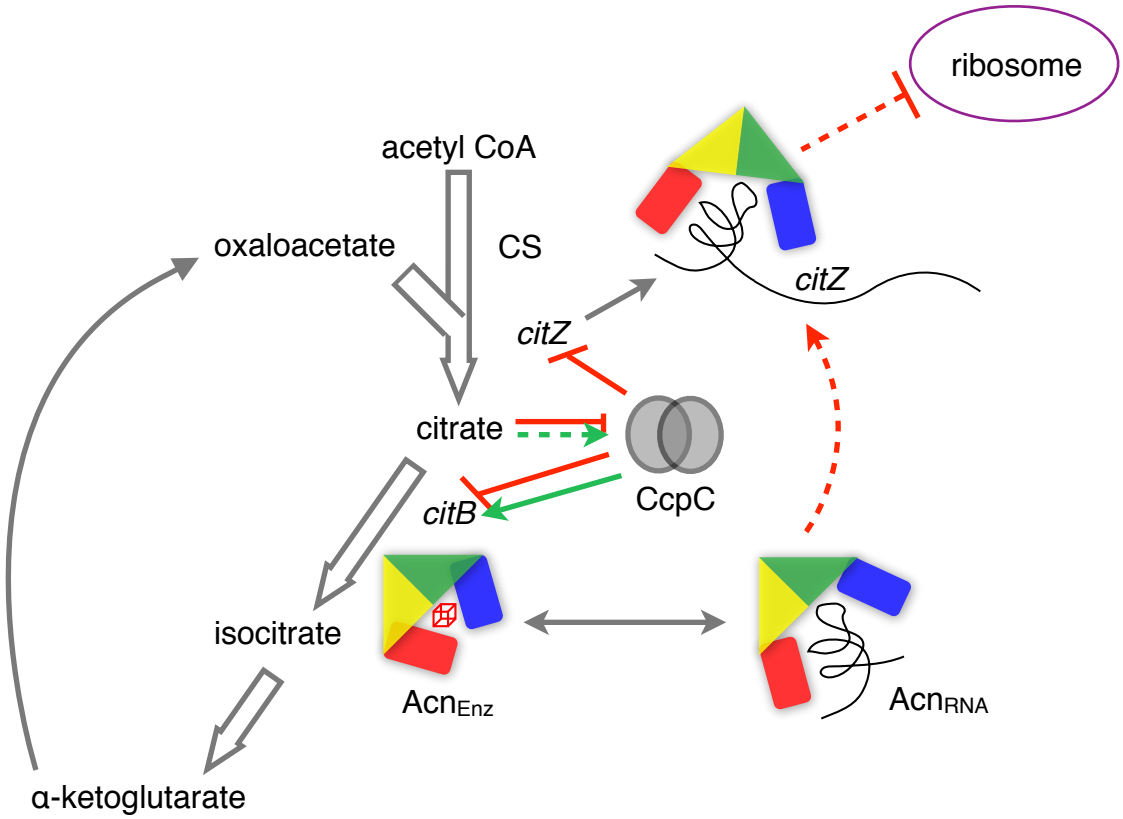

Figure 33. A model for a TCA branch autoregulatory loop. At the transcriptional level, CcpC represses *citZ* and *citB* in the absence of citrate. In the presence of citrate, CcpC repression of *citZ* is alleviated; however, CcpC also becomes a positive regulator of *citB*. The aconitase protein is present in two pools in the cell; the enzymatic form and the RNA-binding form. We hypothesize that the RNA-binding form of Acn interacts with the *citZ* mRNA at the post-transcriptional level to block translation of *citZ*. This model would allow *B. subtilis* to tightly control the concentration of citrate inside the cell using regulation by CcpC and aconitase, an enzyme that can metabolize citrate, making this proposed model a type of autoregulatory loop.

3.2 Roles for aconitase and CcpC in the regulation of citrate synthase

The results presented in this chapter, and previously published data (Jourlin-Castelli *et al.,* 2000), indicate that both aconitase and CcpC contribute to the regulation of citrate synthase in *B. subtilis*. Introduction of a *ccpC* null mutation caused derepression of a *citZ-lacZ* fusion, and levels increased further in combination with a *citB* null mutation. This effect could be seen at the protein level as well: a *ccpC* null mutation resulted in increased citrate synthase protein levels, and higher levels still when combined with a *citB* null (or *citB2* or *citB7*) mutation. These data indicate that aconitase plays a role independent of CcpC in the regulation of citrate synthase, although more work must be done to elucidate the mechanism of aconitase-dependent regulation of *citZ in vivo* (see below).

By incorporating these new data with that of other lab members, an updated model has emerged for the role of aconitase and CcpC in the regulation of the Krebs cycle (Figure 33). During growth on glucose, the *citZ* gene is repressed by CcpA and both the *citZ* and *citB* genes are repressed by CcpC. However, when glucose is exhausted and citrate levels rise, both genes are derepressed and the CitZ and Acn proteins begin to be made. The proteins (along with isocitrate dehydrogenase) metabolize citrate to 2-ketoglutarate. However, aconitase may also bind to the *citZ* RNA and prevent translation of the CitZ protein. We can imagine a possible explanation for this regulation if we consider the relationship of citrate and iron in the cell. Citrate is a chelator of divalent cations, including iron. If citrate levels rise, aconitase is activated by CcpC, resulting in more aconitase protein in the cell. However, the high levels of citrate likely would sequester the available iron away from aconitase, resulting in high levels of the RNA-binding apo-Acn. Acn would then bind to *citZ*, reducing the levels of CitZ in the cell, leading to a drop in citrate levels. This regulatory mechanism would allow the cell to counteract the loss of repression of *citZ* by CcpC in high citrate.

Importantly, this model predicts a dual mechanism for the accumulation of citrate in a *citB* null cell. First, the metabolic roadblock produced by the removal of aconitase enzyme activity causes a build-up of citrate within the cell. Second, the model predicts that the RNA-binding function of aconitase contributes to citrate synthase regulation; in the absence of aconitase, citrate synthase protein accumulates and produces even more citrate. The case of the *citB7* mutant provides strong evidence in support of this model. The *citB7* mutant exhibits very high levels of aconitase activity *in vivo*, yet this strain accumulates citrate in the culture fluid.

Going forward, it will be important to more definitively establish the interaction between aconitase and *citZ* mRNA *in vivo*. One caveat of the experiments I have shown is the lack of a negative control for aconitase:RNA binding. Demonstrating that another RNA of a size similar to that of the *citZ* probe does not bind to aconitase with the same affinity will be necessary to prove this interaction is specific. Additionally, it would be interesting to discover the binding site for aconitase on the *citZ* mRNA. An RNA footprint approach would be useful here.

3.3 Possible role for a *citZ*-specific small RNA in Acn regulation of CS

A recent paper suggests the possibility of yet another level of complexity for the Acn-CS regulation story. Schmalish *et al.* (2010) discovered a small RNA in the intergenic region between *yrhJ* and *yrhK* on the *B. subtilis* chromosome with strong complementarity to the *citZ* leader region. The small RNA, which is regulated by the motility sigma factor, σ^D, is suspected to act as an antisense RNA for *citZ*, but the exact mechanism and the resulting regulation have not been elucidated. Due to the strong sequence complementarity between the *citZ* leader and the *yrhJ-yrhK* small RNA, it is possible that aconitase binds to this small RNA in addition to (or instead of) the *citZ* transcript. In order to determine if the aconitase regulation described here is dependent on the presence of the small RNA, the citrate synthase protein quantitation experiments could be repeated in a *yrhJ-yrhK* small RNA knockout background.

3.4 Possibility of a direct interaction between Acn and CS

In addition to my work examining the role of aconitase in the regulation of citrate synthase expression, I also explored the possibility of a direct, protein-protein interaction between these two proteins. We hypothesized that aconitase might be inhibiting citrate synthase activity, and I tested this hypothesis using purified His_{10}-Acn. I saw no effect on citrate synthase activity when I added His_{10}-Acn to cell extracts or to purified CitZ-His_6 protein. However, as discussed below in Chapter 3, the expression of His_{10}-*citB*$^+$ *in vivo* results in overexpression of *citB-lacZ* fusion, indicating that the function of aconitase is in some manner perturbed by the His_{10} tag. Therefore, I cannot rule out the possibility that the native Acn and CS proteins do interact to add another layer of regulation to this system. To investigate this possibility, the experiments described in this Chapter could be repeated with untagged aconitase protein.

3.5 The elusive single-function mutant

The study of *B. subtilis* aconitase in our laboratory has involved several different attempts to create single-function mutants: that is, aconitase proteins that have lost RNA-binding activity or a enzymatic activity, but not both. The ideal single-function mutant would completely abolish one function but retain wild-type levels of the other. Perhaps unsurprisingly, none of the *citB* mutants I have described in this thesis are true single-function mutants. In this chapter, I showed that the C450S Acn protein is neither an enzyme nor an RNA-binding protein. The C450S Acn protein is stable and produced in high amounts, and has residual aconitase enzyme activity upon activation with iron and sulfur, a fact that suggests that proper folding is not an issue. However, the reasons behind the RNA-binding defect in the C450S strain are unclear. The IRP2 protein, a homolog of IRP1 that is not an aconitase enzyme, is subject to regulation via oxidation of cysteine residues that lie close to the IRE-binding site (Zumbrennen *et al.,* 2009). It is possible that in the absence of the iron-sulfur cluster, the two other cluster-ligating

cysteine residues form a disulfide bond, with each other or with a neighboring cysteine, that prevents RNA binding.

Similarly, the R741E Acn protein, designed to be defective in RNA binding, also exhibits a defect in enzymatic activity compared to wild-type. While it is not as severe a defect as that of the C450S Acn protein, it is still surprising given the expectation that the arginine-741 residue is not involved in enzyme activity. Several arginine residues contribute to enzyme activity in IRP1 (Philpott *et al.,* 1994), but the homolog of R741 in IRP1 (R728) is not one of them. However, a study of "non-enzymatic" residues in IRP1 revealed that mutation of some residues resulted in decreased enzyme activity: Kaldy *et al.* saw higher K_m and V_{max} values for the enzyme activity of certain RNA-binding point mutants (1999), although mutations of R728 were not tested. Interestingly, mutation of a neighboring residue, R732, to glutamate resulted in a 9-fold increase in the K_m (Kaldy *et al.,* 1999). These data and my own results together suggest that the alteration of residues near the RNA binding pocket of aconitase can have unplanned effects on enzymatic activity. It remains to be seen if the Acn_{citB5} protein also exhibits lower enzymatic activity; I will explore this issue in the overall Conclusions and Perspectives (see below).

Beyond these two mutants, it is worthwhile to consider one other *citB* mutant created by a member of our laboratory. The *citB517* strain, possessing a C517A mutation, is unstable. When the *citB517* strain was plated from frozen stocks, two colony morphologies were evident: Spo^+ and Spo^-. As mentioned above, I readily obtained revertants that appear Spo^+ when growing up my *citB2* strain. Given that I initially (inadvertently) isolated the *citB2* strain with a *citZ* suppressor mutation (*citZ340*), I hypothesize that the Spo+ colony morphology in the *citB517* frozen stocks is due to the appearance of true revertants (from C517A back to C517) or extragenic suppressors that counteract a similar citrate accumulation phenotype. This high reversion rate calls into question the residual RNA-binding activity of C517A Acn. It is very likely that the *citB517* culture from which this protein was isolated was populated by a considerable number of

revertants. Therefore, the retention of RNA-binding ability by this purified protein may be due to contamination by wild-type Acn.

Ultimately, these examples lead me to consider other possibilities for the creation of an aconitase mutant defective in a single function. To create an enzymatically dead mutant of aconitase that possesses RNA-binding activity, it might be prudent to avoid the established technique of mutating the cluster-ligating cysteine residues. Instead, there are specific catalytic residues that might prove good targets for mutagenesis. In the canonical pig mitochondrial aconitase sequence, they are Histidine-101 and Serine-642 (Voet *et al.,* 2004). While these residues are conserved in IRP1, *B. subtilis* aconitase posesses a leucine residue at the position corresponding to His-101. This may indicate that the *B. subtilis* aconitase mechanism of action is slightly different than that described for mammalian aconitases. The catalytic Ser-642 residue is conserved in *B. subtilis* (Ser-792), however, making it a good candidate for mutagenesis. It is possible that an S792A mutant would behave more similarly to wild-type aconitase. Mutation of the S792 residue should not affect iron-sulfur cluster insertion, and therefore instead of being stuck in the apo-Acn form, this mutant could switch between the two protein conformations.

Creation of an RNA-binding mutant that possesses wild-type aconitase activity will likely be more difficult. Through the analysis of IRP1 residues implicated in RNA-binding, and the comparison of the *B. subtilis* aconitase sequence to the published crystal structure of IRP1 in complex with its IRE target (Walden *et al.,* 2006), specific residues could be identified for analysis. By mutating several different residues invidually and testing the mutant proteins en masse for aconitase enzyme activity as well as RNA-binding ability, a suitable mutant may be discovered.

3.6 Other examples of aconitase-mediated regulation of the TCA branch enzymes

Prior to the writing of this thesis, a study from a different group corroborated some of the results presented in this chapter. This group created a *citB5*-like mutant by introducing two point mutations into *B. subtilis* aconitase: R741E and Q744E (Gao *et al.,* 2010). While the authors did not purify this protein to test its activities *in vitro*, they demonstrated that strains expressing this mutant *citB* allele exhibited higher levels of *citB-lacZ* expression, aconitase protein, and aconitase activity in cell extracts. These results agree with ours concerning the *citB5* and *citB7* mutants.

More interestingly, a study in the Gram-negative bacterium *Sinorhizobium meliloti* demonstrates that aconitase (*acnA*) mutants exhibit very poor growth and are outcompeted by psuedorevertants (Koziol *et al.,* 2009). The cause of this phenotype was traced to the overaccumulation of citrate in these strains; a citrate synthase (*gltA*) mutation suppressed the poor growth phenotype.

In addition, there is evidence of aconitase autoregulation in *E. coli*. In a study by Tang *et* al.*,* binding of both aconitase proteins, AcnA and AcnB, to the 3' UTRs of their own transcripts was demonstrated, and this binding resulted in an increase in newly translated AcnA and AcnB proteins in an *in vitro* transcription-translation assay (1999). In addition, aconitase levels were shown to increase in the presence of oxidative stress, despite loss of aconitase activity, suggesting that the apo-Acn proteins activate this autoregulatory loop (Tang *et al.,* 1999).

Chapter 2: Investigation of the regulation of sporulation by aconitase

As described in the Introduction, Alisa Serio discovered a role for aconitase in the regulation of late-sporulation gene expression during her graduate work. I sought to continue this work through a combination of *in vivo* and *in vitro* approaches. The following chapter of this thesis describes my exploration of how aconitase regulates the *gerE* mRNA and the impact of that regulation on cell physiology. Part of this work has been published in the Journal of Bacteriology (Serio, A.W., K.B. Pechter, and A.L. Sonenshein, 2006).

1 The *citB5* mutation causes a delay in GerE protein expression

Serio had identified *gerE* as a gene encoding a sporulation-specific transcription factor that is differentially expressed in the *citB5* mutant. The *citB5* mutant accumulates *gerE* mRNA later in sporulation than does the wild-type strain (Serio *et al.,* 2006a). We hypothesized that this delay in *gerE* mRNA accumulation was due to the lower affinity of the Acn_{citB5} protein for the *gerE* 3' UTR, resulting in its degradation by nucleases. Furthermore, we hypothesized that this would result in a delay in the appearance of GerE protein, which would cause altered expression of GerE-regulated genes of the σ^K regulon. To test this hypothesis, I analyzed GerE protein levels in the *citB5* mutant.

I grew strains AWS144 (wild-type), AWS133 (*citB5*) and EUDC9901 (*gerE* null) in DS medium; since AWS133 is a merodiploid [*citB5*-His_6::pAWS42*(cat)*], the medium for this strain was supplemented with chloramphenicol to prevent loss of the plasmid and the *citB5* allele. *B. subtilis* cells growing in DS medium initiate sporulation at the exit of the exponential growth phase (T_0). Sporulation takes about 7 - 8 hours, and the *gerE* mRNA is transcribed late in the process (Cutting *et al.,* 1986). Therefore, beginning at 6 hours after T_0, I took samples every 30 minutes and harvested the cells by centrifugation. To obtain the same number of cells per sample, I measured the A_{600} and then took a sample equivalent to 5 ml cells at A_{600} = 1.0. I treated the cells with lysozyme to generate cell extracts, boiled them in SDS-PAGE sample buffer, clarified the samples by centrifugation and analyzed equivalent volumes (representing an equal number of cells)

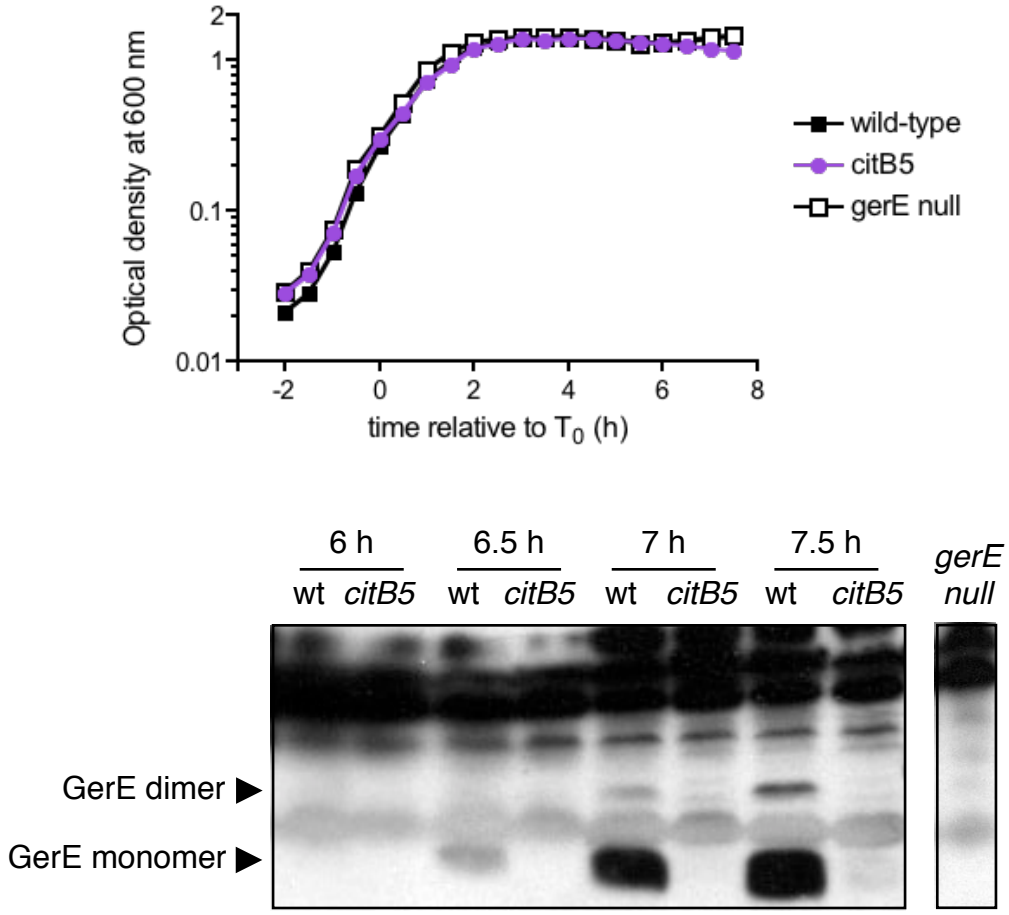

Figure 34. GerE protein expression during sporulation in the *citB5* mutant. Strains AWS144 (*citB*$^{+}$), AWS133 (*citB5*) and EUDC9901 (*gerE* null) were grown in DSM to initiate sporulation (top). Cell lysates were isolated from stationary phase cultures and analyzed by SDS-PAGE and Western blot with polyclonal antibody raised to *B. subtilis* GerE (bottom). Times are expressed as hours after T_0. Cell extract from the *gerE* null at T = 7.5 is presented as a control for antibody specificity. GerE dimer and monomer are indicated by the arrows.

by immunoblotting with polyclonal antibodies raised against GerE (Kuwana *et al.,* 2004). In Figure 34, a representative blot is shown. There are several cross-reacting bands on this blot that serve as loading controls. Both GerE monomer and a small amount of SDS-resistant GerE dimer are indicated by the arrows. By 6.5 hours after T_0, GerE protein was visible in the wild-type strain, but not in the *citB5* mutant strain. The level of GerE protein in the wild-type strain continued to rise at the 7 and 7.5 hour time points. However, the *citB5* mutant did not begin to accumulate GerE protein until one hour after the wild-type strain; at the 7.5 hour time point, a faint, diffuse band is present.

This result, along with Serio's data indicating a delay in the appearance of *gerE* mRNA in the *citB5* mutant, strongly support a role for aconitase in the regulation of the *gerE* message. In addition, as discussed in the Introduction, Serio demonstrated that purified His_{10}-Acn binds to the *gerE* 3' UTR *in vitro*, but His_{10}-Acn_{citB5} does so with lower affinity. The following sections of this chapter describe my work to define a binding site for Acn on the *gerE* mRNA.

2 Approximation of the *gerE* 3' terminus

To begin my search for an aconitase binding site on the *gerE* mRNA, it was first necessary to define the limits of the *gerE* transcript. In a study by Cutting *et al.* (1986), the authors identified by Northern blotting a *gerE* transcript. The authors estimated the transcript to be approximately 300 nucleotides (n) in length. Given the diffuse nature of the bands, however, it was difficult to be certain of that measurement. Furthermore, if the 300 n result were correct, the *gerE* 3' UTR would have to be very short, likely less than 50 n, a factor that would significantly limit the possible aconitase binding sites. In the hope of obtaining a more definitive result, I used two different approaches to determine the *gerE* 3' terminus.

2.1 The *gerE* transcript extends to the beginning of *ysmB* by RNase protection

To determine the 3' terminus of the *gerE* transcript, I utilized an RNase protection assay (RPA). RNase protection involves annealing total cellular mRNA to a radioactive antisense RNA probe that corresponds to a specific mRNA of interest. After annealing, the mixture is digested with RNase T2, which specifically degrades single stranded RNA. The digested mixture is then run on a denaturing gel and the radioactive signal is detected. Any resulting bands are the result of the presence of the mRNA of interest, which anneals to the radiolabelled probe and prevents its digestion by RNase T2. This technique can be used to approximate the 3' end of a transcript if the probe is designed to be longer than the expected transcript; the molecular weight of the RNase-resistant fragment allows one to deduce the 3' end.

In my case, I needed an antisense probe that would anneal to the *gerE* 3' UTR and extend beyond the expected 3' end of the *gerE* mRNA. To do this, I digested pAWS60 with XcmI, gel-purified the product, and performed *in vitro* transcription from the T7 promoter to produce an RNA probe. It is important to note that the 5' end of this probe is not homologous to *gerE*: there are 15 bp between the T7 promoter and the 3' end of the *gerE* construct on pAWS60 that are included in the antisense probe. To create molecular weight markers of known size (155, 216, 266 bases), I separately digested pAWS60 with three other restriction enzymes (BseRI, NdeI, EcoNI) and generated RNAs by *in vitro* transcription using the T3 RNA polymerase and the digested plasmids as templates.

To obtain wild-type RNA for analysis by RPA, I grew strain JH642 in DS medium and harvested cells 5 and 6 hours after the initiation of sporulation (T_o). I prepared RNA from these samples and hybridized the total RNA to the radiolabelled antisense *gerE* 3' UTR probe described above. The RNA hybrids were then digested with RNase T2 and run on a denaturing acrylamide gel along with undigested sample (Figure 35). The first

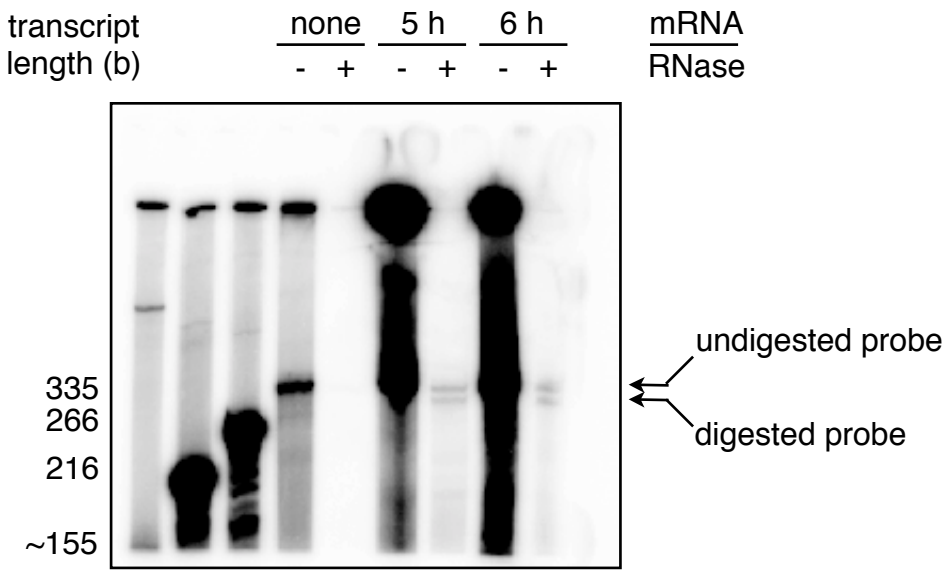

Figure 35. The *gerE* transcript extends beyond the start codon of *ysmB* by RNase protection assay. RNA was prepared from sporulating cultures of strain JH642 (wild-type) at the indicated time points. Total cellular RNA was hybridized to a radiolabelled antisense RNA probe generated by *in vitro* run-off transcription of the pAWS60 plasmid disgested by XcmI using T7 RNA polymerase. The RNA hybrid was digested with RNAse T2, which degrades single-stranded RNA. Digested and undigested samples were run on a denaturing polyacrylamide gel and RNA was detected using a phosphorimager. Molecular weight markers were generated from *in vitro* run-off transcription of pAWS60 digested with BseRI, NdeI and EcoNI.

three lanes are the RNA markers, and the lengths of these and the undigested probe (no mRNA, no RNase) are indicated to the left of the gel. When RNase was added to the probe alone, it was completely digested. When mRNA from the 5 or 6 hour time point was hybridized to the probe, two bands were visible in the digested (+RNase) sample. The top band corresponded to the undigested probe (335 b). The bottom band of the doublet was slightly shorter than the undigested probe. Recall that 15 bases of the probe were not homologous to *gerE* and therefore were not protected by hybridization. The smaller band was likely to be caused by the digestion of those exogenous 15 b. Therefore, from this experiment I concluded that the *gerE* transcript must extend at least to the end of the pAWS60 probe; i.e., the *gerE* transcript extends at least to the start codon of *ysmB*. In order to bolster this conclusion, I used a second approach to approximate the *gerE* 3' terminus: RT-PCR.

2.2 The *gerE* transcript extends to the beginning of *ysmB* by RT-PCR

To approximate the *gerE* 3' terminus using RT-PCR, I used the RNA samples described above to generate *gerE*-specific cDNA with four different oligos: gerER, OKP22, OKP20, and ysmBR2. In addition, a 16S rRNA specific primer, rRNA16SR, was used for cDNA synthesis. As shown in the diagram at the top of Figure 36, the four *gerE*-specific primers anneal to increasingly downstream portions of the *gerE* 3'UTR; the final primer, ysmBR2, anneals after the stop codon of *ysmB*. After first-strand cDNA synthesis with these reverse primers, the gerEFRT forward primer was used in conjunction with each of the reverse primers in separate reactions to amplify any cDNA present for detection by agarose gel electrophoresis. For each reaction, product would indicate a continuous transcript from gerEFRT to that particular reverse primer.

The bottom half of Figure 36 displays the results of this experiment for two RNA samples from strain JH642 (4 h, 5 h). On the bottom left panel, the control genomic DNA reactions, indicating expected product size, are shown. In the middle panel are the reactions using the JH642 4 hour cDNA as a template. Notice that product was obtained

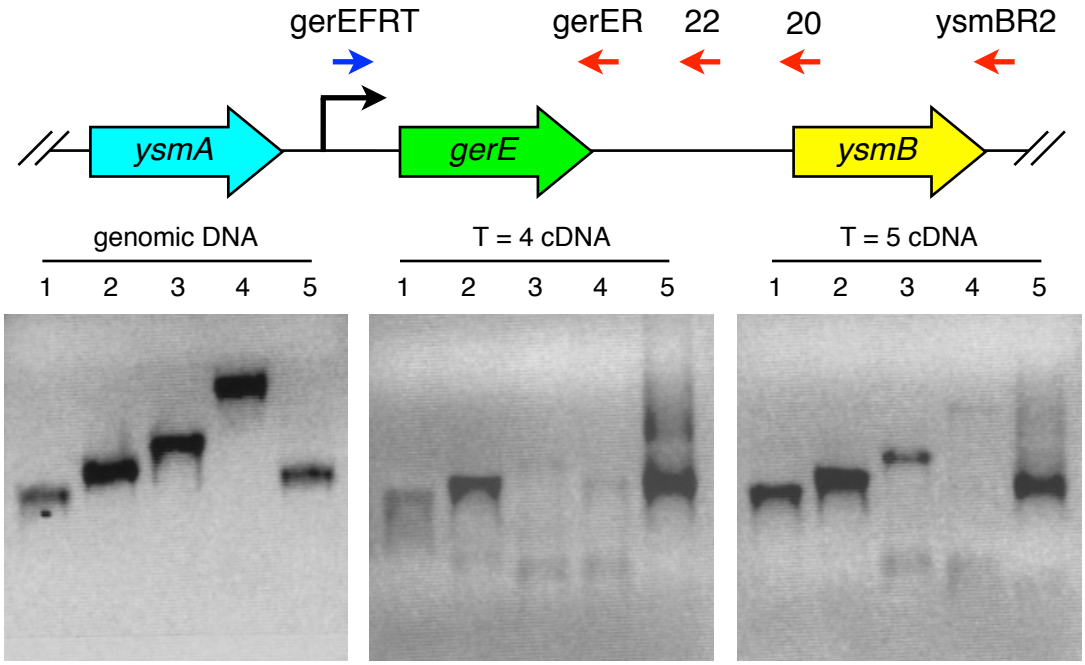

Figure 36. The *gerE* transcript extends beyond the start codon of *ysmB* by RT-PCR. RNA was prepared from sporulating cultures of strain JH642 (wild-type) at the indicated time points. cDNA was generated using Superscript II reverse transcriptase (Invitrogen) and the reverse primers gerER, OKP22, OKP20, ysmBR2 and rRNS16SR. The gerEFRT forward primer was used along with the reverse primers to amplify the cDNA products in a PCR reaction. The products were visualized by agarose gel electrophoresis. Templates used are indicated above each gel panel. The lane numbers indicate reactions with reverse primers: 1, gerER; 2, OKP22; 3, OKP20; 4, ysmBR2. Reaction 5 was performed with control 16S rRNA primers rRNA16SF and rRNA16SR. Primers OKP22 and OKP20 are abbreviated 22 and 20, respectively.

for the first two *gerE*-specific reactions (gerEFRT and gerER; gerEFRT and OKP22) but not for the last two (gerEFRT and OKP20; gerEFRT and ysmBR2). The 16S rRNA control reaction shows a positive result. Negative control reactions, performed with total RNA to demonstrate a lack of genomic DNA contamination, are not shown here but did not produce product. In the bottom right panel, the *gerE* and 16S rRNA reactions were repeated with the 5 hour time point cDNA as template. At this time point, there was ample product visible for the first three reactions (through OKP20) and a faint band for the ysmBR2 reaction.

This result indicates that the *gerE* transcript extends at least to the annealing site of the OKP22 primer at the 4 hour time point in the JH642 strain. It also indicates that at the 5 hour time point, the *gerE* transcript extends (at least in some of the molecules) to the site of the ysmBR2 primer, at the end of the *ysmB* gene. Knowing that the *gerE* transcript includes these sequences allowed me to manipulate the *gerE* RNA to look for possible binding sites of aconitase.

3 Role of *gerE* stem-loop sequences in GerE expression and function

Given the similarity of *B. subtilis* aconitase to the eukaryotic IRP1 protein, we hypothesized that the binding site for aconitase would be similar to that of the iron response element (IRE) stem-loop structures to which IRP1 binds. In Figure 37, two putative stem-loop sequences in the *gerE* 3' UTR, designated SL1 and SL2, are described. The SL2 stem-loop was identified by Alisa Serio and was the putative target she suggested was responsible for the *in vitro* binding of aconitase to the *gerE* 3' UTR RNA (Serio *et al.,* 2006a). I identified the SL1 stem-loop sequence using Mfold, an RNA secondary prediction algorithm (Zucker 2003). The locations of the SL sequences on the *gerE* RNA are indicated; SL1 is just 9 bp downstream from the stop codon of *gerE*, while SL2 is 58 bp downstream from the *gerE* stop. In Figure 38, the predicted structure of each stem-loop is shown in comparison to the known consensus sequences and

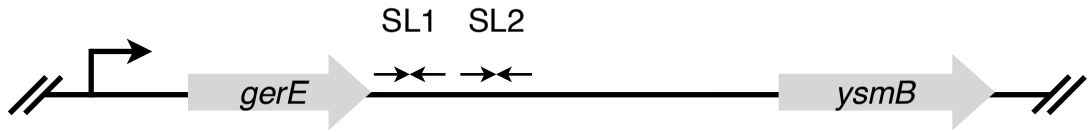

gerE ORF >>> UTR SL1 SL2

5′GAGCTAGAGCTTtaatccttgccggtattccttctttggaaggagccggttattgctgtttgtttggaacattcgaaaccatatttggaatgctgtg

3′

Figure 37. Two putative stem-loop structures in the *gerE* 3' UTR. The *gerE* locus is shown in cartoon representation (top) along with the sequence of the last several codons of the ORF and first portion of the 3' UTR (bottom). The sequences of the putative stem-loop structures SL1 and SL2 are underlined; they are represented by inverted arrows in the cartoon, which is not to scale. In addition, the downstream *ysmB* gene, encoding a hypothetical protein, is shown.

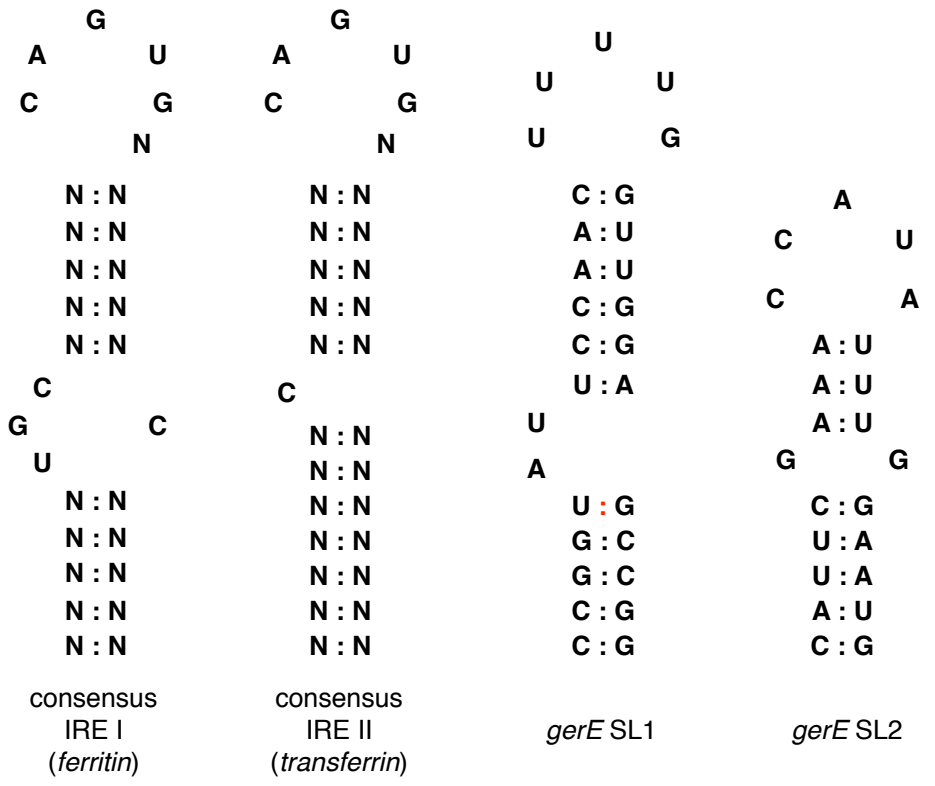

ΔG (kCal/mol)	(*-3.8*)	(-6.7)	-17.5	-4.7

Figure 38. Comparison of the putative *gerE* stem-loops and eukaryotic IRE sequences. Comparison of sequence and structure of eukaryotic IRE consensus forms and putative *gerE* stem-loops (SL). Gibbs free energy values were computed using Mfold (Zucker 2003). Parentheses surround the free energy values for the IRE consensus sequences to highlight that they were calculated from the human ferritin and transferrin sequences.

structures of the two IRE types, ferritin-like and transferrin-like. In addition, the Gibbs free energy (ΔG) of each structure, as calculated by Mfold, is shown. All of the structures have negative ΔG values, indicating that they are energetically favorable under the conditions of the calculation (37°C, 1 M total concentration univalent cations) (Zucker 2003).

Given the proximity of the SL1 and SL2 sequences with the *gerE* stop codon and their similarities to the eukaryotic IRE structures, I hypothesized that one or both of the stem-loop structures could serve as the binding site for aconitase. Since altering the ability of aconitase to bind *gerE* mRNA led to a delay in appearance of GerE, we hypothesized that deleting the site of binding would have the same effect. Thus, to study the contribution of the SL1 and SL2 stem-loops to the aconitase:*gerE* interaction, I removed these sequences genetically and looked at the effect of those mutations *in vivo*.

3.1 Construction of the *gerEΔSL1* and *gerEΔSL2* mutants

To create *gerE* mutants that lacked either SL1 or SL2, I mutagenized the *gerE* 3' UTR using site-directed mutagenesis. I created three constructs: *gerE*$^+$, *gerEΔSL1*, and *gerEΔSL2*. Each construct contains the *gerE* gene flanked by approximately 250 bp of upstream and downstream sequence. The *gerE*$^+$ construct contains the wild-type 3' UTR sequence. To create the *gerEΔSL1* construct, I used mutagenic primers to remove a 31 bp sequence encompassing the 29 bp SL1 sequence (plus one base-pair at each end). Similarly, for the *gerEΔSL2* construct I used mutagenic primers to remove the 27 bp SL2 sequence. For each of these constructs, the *gerE* coding sequence is unchanged. The *gerE*$^+$, *gerEΔSL1*, and *gerEΔSL2* constructs were each ligated to an integrative *B. subtilis* vector, pHK23 (Belitsky *et al.,* 2008), which contains upstream and downstream sequences of the *amyE* gene flanking a multiple cloning site and *erm* resistance cassette. The resulting plasmids (pKP11, pKP16, and pKP7) were introduced into a *gerE* null strain of *B. subtilis* (KBP9) at the non-essential *amyE* locus by homologous recombination. The loss of amylase activity due to the *amyE* insertion was confirmed in

transformants using a starch test. Additionally, the genotype of the resulting strains KBP15 (*gerE::kan amyE::gerE*$^+$), KBP24 (*gerE::kan amyE::gerEΔSL1*), and KBP11 (*gerE::kan amyE::gerEΔSL2*) was confirmed by PCR amplification of genomic DNA and subsequent DNA sequencing.

3.2 The SL1 sequence is required for proper GerE expression, SL2 is not

To analyze the effect of the *gerEΔSL2* mutation, I grew strains AWS96 (wild-type), KBP9 (*gerE* null), KBP15 (*gerE*$^+$) and KBP11 (*gerEΔSL2*) in DS medium and took samples every hour between 5 and 9 hours after T_0 as described for the GerE detection experiments above. As before, samples were analyzed by immunoblot using polyclonal antibodies raised against GerE. Note that the strains designated *gerE*$^+$ and *gerEΔSL2* have the only functional copy of *gerE* at the *amyE* locus. The strain marked "wild-type" has the *gerE*$^+$ allele at the *gerE* locus. As shown in Figure 39, GerE expression in the *gerEΔSL2* mutant was no different than in the *gerE*$^+$ complemented strain. Both the *gerE*$^+$ complement and *gerEΔSL2* mutant exhibited slightly lower expression than the wild-type strain at the 6 hour time point, but at the later time points the GerE expression levels in these strains were indistinguishable from one another. This experiment indicates that SL2 is not important for GerE protein accumulation during sporulation. If perturbation of the aconitase:*gerE* interaction is sufficient to cause a delay in GerE protein accumulation, as seen in the *citB5* mutant, then the SL2 sequence cannot be the binding site for aconitase.

To perform the analogous experiment for the *gerEΔSL1* strain, I grew strains AWS96 (wild-type), KBP9 (*gerE* null), KBP15 (*gerE*$^+$), KBP24 (*gerEΔSL1*) in DS medium and took samples every hour between 6 and 9 hours after T_0 as described above. In this case, I generated cell extracts by sonication, clarified the extracts by centrifugation, and measured the total protein concentration using the Bradford assay. I analyzed equivalent amounts of protein (5 μg) by immunoblot and detected GerE as described above. The results of this experiment can be seen in Figure 40. Strikingly, at the 6 and 7 hour time

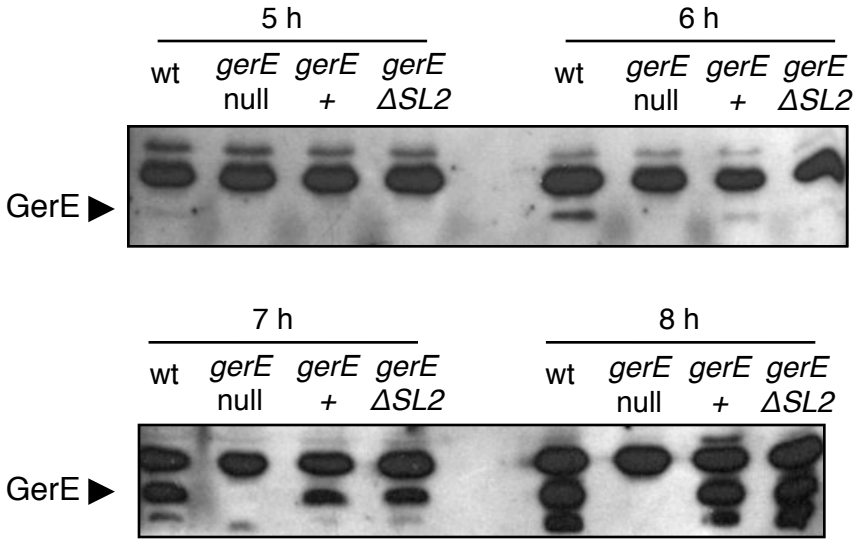

Figure 39. GerE protein expression in the *gerEΔSL2* mutant. Strains AWS96 (wild-type), KBP9 (*gerE* null), KBP15 (*gerE*$^{+}$), and KBP11 (*gerEΔSL2*) were grown in DSM to initiate sporulation. Cell lysates were isolated from stationary phase cultures and analyzed by SDS-PAGE and Western blot with polyclonal antibody raised to *B. subtilis* GerE. Times are expressed as hours after T_0. The arrows indicate GerE.

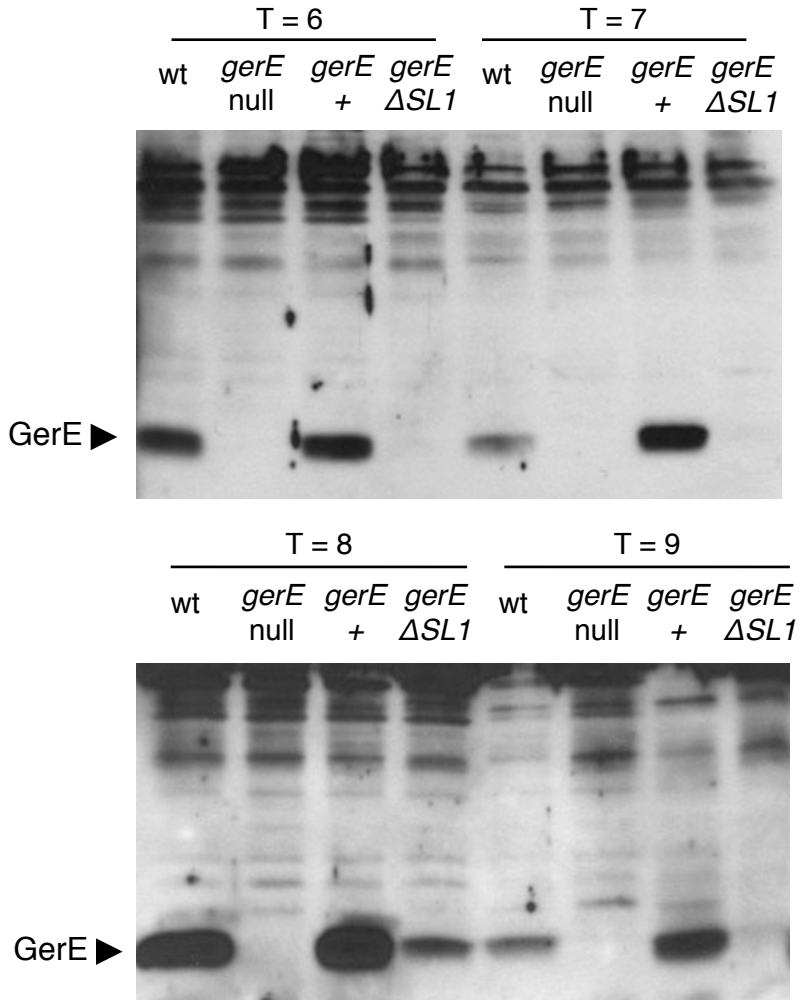

Figure 40. GerE protein expression in the *gerEΔSL1* mutant. Strains AWS96 (wild-type), KBP9 (*gerE* null), KBP15 (*gerE*$^{+}$), and KBP24 (*gerEΔSL1*) were grown in DSM to initiate sporulation. Cell lysates were isolated from stationary phase cultures and analyzed by SDS-PAGE and Western blot with polyclonal antibody raised to *B. subtilis* GerE. Times are expressed as hours after T_0. The arrows indicate GerE. A representative experiment of 2 is shown.

points GerE was visible in the wild-type and *gerE*$^{+}$ strains, but not in the *gerEΔSL1* mutant. At the 8 hour time point, a low level of GerE was visible in the *gerEΔSL1* mutant strain, but in the 9 hour sample for the same strain there was barely any detectable GerE protein. These data demonstrate that the *gerEΔSL1* mutant exhibited altered GerE protein levels compared to the *gerE*+ strain in sporulating cultures, indicating that the SL1 sequence is required for proper GerE protein accumulation during sporulation.

3.3 The SL1 sequence is not required for proper spore formation

After discovering the altered kinetics of GerE protein accumulation in the *gerEΔSL1* mutant strain, we questioned what effect this would have on the formation of viable spores. To explore this, we first considered the phenotype of a *gerE* null mutant.

The GerE protein is necessary for the activation and repression of a host of genes involved in the late stages of sporulation (Eichenberger *et al.,* 2004), and *gerE* null cells exhibit a defective spore coat (Moir *et al.,* 1979). Despite published work to the contrary (Moir 1981), this spore coat defect correlated with in a mild heat-resistance defect in *gerE* null spores in my hands (see below). A stronger phenotype was found in a recent study in which Ghosh *et al.* (2008), demonstrated that *gerE* null spores exhibit a dramatic defect in sodium hypochlorite (NaClO, or more commonly, bleach) resistance . Given this knowledge, I chose to test the resistance of *gerEΔSL1* spores to sodium hypochlorite.

To measure the effect of the *gerEΔSL1* mutation on NaClO-resistance, I grew strains AWS96 (wild-type), KBP9 (*gerE* null), KBP15 (*gerE*$^{+}$) and KBP24 (*gerEΔSL1*) in DS medium and took samples 7 hours after T_0. Four samples were taken for each strain, and sample volumes were normalized so each was equivalent to 1 ml cells at an OD_{600} of 1.0. The cells were pelleted by centrifugation and then resuspended in 1 ml buffer (50 mM KPO_4, pH 7) containing NaClO at three different dilutions of a 5.25% commercial stock: 10^{-2}, 10^{-3}, and 10^{-4}. The remaining sample was treated with buffer alone to provide a total viable count control. The cell suspensions were incubated at room temperature for

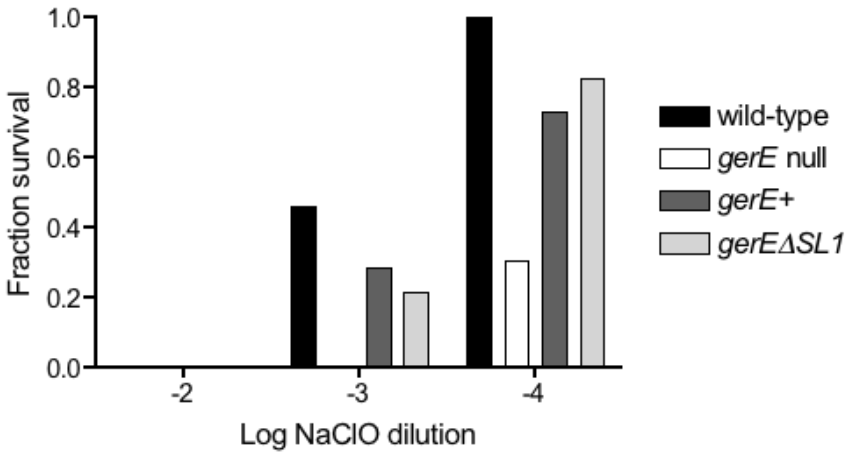

Figure 41. The *gerE* SL1 sequence is not required for NaClO-resistant spore formation. Strains AWS144 (wild-type), AWS133 (*citB5*), KBP9 (*gerE* null), KBP15 (*gerE+*) and KBP24 (*gerEΔSL1*) were grown in DS medium. Samples were taken 7 hours after the initiation of sporulation (T_0). Samples were treated with the indicated dilutions of a commercial stock of NaClO (5.25%) and quenched with sodium thiosulfate prior to plating to determine NaClO-resistant CFU.

15 minutes and then diluted 1:10 in sodium thiosulfate (1%) to quench the NaClO. The quenching reactions were incubated at room temperature for 10 minutes. Samples were serially diluted further in dH2O and plated on DS medium to determine NaClO-resistant and total colony forming units (CFU). All strains demonstrated total viable CFU between 1 and 2 x 10^8, making it possible to compare the fraction of total viable CFU that survived NaClO treatment between different strains. The results of this experiment are shown in Figure 41. Notice that at the highest concentration of NaClO tested (10^{-2} dilution), none of the strains survived NaClO treatment. However, treatment with the 10^{-3} dilution of NaClO resulted in ~50% survival in the wild-type spores and <1% survival in the *gerE* null strain. This defect could be partially complemented by the addition of the *gerE*+ allele at the *amyE* locus in strain KBP15 (*gerE*$^+$); this strain did not reach wild-type levels of NaClO resistance but the phenotype was in stark contrast with the *gerE* null strain. The *gerEΔSL1* demonstrated survival levels nearly identical to those of the *gerE*$^+$ strain. At the lowest concentration of NaClO (10^{-4}) tested, the wild-type strain was 100% resistant, while the *gerE* null survival level was 30%. The *gerE*$^+$ and *gerEΔSL1* strains exhibited an equally intermediate phenotype. These data indicate that the *gerEΔSL1* strain is not defective in NaClO-resistant spore formation, suggesting that the GerE protein accumulation defect does not manifest in sporulation defect as measured by this assay.

4 The SL1 sequence is not required for His_{10}-Acn binding to *gerE* RNA *in vitro*

To determine if the SL1 sequence is required for aconitase to bind to the *gerE* 3' UTR *in vitro*, I created a *gerEΔSL1* construct for use as an *in vitro* transcription template. I amplified a 340 bp fragment of plasmid pKP15, which contains the *gerEΔSL1* construct, and ligated it to the pBluescript KS vector, a proprietary Stratagene vector that has T3 and T7 RNA polymerase promoters flanking a multiple cloning site. The resulting plasmid, pKP17, contains the 3' half of the *gerE* open reading frame and the 3' UTR with the SL1 sequence removed. In order to create *gerE* and *gerEΔSL1* templates for *in vitro* run-off transcription, I amplified 462 and 431 bp fragments from pAWS100 and pKP17, respectively, containing the T7 promoter site upstream of the *gerE* sequence. In addition, to create a positive control template, I amplified a 470 bp fragment of pAWS106 containing the T7 promoter and the *fliT* 3' UTR.

To test binding of the *gerE*, *gerEΔSL1*, and *fliT* RNAs to aconitase, I synthesized radiolabelled RNA using the aforementioned PCR products and T7 RNA polymerase. I determined the specific activity of the probes by scintillation counting and combined 0.25 nM RNA with a range of concentrations of wild-type His_{10}-Acn (purification described in Chapter 4) from ~3 - 780 nM. The reactions were allowed to equilibrate prior to filtration through a nitrocellulose membrane as described in Chapter 1. Included in these reactions was 20 μg/ml of yeast tRNA to act as a nonspecific competitor. Two things were evident from these data, which are presented in Figure 42. First, aconitase was able to retain a large fraction of the *fliT* RNA (~90% at the highest concentration of Acn) while only ~30% of the *gerE* RNAs were retained at the same concentration. Second, aconitase bound to the *gerE* and *gerEΔSL1* RNAs with identical affinity. These results suggest that SL1 is not essential for *gerE* binding to aconitase *in vitro*. In addition, they suggest that the aconitase:*gerE* interaction is one of lower affinity than for other targets, such as *fliT*.

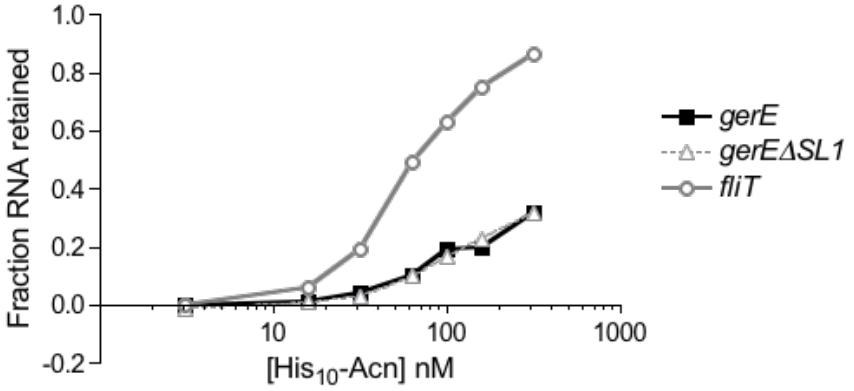

Figure 42. The *gerE* SL1 sequence is not necessary for the aconitase:*gerE* interaction *in vitro*. Radiolabelled *gerE*, *gerESL1* and *fliT* RNA was synthesized by *in vitro* run-off transcription with the T7 RNA polymerase. Each RNA was mixed with increasing concentrations of His10-Acn and the reactions were allowed to equilibrate prior to passage through a nitrocellulose membrane filter. The RNA retained on the filter was detected by scintillation counting, the background counts subtracted, and the fraction of the input RNA calculated. Although the data are from a single experiment, all RNAs were assayed in other experiments and gave similar results.

5 Evidence for targets of aconitase beyond *gerE*

The *gerE* target was originally studied as a means of explaining the sporulation defect in the *citB5* mutant (Serio *et al.,* 2006a). The above experiments have left much doubt as to the importance of the aconitase:*gerE* interaction in sporulation. Could an aconitase-dependent effect on *gerE* be solely responsible for the defect in the *citB5* strain? The two experiments presented below explore this question.

5.1 The *citB5* mutation is epistatic to a *gerE* null mutation in a sporulation assay

One of the clearest ways to clarify the importance of *gerE* in the *citB5* sporulation defect is to look at the phenotypes caused by these two mutations singly and in combination. To do this, I grew strains AWS144 (wild-type), AWS133 (*citB5*), KBP9 (*gerE* null), and KBP10 (*citB5 gerE*) in DS medium and took samples at 7 and 27.5 hours after T_0. I incubated the samples at 80°C for 15 minutes prior to plating on DS medium to determine heat-resistant CFU. The results of this experiment are shown in Figure 43. In my hands, the *citB5* phenotype was not as dramatic as the published values: at the 7 hour time point it had a 5-fold defect in spore formation, while Serio found a difference of nearly 100-fold. It is likely that the difference in results is due in part to the arbitrary designation of T_0; my T_0 may be later than Serio's. Regardless, the phenotype I saw was reproducible. Moreover, the *gerE* phenotype did not resemble the *citB5* defect. The *gerE* null cells sporulated slightly less well than the wild-type strain at the 7 hour time point, but at 27.5 hours the gap widened to a 10-fold difference in heat-resistant spore formation. If a defect in GerE protein accumulation were responsible for the *citB5* phenotype, one would expect the phenotype of the *citB5* mutant to resemble that of the *gerE* null, but it did not. Finally, the combination of these two mutations produced a phenotype nearly identical to the *citB5* mutation alone, indicating that the *citB5* mutation is epistatic to the *gerE* null mutation in reference to the sporulation phenotype.

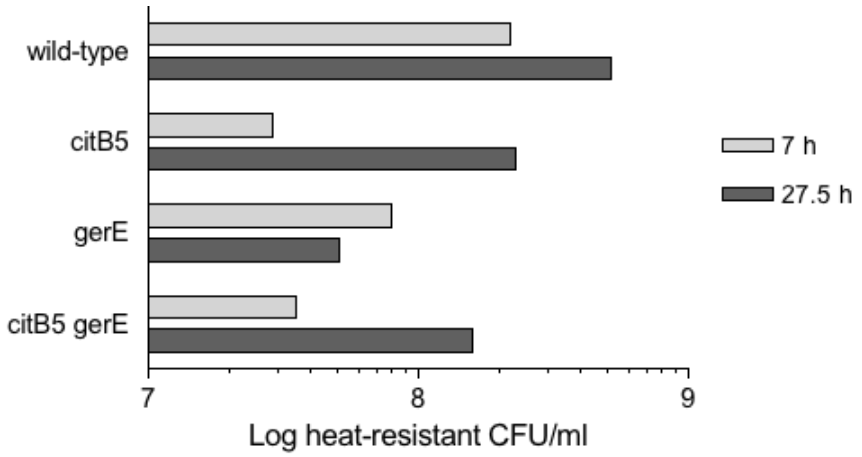

Figure 43. The *citB5 gerE* double mutant sporulation phenotype resembles the *citB5* single mutant. Strains AWS144 (wild-type), AWS133 (*citB5*), KBP9 (*gerE* null) and KBP10 (*citB5 gerE*) were grown in DS medium and sampled at the indicated time points. Samples were incubated at 80°C for 15 minutes prior to plating to determine heat-resistant CFU. Although the data shown are from a single experiment, all strains were assayed in other experiments and gave similar results.

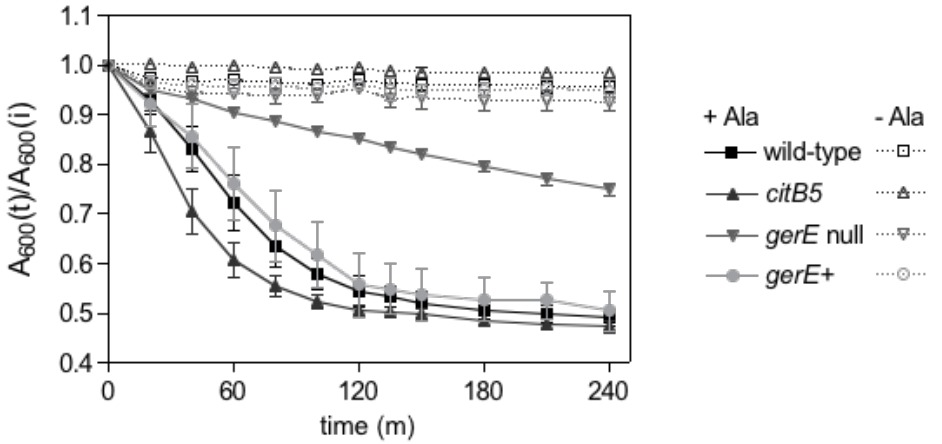

Figure 44. The *citB5* mutant does not possess the characteristic *gerE* null germination defect. Strains AWS144 (wild-type), AWS133 (*citB5*), KBP9 (*gerE* null) and KBP15 (*gerE*$^+$) spores were prepared from DS medium cultures grown for 72 hours. Spores were washed extensively prior to heat activation at 70°C and dilution in room-temperature buffer with or without L-alanine, a *B. subtilis* germinant. The absorbance at 600 nm was measured immediately after dilution and then followed at 20-30 intervals for 4 hours. The ratio of the absorbance at a specific time point compared to the initial absorbance reading was calculated. Results shown are the mean and standard deviation of three independent biological replicates.

5.2 *citB5* spores do not have a germination defect

To further examine the contribution of an aconitase:*gerE* interaction to the *citB5* mutant phenotype, I examined the germination phenotype of the *citB5* mutant. The *ger* loci were so named because mutations in those genes, including *gerE*, exhibit defects in germination assays that measure the loss of absorbance as spores rehydrate and transition from phase-bright to phase-dark (Moir *et al.,* 1979). If *gerE* plays a large role in the *citB5* phenotype, one would expect the *citB5* strain to have a germination defect similar to the *gerE* strain itself.

To test this, I grew strains AWS144 (wild-type), AWS133 (*citB5*), KBP9 (*gerE* null), KBP15 (*gerE*$^+$) in DS medium for ~72 hours to allow the vast majority of cells in the culture to sporulate. I harvested the cultures by centrifugation at 4°C and washed the spores four times in cold deionized water. Heat-activation is commonly used to prepare spores for germination; the mechanism of this effect is not known but likely involves a 'loosening' of the spore coat that gives germination receptors access to solvent (Setlow 2003). I heated spore suspensions to 70°C for 15 minutes and then diluted the spores to A_{600} ~ 0.7 (to keep the assays in the linear range of the spectrophotometer) in 10 mM Tris (pH 8.4) with or without 10 mM L-alanine, a known *B. subtilis* germinant. The dilution and all subsequent steps were performed at room temperature. I then followed the absorbance at 600 nm at 20-30 minute intervals for four hours. These data are presented as the ratio of the absorbance at each time point to the initial absorbance value [$A_{600}(t)/A_{600}(i)$] so that the rate of germination can be compared across strains. In Figure 44, it is apparent that all the spore suspensions maintained a constant absorbance ratio without the addition of germinant. However, for the wild-type, *citB5* and *gerE*$^+$ spores, the addition of L-alanine triggered a drop in the absorbance ratio that continued rapidly over the course of 1-2 hours before leveling off. The *gerE* null spores, in comparison, exhibited a slow, steady decrease in the absorbance ratio over the four-hour experiment. The *citB5* mutant spores clearly did not have a *gerE* null-like germination

phenotype. In fact, the *citB5* mutant exhibited a reproducible hyper-germination phenotype; that is, the *citB5* strain responded more rapidly to the addition of L-alanine. This experiment was performed in triplicate and the *citB5* hyper-germination effect was seen in each individual biological replicate.

It is clear from this experiment that the *citB5* mutant germination phenotype is very different from that seen in *gerE* null spores. Therefore, again it seems unlikely that the *citB5* defect in sporulation is due solely to the aconitase:*gerE* interaction.

6 Discussion

The experiments presented in this chapter have furthered our understanding of the regulation of *gerE* by aconitase in *B. subtilis*, but they have also produced conflicting results.

6.1 The role of SL1 in GerE protein accumulation

Initially, I demonstrated that GerE protein accumulation is delayed in the *citB5* mutant strain. While the GerE protein was first detected 6.5 h after T_0 in the wild-type strain, it was only visible as a faint band 1 h later in the *citB5* mutant. Previous results indicated that *gerE* mRNA begins accumulating ~3.5 h after T_0 (in the published experiment, T_0 occurred at approximately 4 hours of growth), and did not reach comparable levels in the *citB5* strain for another 2 h (Serio *et al.,* 2006a). My results do not offer information on when the GerE protein levels reach comparable levels to the wild-type, if they do so at all. Still, it is clear from the results presented above that the delay in *gerE* mRNA accumulation in the *citB5* mutant reported previously carries over to the GerE protein level.

After establishing that GerE protein accumulation is delayed in the *citB5* mutant, I attempted to define the limits of the *gerE* transcript using RT-PCR and RNase protection, for the purpose of locating an IRE-like element within the 3' UTR. Both experiments suggested that *gerE* mRNA extends beyond the intergenic region between

gerE and the downstream gene, *ysmB*, although the RT-PCR result suggests that the *gerE* mRNA is predominantly monocistronic; the amplification of cDNA for a primer set including the *ysmB* open reading frame was very faint. However, neither of these approaches provided a specific 3' end for the *gerE* mRNA. In eukaryotes, the position of a 5' IRE relative to the mRNA cap is known to be important for preventing translation of target mRNAs, such as ferritin (Goossen *et al.,* 1992). For IREs located in the 3' UTR, the importance of IRE position is less clear; the canonical transferrin RNA exhibits 5 IREs spread out over approximately 1 kb in the 3' UTR (Koeller *et al.,* 1989). Given this, I analyzed the length of the *gerE* 3' UTR (~250 b) for potential stem-loop structures and discovered two with structural similarities to the IRE consensus sequences.

In my *in vivo* experiments with the *gerEΔSL1* and *gerEΔSL2* mutants, deletion of the SL2 sequence had no effect on GerE protein accumulation, but deletion of the SL1 sequence caused a 2 hour delay in the appearance of GerE protein as well as lower total levels of protein. However, my follow-up experiments are not easily reconciled with this *in vivo* result. The *gerEΔSL1* mutation's effect on GerE protein accumulation did not manifest phenotypically in sporulation and germation assays. Furthermore, the absence of the SL1 sequence had no effect on aconitase binding to the *gerE* RNA *in vitro*. However, given the known issues with the N-terminal His_{10}-Acn (see chapter 3) I used in my *in vitro* experiments, it is possible that the aconitase:*gerE* interaction seen in these experiments is not physiologically relevant, and that an untagged aconitase protein could discriminate between the *gerE* and *gerEΔSL1* RNAs. This concern is part of a larger issue, however. How relevant is any His_{10}-Acn interaction previously seen with *gerE*?

6.2 Is the aconitase:*gerE* interaction real?

Alisa Serio demonstrated that N-terminally His-tagged wild-type aconitase protein binds *in vitro* to a fragment of *gerE* RNA containing the 3' UTR. The dissociation constant (K_d) determined for this interaction was ~4 nM, indicating a high level of affinity (2006a). My experiments with untagged aconitase paint a very different picture

of the affinity of this protein for RNA. Aconitase binds to *citZ* and *fliT* with an affinity in the mid-to upper nM range; no specific dissociation constant has been calculated but my experiments suggest it would be on the order of ~250 nM. The approximate K_d I obtained is corroborated by a similar, if slightly stronger, affinity of binding (~100 nM) seen by Claudia Alén in her original analysis of the RNA-binding properties of untagged aconitase (1999), suggesting that the >10 fold increase in affinity for RNA demonstrated by His_{10}-Acn might be due to nonspecific binding of the negatively charged RNA to the positively charged ten histidine residues. In order to test this possibility, a protein with a His tag known not to bind RNA could be tested in a *gerE* binding assay after adding a His_{10} tag.

6.3 *gerE* null sporulation phenotype

Another aspect of the experiments presented above was further clarification of the *gerE* sporulation defect which heretofore had been confusing in the literature. In my hands, the *gerE* null mutant exhibits a reproducible defect in a heat-resistant spore formation. An early study characterizing the *gerE* null mutant found the percent survival of wild-type and *gerE* null cells to heat-treatment (90°C) to be equivalent (Moir 1981). The percent survival is not the best way to present spore formation because total cell viable counts can vary. In fact, the *gerE* null cells produced inconsistent levels of total viable counts in my hands. The NaClO-resistant spore formation assay did not have this issue, suggesting that the permissive conditions in this assay (treatment in phosphate buffer followed by sodium thiosulfate) may protect *gerE* cells and spores from the shock of plating directly onto DS medium plates.

6.4 Does aconitase have multiple sporulation specific mRNA targets?

In this chapter, I presented two pieces of evidence that aconitase has sporulation-specific targets beyond *gerE*. First, I found that a *citB5* mutation is epistatic to the *gerE* null mutation in a sporulation assay. If *gerE* were the only relevant target for aconitase in sporulation, and moreover the target responsible for the phenotype of a *citB5* mutant,

I would expect the situation to be reversed. The complete removal of *gerE* from a *citB5* strain would result in a *gerE* null-like phenotype. Since this was not the case, it is reasonable to assume that the *citB5* mutation has effects beyond *gerE*.

Another result that suggests multiple sporulation-specific targets for aconitase is the different germination phenotypes of *gerE* null and *citB5* strain-derived spores. In fact, these mutations had opposite effects on germination. The *gerE* null appeared to respond very slowly to germinants, while the *citB5* strain exhibited a hyper-germination phenotype. The exact reasons for the *citB5* germination phenotype are unknown, but it is likely that they stem from the altered *cot* gene expression evident in this strain. The *cot* genes, which encode spore coat proteins, are expressed at lower levels than in wild-type cells (Serio *et al.,* 2006a). Perhaps the lower levels of *cot* gene expression during sporulation make mature *citB5* spores more sensitive to germinants. A less dense spore coat could allow greater accessibility of the germination receptors to solvent. However, the coat would still have to be significantly protective to maintain full heat resistance at late time points, as *citB5* spores do not demonstrate any defect in heat-resistant spore formation when assayed post-24 hours. Going forward, it would be interesting to determine if the hypergermination phenotype seen here is specific to germination triggered by L-alanine or if it also applies to the cogerminant combination of L-asparagine, glucose, fructose and potassium ions (Corfe *et al.,* 1994).

To determine all of the direct sporulation-specific targets of aconitase, and to clarify whether or not *gerE* is a target of aconitase *in vivo*, a pull-down approach could be employed. In such an experiment, purified, untagged Acn would be incubated with total *B. subtilis* RNA and Acn:RNA complexes would be isolated using anti-Acn antibodies attached to beads. Alternatively, aconitase could be immobilized on a column and total RNA could be passed over it. RNAs that stay bound after washing would be eluted, perhaps by displacement with citrate. Another possibility is one I describe in the next chapter, i.e., using a modified version of the new purification scheme to detect

aconitase:RNA complexes in cell extracts. In all of these cases, the RNAs detected would be isolated, reverse transcribed to cDNA, and analyzed either by a microarray approach or by using deep sequencing.

Chapter 3: Purification of aconitase from *B. subtilis*

In any complex biological system, the observed phenotype is the result of thousands of molecular interactions. Studying these interactions en masse has great merit, but individual interactions are best studied with purified components. Here I describe two methods for the purification of aconitase. The first makes use of a histidine tag at the amino terminus of the protein; the second is a purification of untagged aconitase protein by using automated Fast Pressure Liquid Chromatography (FPLC) systems.

1 Characterization of N-terminal His-Acn proteins

I first purified aconitase utilizing an amino-terminal decahistidine affinity tag. Previously, a carboxy-terminal hexahistidine tagged version of wild-type aconitase, constructed by Boris Belitsky and modified by Alisa Serio for purification of *citB5* aconitase as used. However, the C-terminal tag did not result in a very pure preparation of aconitase; there were contaminating proteins present that complicated the interpretation of *in vitro* binding assays. In an attempt to circumvent this issue, Serio introduced an N-terminal His_{10} tag to wild-type aconitase and found that the preparation was much more pure than the C-terminally purified proteins. Therefore, I used this approach to purify both wild-type and the C450S mutant discussed earlier. I describe the purification process below, as well as an analysis of the proteins *in vitro* and *in vivo*.

1.1 Purification of wild-type and C450S mutant His-Acn

Briefly, I grew AWS198 [His_{10}-*citB*$^{+}$*::*pAWS50(*cat*)] and KBP55 [His_{10}-*citB2::*pKP12(*cat*)] in DSM supplemented with chloramphenicol to prevent loss of the integrated plasmid. (The construction of strain KBP55 is described in Chapter 1.) I harvested the cells at early stationary phase by centrifugation. The pellets were resuspended in buffer containing a strong reducing agent (0.5 mM DTT) to prevent oxidation of the Fe-S cluster, subjected to two rounds of breakage in a French press, and sonicated to break up genomic DNA. The extract was clarified by centrifugation and dialyzed to remove the dithiothreitol, which can interfere with metal-affinity binding. I

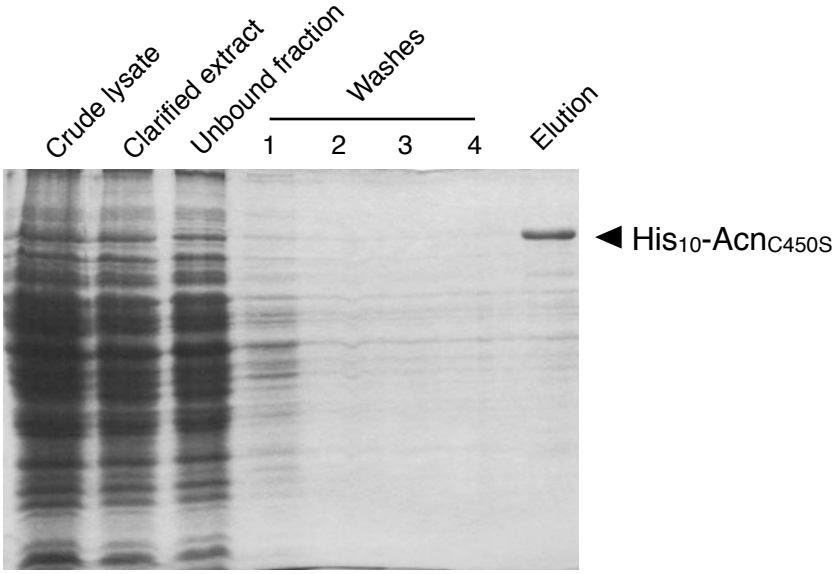

Figure 45. Purification of His_{10}-Acn_{C450S}. Strain KBP55 was grown in DS medium and harvested at the exit of the exponential growth phase by centrifugation. Crude lysate was generated (lane 1), clarified by centrifugation (lane 2) and bound to metal-affinity resin. The unbound fraction (lane 3) was removed by centrifugation and the resin was washed four times in buffer containing 10 mM imidazole (lanes 4-7) to remove non-specific proteins. His_{10}-Acn_{C450S} was eluted in buffer containing 250 mM imidazole (lane 8). Samples were analyzed by SDS-PAGE followed by staining with Coomassie blue.

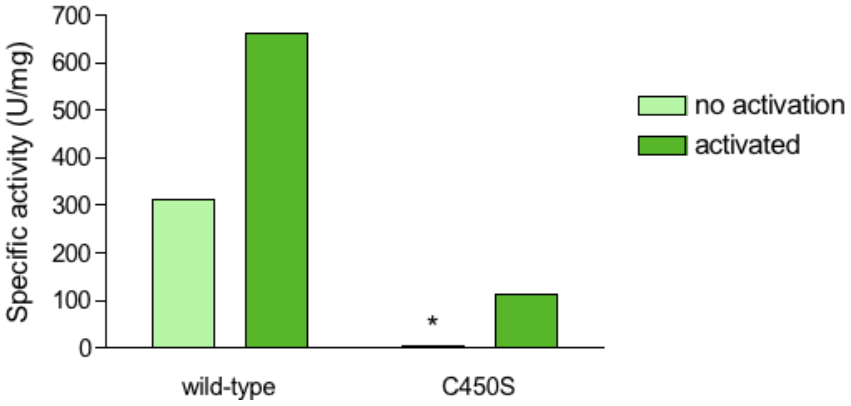

Figure 46. Specific activity of wildtype and C450S His_{10}-Acn. The specific activity of purified wild-type and C450S His10-Acn was measured before and after activation with exogenous Fe and S. The asterisk indicates that the unactivated His_{10}-Acn_{C450S} sample was below the limit of detection of the assay.

incubated the dialyzed lysate with metal-affinity resin in buffer containing β-mercaptoethanol (7 mM) to allow His_{10}-Acn to bind; β-mercaptoethanol is a weaker reducing agent than dithiothreitol and is suitable for use with metal-affinity resins in concentrations below 10 mM. Aconitase was eluted from the resin in buffer containing imidazole, dialyzed against a buffer containing 50% glycerol, and stored at -20°C. I took samples throughout the purification process and analyzed them by SDS-PAGE followed by staining with Coomassie blue to visualize total proteins. A representative gel, depicting the purification of His_{10}-Acn_{C450S}, is shown in Figure 45.

1.2 Specific activity of wild-type and C450S His-Acn *in vitro*

I determined the specific activity of His_{10}-Acn and His_{10}-Acn_{C450S} before and after activation *in vitro* with added reduced iron and sulfur. The results of this experiment can be found in Figure 46. The wild-type His_{10}-Acn protein exhibited a higher specific activity than the His_{10}-Acn_{C450S} protein, which demonstrated residual activity only after activation. Thus, mutation of one of the cluster-ligating cysteine residues results in a substantial loss in aconitase enzyme activity.

1.3 *citB-lacZ* is overexpressed in His-Acn strains *in vivo*

The ease and simplicity of utilizing an N-terminal His_{10} tag made it the obvious choice for purification purposes. However, that changed with an unexpected discovery concerning the *in vivo* phenotype of strains expressing an N-terminally His-tagged aconitase protein. To compare *citB-lacZ* expression in *citB2* and *citB*$^+$ strains to wild-type, I introduced genomic DNA from strain AWS173 into strains AWS198 and KBP55 by transformation. The resulting strains were KBP91 [His_{10}-*citB*$^+$*::*pAWS50(*cat*) *amyE::citBp21-lacZ tet*] and KBP92 [His_{10}-*citB2::*pKP12(*cat*) *amyE::citBp21-lacZ tet*], respectively. In addition, although I did not go on to purify the His_{10}-*citB7* protein, I introduced genomic DNA from strain AWS198 to strain KBP81, producing strain KBP82 [His_{10}-*citB7::*pAWS50(*cat*) *amyE::citBp21-lacZ tet*].

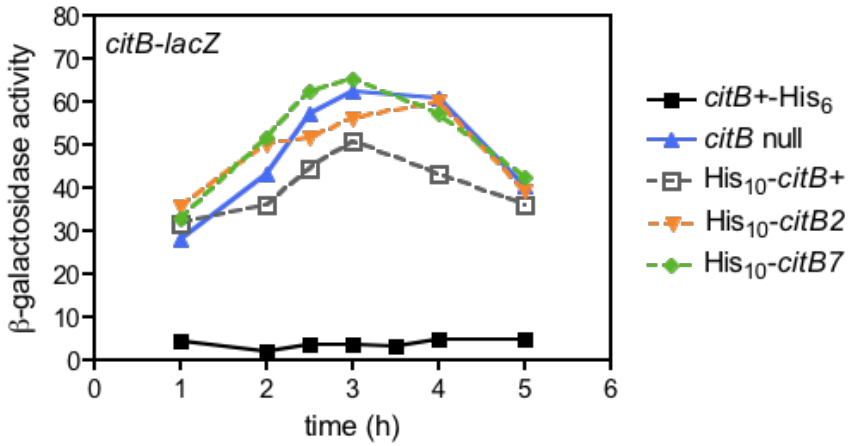

Figure 47. The *citB-lacZ* fusion is hyperexpressed in strains expressing an N-terminal His_{10}-tagged aconitase protein. Strains AWS176 (*citB*$^{+}$-His_6), AWS174 (*citB* null), KBP91 (His_{10}-*citB*$^{+}$), KBP92 (His_{10}-*citB2*), and KBP82 (His_{10}-*citB7*) were grown in DS medium and sampled at the indicated time points to determine β-galactosidase activity. The data shown are from a representative experiment of 2. Overall trends were preserved despite variability in calculated Miller Units.

To measure the expression of *citB-lacZ* in these various mutants, I grew strains KBP91, KBP92, and KBP82 along with strains AWS176 (*citB*$^{+}$-His$_6$) and AWS174 (*citB* null) in DS medium and compared their *citBp-lacZ* expression (Figure 47). It is clear from this experiment that the presence of the N-terminal His$_{10}$ tag on otherwise wild-type aconitase caused an increase in *lacZ* expression to the levels seen in the *citB* null mutant. This increase was specific to the N-terminal tag; the C-terminally tagged strain (*citB*$^{+}$-His$_6$) exhibited low, wild-type levels of *citB-lacZ* expression. There were two possible explanations for the increase seen in the N-terminal His-tagged strains. First, the His$_{10}$-tag might render aconitase enzymatically inactive *in vivo*. However, the enzymatic assay (see above) I performed on the purified His$_{10}$-Acn suggests it is an active enzyme. Furthermore, strain KBP91 (His$_{10}$-*citB*$^{+}$) is a glutamate prototroph, indicating it produces ample aconitase protein to fuel the cell's glutamate requirement. The second possibility is that the overexpression of *citBp-lacZ* seen in Figure 47 is due to a perturbation of RNA-binding by the His$_{10}$ tag. I had no evidence to support or reject this hypothesis, but we discontinued the use of the N-terminal His$_{10}$ tag to study aconitase. While I considered returning to the C-terminal His$_6$ tag approach, I decided to eliminate all tags and purify aconitase using a protocol based on classical techniques with the advantages of modern, automated purification technology.

2 A new, FPLC-based purification scheme for aconitase

To purify aconitase without the use of affinity tags, I turned to classical techniques that exploit the inherent biochemical properties of a specific protein to separate it from the thousands of other proteins present in a cell extract. Luckily, I did not need to develop the purification scheme from scratch: a former member of the lab, Douglas Dingman, purified *B. subtilis* aconitase 25 years ago (1987). As described in the Introduction, Dingman used a combination of ammonium sulfate precipitation, size exclusion chromatography, anion-exchange chromatography, and a final gel filtration

chromatography step to produce a pure preparation of aconitase. I kept the essence of this four-step scheme but modified it for use with the Fast Pressure Liquid Chromatography (FPLC) systems available to me: the Akta (GE Healthcare) and the BioLogic DuoFlow (Bio-Rad). The resulting purification scheme is outlined in Figure 48. In the following section, I detail the new purification protocol with examples of steps from the purification of wild-type, R741E and C450S aconitase proteins.

2.1 Preparation of cells and extracts

To prepare cells for the purification of aconitase, I grew strains KBP94 (wild-type), KBP81 (*citB7*) and KBP22 (*citB2 citZ340*) in DS medium. I used strain KBP22 instead of strain KBP118 (*citB2*) because of consistent problems with reversion in the *citB2* culture population. The culture volumes ranged from 500 ml to 2 L; however, cell extract equivalent to a 500-ml culture was the maximum input volume for the gel filtration step. As is the case with all *B. subtilis* growth experiments reported here, the cultures were vigorously aerated and supplemented with iron. The cultures were harvested in late exponential phase (A_{600} = 0.8 - 1.0) by centrifugation. Cell pellets were washed twice in a 20 mM Tris-citrate buffer (20 mM Tris, 20 mM citrate; pH adjusted to 7.35 with NaOH) prior to storage at -80°C. I thawed the cell pellets and resuspended them in the same buffer. The resuspensions were kept on ice. I used 2 - 3 rounds of passage through a French press to break the cells and then sonicated them to break up genomic DNA. I clarified the cell extracts by centrifugation and then proceeded to the ammonium sulfate precipitation step.

2.2 Ammonium sulfate precipitation

I collected proteins that precipitated with $(NH_4)_2SO_4$ between 40% and 85% of saturation. Ammonium sulfate was added slowly with gentle stirring on ice over a 30 - 45 minute period. To counteract the effect of ammonium sulfate on buffer pH, 5 µl NaOH (1N) was added for every gram of $(NH_4)_2SO_4$ added. I collected the proteins precipitated

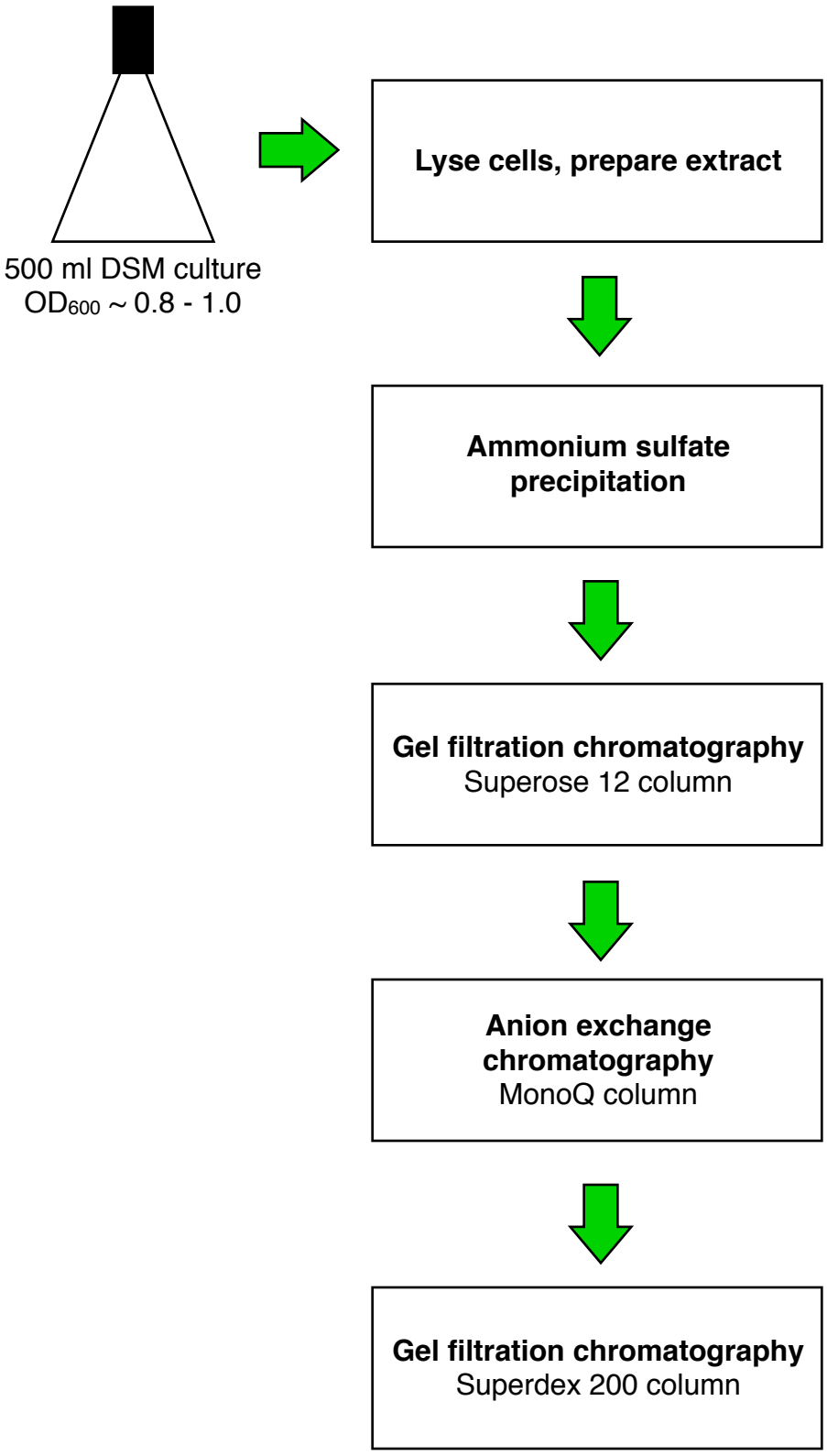

Figure 48. Aconitase purification scheme. The purification scheme for aconitase described in this Chapter is outlined.

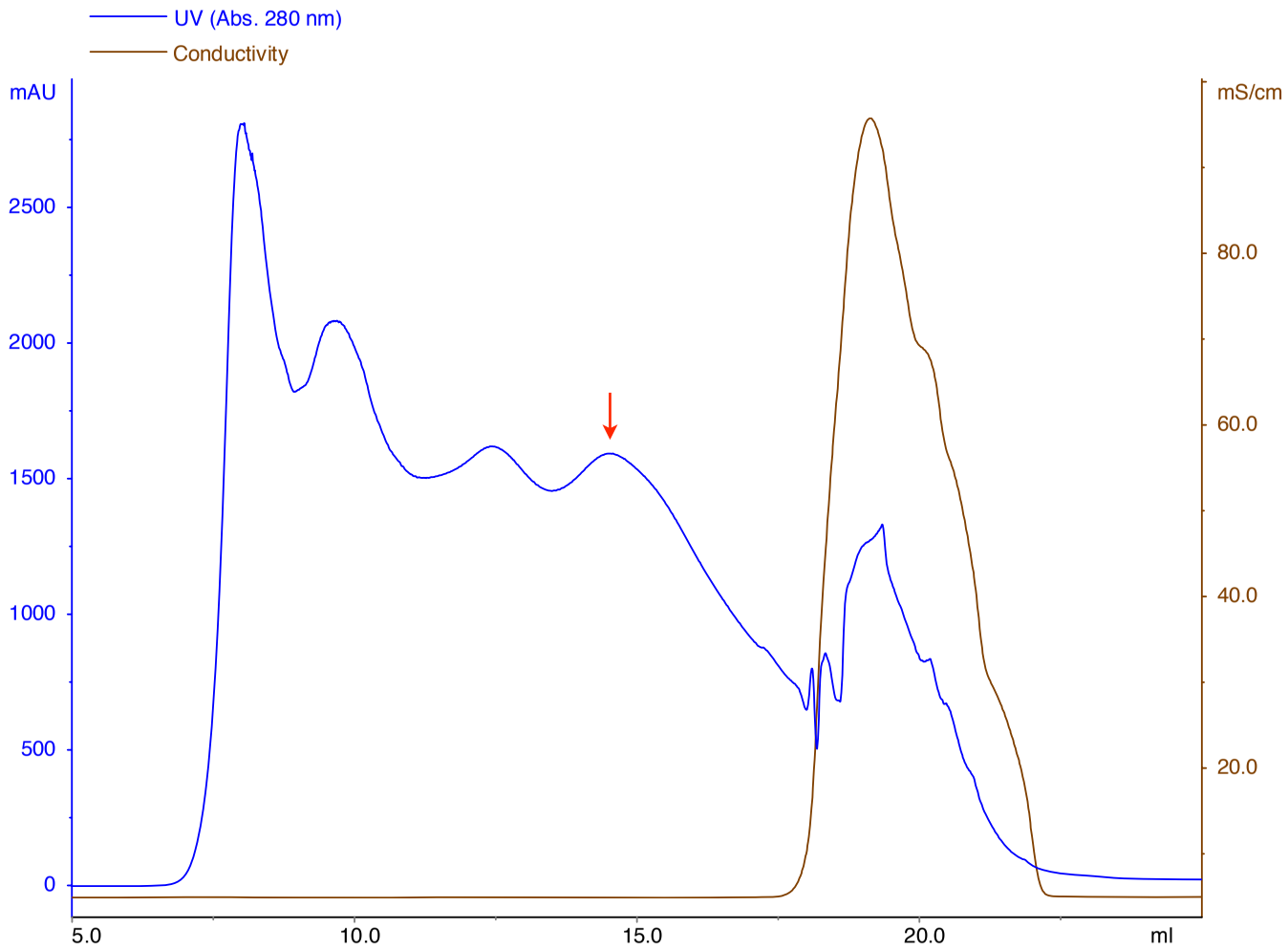

Figure 49. Gel filtration of wild-type *B. subtilis* cell extract via a Superose 12 column. Ammonium sulfate-precipitated proteins were resuspended in 20 mM Tris-citrate (pH 7.35) and injected onto a Superose 12 column connected to an AKTA FPLC system (GE Healthcare). Approximately 1 column volume of the same buffer was used to elute proteins; Aconitase eluted in the peak indicated by the red arrow.

at 85% of saturation by centrifugation, discarded the supernatant, and continued to the gel filtration step with the aconitase-containing pellet.

2.3 Preparations for use of FPLC

Prior to use of the FPLC systems, there were several considerations. First, the redissolved ammonium sulfate pellets were filter-sterilized prior to loading on the Superose 12 column to remove any solid matter that could clog the system. Second, all buffers were filter-sterilized and cooled to 4°C prior to use to remove solid matter and to prevent the injection of air into the system. Next, a volume of 20 mM Tris-citrate (pH 7.35) large enough to accomodate both Superose 12 and MonoQ runs was prepared in a single batch (1 L) to prevent even minute differences in conductivity that might occur in separately prepared batches of buffer. The importance of this is discussed below. Finally, when injecting samples, great care was taken to prevent injecting air into the system.

2.4 Gel filtration chromatography

I used gel filtration to begin separating aconitase from other proteins in the resuspended 85% ammonium sulfate precipitate. By using a Superose 12 column, I could separate very large and very small proteins from aconitase. To do this, I resuspended the ammonium sulfate-precipitate in 20 mM Tris-citrate (pH 7.35). If necessary, I concentrated the resuspension to ~1 ml prior to loading the sample on the Superose 12 column using a 1 ml loop.

The maximum amount of resuspended precipitate injected was equivalent to the precipitate obtained from a 500 ml culture. The protein contained in this 500-ml volume is the largest amount that can be separated efficiently by the Superose 12 column. (Improper separation on the Superose 12 column resulted in certain contaminants remaining in the aconitase-containing fraction that prevented aconitase from binding to the anion-exchange column in the next step of the purification.) Proper separation allowed me to isolate aconitase from those contaminants and to obtain a distinct

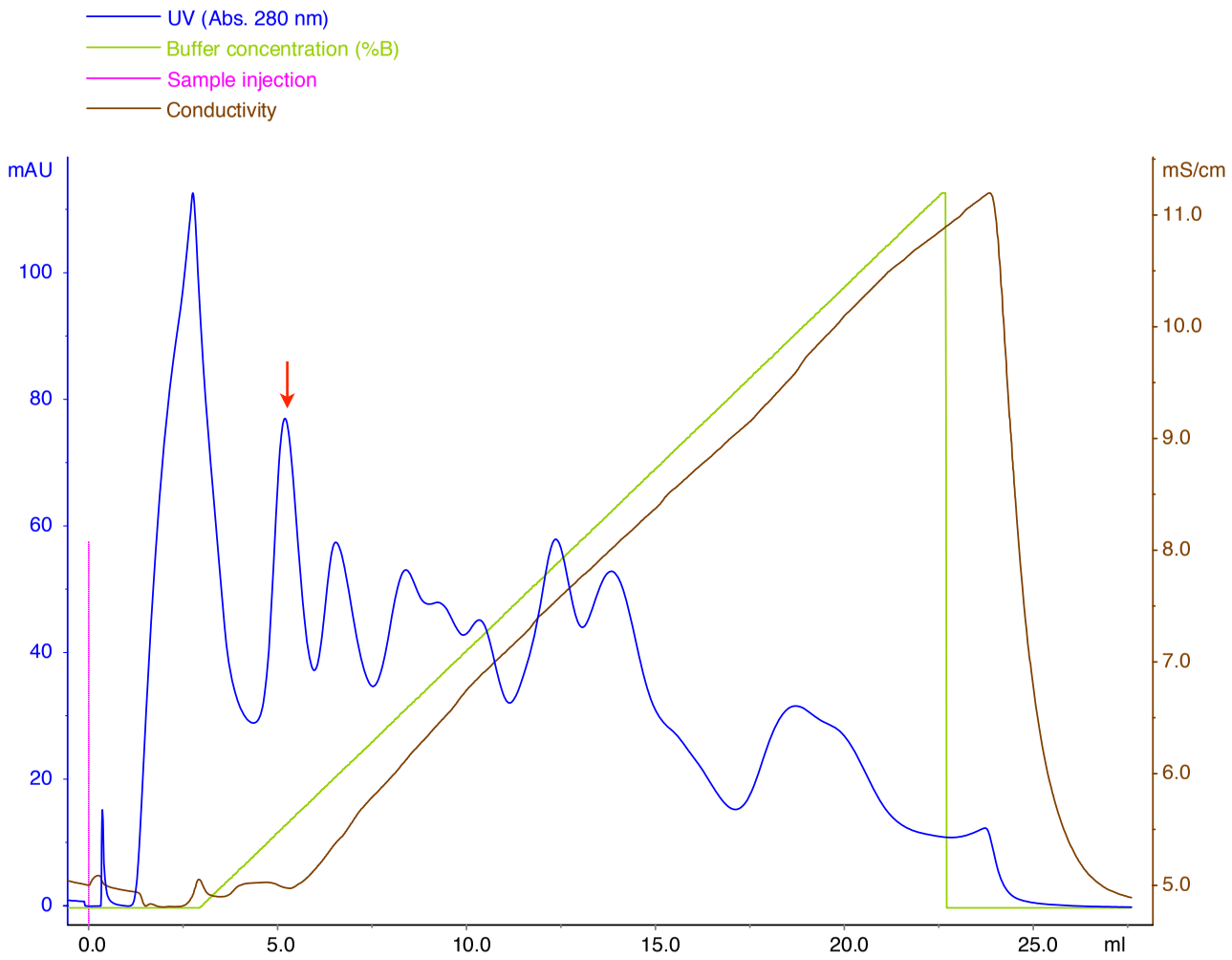

Figure 50. Anion exchange chromatography of wild-type *B. subtilis* cell extract via a MonoQ column. Superose 12 fractions Superose 12 fractions from a $(NH_4)_2SO_4$-precipitated KBP94 cell extract were pooled and injected onto a MonoQ column connected to an AKTA FPLC system (GE Healthcare). A linear gradient of 20 mM - 60 mM Tris-citrate (pH 7.35) was used to elute proteins from the column. The aconitase-containing peak is indicated by the red arrow.

aconitase peak during anion-exchange elution. Therefore, ammonium sulfate precipitates corresponding to a larger volume were divided (for example, into fourths for 2 L) prior to centrifugation and stored at 4°C before independent resuspension and injection in separate Superose 12 runs.

In Figure 49, a representative Superose 12 column run using KBP94 (wild-type) extract is shown. The AKTA system collected 250 µl fractions throughout the run in a 96-well microtiter plate. In addition, the system provided real-time monitoring of the protein concentration and conductivity of the solution with a built-in UV spectrophotometer and conductivity meter. In the case of the KBP94 and KBP81 (*citB7*) samples, I used the aconitase enzyme activity assay to test fractions from each of the absorbance peaks. For KBP22 (*citB2 citZ340*) (enzymatically inactive) cell extracts, I used my knowledge gained from the other two purification schemes to identify candidate fractions and then confirmed the presence of aconitase using an SDS-PAGE gel stained with Coomassie blue. For all samples, aconitase eluted as a component of the final major peak prior to salt elution (see red arrow). In some cases, the UV spectra did not resolve into four separate, pre-salt elution peaks due to a high protein concentration: instead, two major peaks were evident, and aconitase again eluted in the second peak prior to salt elution.

2.5 Anion exchange chromatography

I pooled the Superose 12 fractions containing aconitase (< 1.5 ml total volume) and injected them directly onto the MonoQ column on the AKTA for anion exchange chromatography. The column was washed with 2 column volumes (CV) of 20 mM Tris-citrate (pH 7.35) and eluted with a linear gradient of 20 mM to 60 mM Tris-citrate (both pH 7.35). As in the previous step, 250 µl fractions were collected and I used the UV spectrum to identify candidate fractions and test them by either an enzyme activity assay or by SDS-PAGE analysis with Coomassie blue staining.

In all cases, aconitase binding to the MonoQ column was quite weak and eluted at the very beginning of the gradient. In Figure 50, a representative run of a wild-type sample is shown. The second peak in the UV spectrum contains aconitase; the fraction begins eluting as the linear gradient begins, even before the conductivity meter registers a difference in conductivity in the solution leaving the column. Despite the weakness of aconitase binding, the eluted fraction was extremely pure. In most runs the purity was greater than 90% aconitase on an SDS-PAGE gel. For example, in Figure 51, a representative run of a KBP22 (*citB2 citZ340*) sample was analyzed by SDS-PAGE and Coomassie blue staining to determine the aconitase-containing fractions. The B4 fraction of the MonoQ column contains some smaller molecular weight bands but is overwhelmingly comprised of Acn_{C450S}.

Notably, this purification step provided further evidence that the *citB7* strain overexpresses the aconitase protein. In Figure 52 a representative run of a KBP81 (*citB7*) sample on the MonoQ column is shown. It is evident that the aconitase peak is much larger than in the wild-type strain. In addition, I analyzed the purification of aconitase from KBP81 (*citB7*) by SDS-PAGE and Coomassie blue staining (Figure 51, top). The portion of the cell extract comprised of aconitase is much higher in the *citB7* strain than in the *citB2 citZ340* strain, indicating once again that KBP81 overexpresses aconitase, as discussed in Chapter 1.

Due to the weak binding of aconitase to the MonoQ column, this purification step required special considerations to ensure success. First, the same batch of 20 mM Tris-citrate (pH 7.35) buffer was used for both the Superose 12 and MonoQ column runs for a particular sample. This prevented any differences in conductivity from eluting the aconitase in the “flow-through” fraction of the MonoQ column (the first peak visible on the UV spectrum). Second, the pooled Superose 12 fractions were not concentrated prior to loading on the MonoQ column. Concentration via a spin column resulted in an increase in the conductivity of the sample, causing aconitase to elute in the flow-through

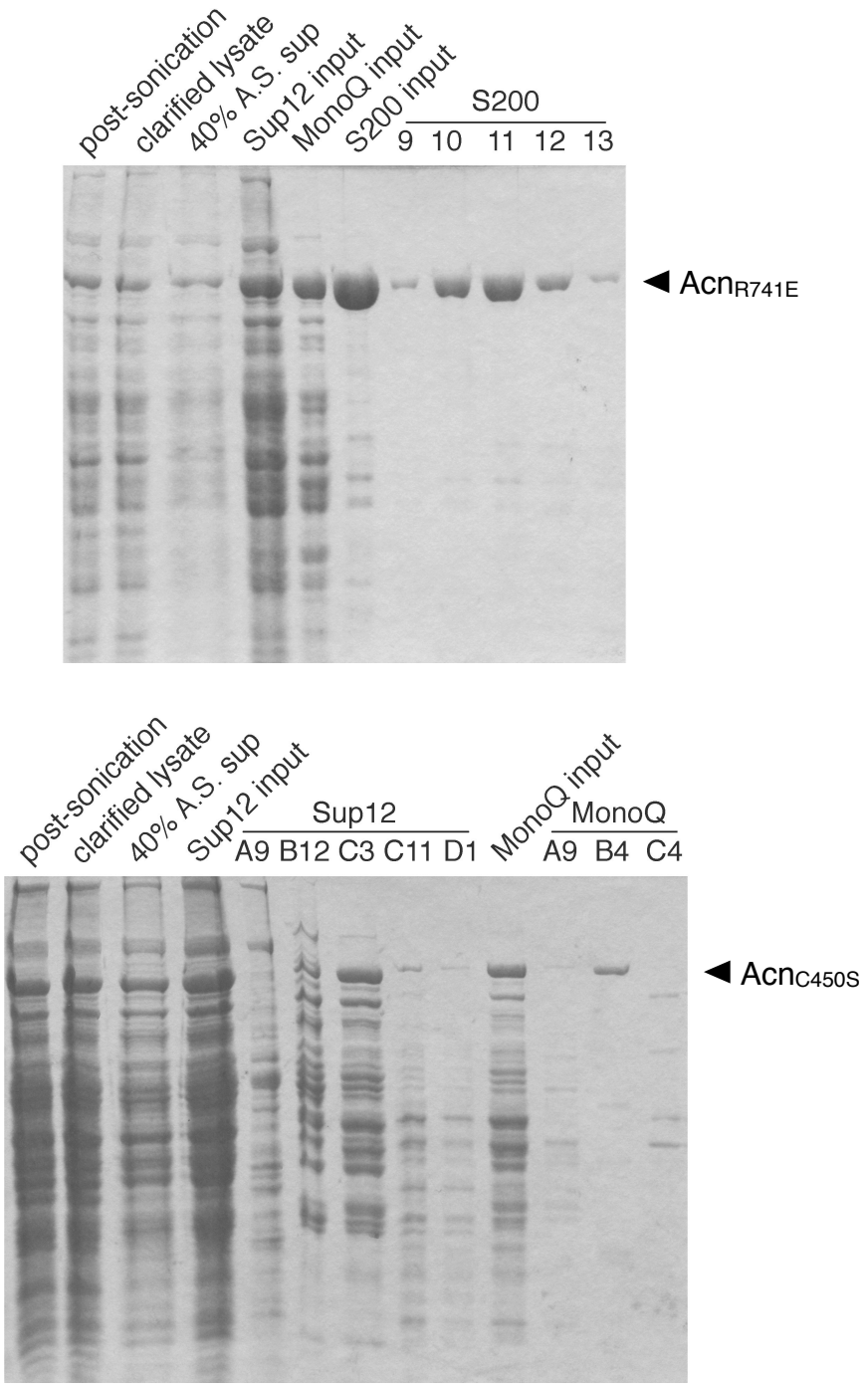

Figure 51. Analysis of the purification of R741E and C450S mutant Acn proteins by SDS-PAGE. Strains KBP81 (*citB7,* top panel) and KBP118 (*citB2*, bottom panel) were grown in DS medium and cells were harvested by centrifugation. Cell extracts were generated and samples were taken during the purification process as noted in lane descriptions. The volume sample analyzed varied between samples to prevent overloading; however, fractions grouped together were analyzed in equal volumes and are directly comparable. Bands corresponding to the aconitase mutants are indicated by the labeled arrows.

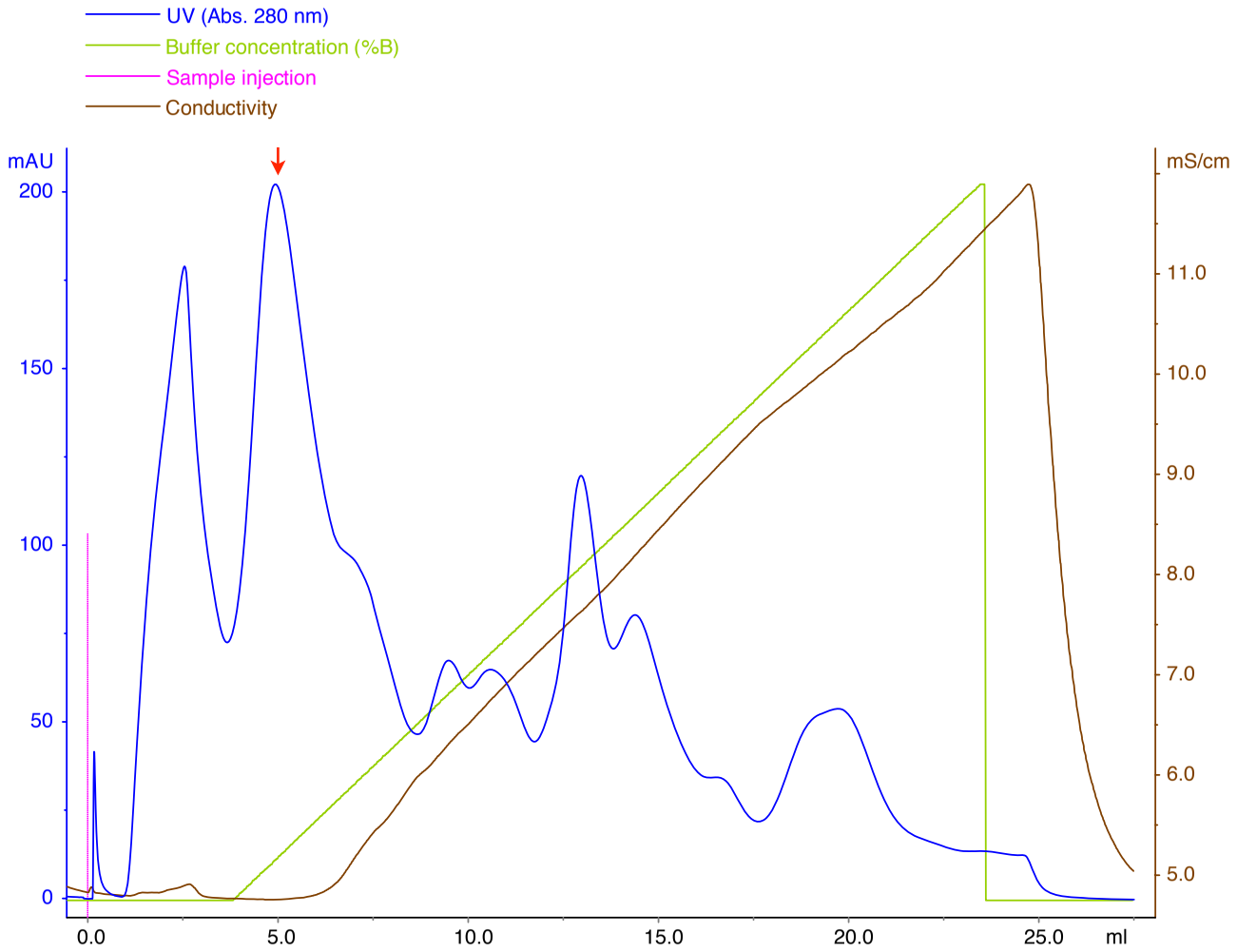

Figure 52. Anion exchange chromatography of *citB7 B. subtilis* cell extract via a MonoQ column. Superose 12 fractions from a $(NH_4)_2SO_4$-precipitated KBP81 cell extract were pooled and injected onto a MonoQ column connected to an AKTA FPLC system (GE Healthcare). A linear gradient of 20 mM - 60 mM Tris-citrate (pH 7.35) was used to elute proteins from the column. The aconitase-containing peak is indicated by the red arrow.

fractions of the MonoQ column run. We hypothesize that this increase in conductivity following concentration was due to the selective binding of aconitase to the citrate in the 20 mM Tris-citrate buffer; thus, it was preferentially retained in the concentrate instead of passing through the concentration filter.

2.6 Gel filtration chromatography

Following the anion exchange chromatography step, the fractions containing aconitase were pooled and concentrated using a spin column (< 0.5 ml final volume). At this point in the protocol, any increase in the conductivity of the buffer due to retention of citrate in the concentration was of no concern because the Superdex 200 (S200) column was also used to replace the buffer with one that did not contain citrate. I injected the sample onto the S200 column connected to the BioLogic DuoFlow system and collected fractions throughout the run.

Aconitase eluted in a peak centered at the 14.5 ml mark, seen in the representative runs in Figure 53. For wild-type and C450S aconitase proteins, the major peak was followed by a smaller shoulder, but for the R741E preparation only a single peak was present. In all three cases, SDS-PAGE analysis confirmed the major peak was aconitase. In addition, analysis of the shoulder in the wild-type and C450S suggested this fraction was aconitase, as well. In the interest of consistency, I chose to pool the major peak fractions for all six preparations and did not include the shoulder fractions. Fractions were pooled and concentrated with a spin column. The concentrated proteins were diluted 1:1 with 100% glycerol and stored at -20°C.

2.7 Aconitase preparations: concentration, activity, and purification factor

The final six aconitase preparations I obtained are summarized in Figure 54 and Table 7. In Figure 54, each of the final six preparations was analyzed by SDS-PAGE followed by staining with Coomassie blue. In Table 7, the protein concentrations, as determined by the Bradford assay, are listed along with activity values obtained using the aconitase activity assay. As discussed in Chapter 1, the mutant proteins demonstrated

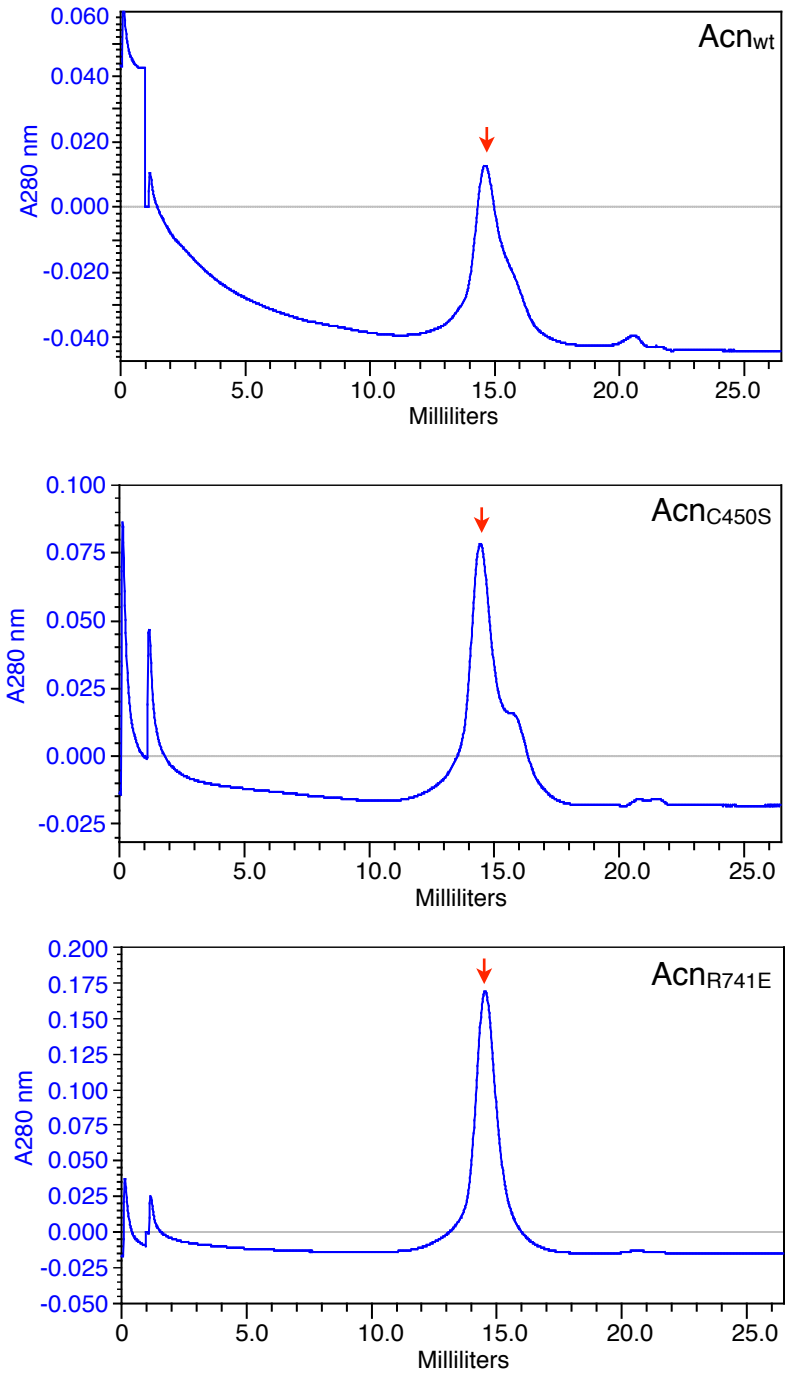

Figure 53. Gel filtration chromatography of aconitase via a Superdex 200 column. MonoQ fractions containing wild-type, C450S, or R741E Acn were separately pooled, concentrated with a spin column (Millipore), and injected onto a Superdex 200 column connected to a BioLogic DuoFlow system (BioRad). Column equilibration and sample run were performed in a 20 mM Tris (pH 7.5), 70 mM KCl buffer. For each spectrum, the aconitase peak is indicated with a red arrow.

Table 7. Comparison of purified wild-type, C450S and R741E Acn proteins. The six purified wild-type, C450S and R741E aconitase preparations are compared for concentration, total approximate volume of entire prep, and specific activity (without activation). The specific activity shown is the mean and standard deviation of two technical replicates.

Aconitase	Prep	Concentration (mg/ml)	Total Approx. Volume (ml)	Specific activity (U/mg)
wild-type	1	0.16	0.1	2478 ± 229
	2	0.23	0.2	2862 ± 206
C450S	1	0.38	0.2	10 ± 14
	2	0.36	0.3	0 ± 30
R741E	1	0.31	0.8	273 ± 35
	2	0.29	0.9	560 ± 215

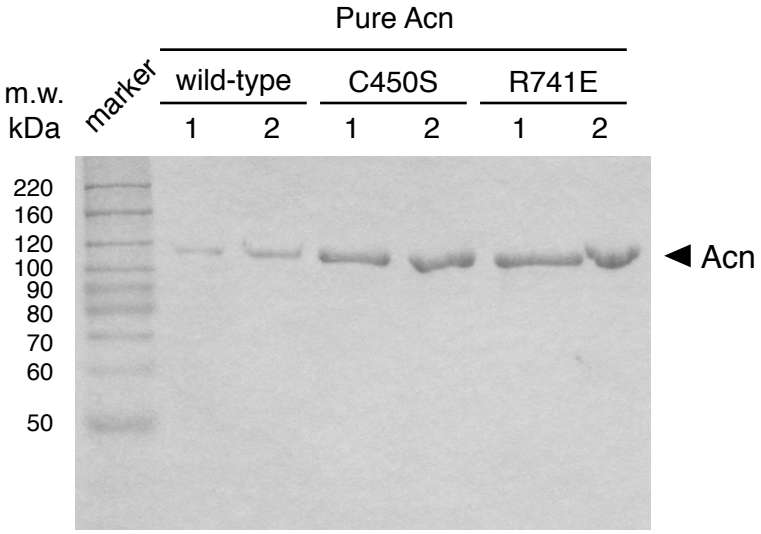

Figure 54. Analysis of final aconitase preparations by SDS-PAGE. Aliquots (5 µl) from each of the six aconitase preparations were analyzed by SDS-PAGE followed by staining with Coomassie blue. Molecular weight markers are noted.

lower activity than wild-type. In addition, there was variability in the activities of the two wild-type preparations. This is likely due to handling differences during the independent preparation process.

The overall purification factor of the wild-type aconitase purification can be estimated by comparing the known cell extract activity in the wild-type strain (KBP94) to the final pure preparations. The purified proteins were harvested from late exponential phase cultures, therefore I will compare cell extracts taken at this stage of growth. In Figure 18, the wild-type cell extract demonstrated 142 units of activity per mg of total protein at 3.5 hours of growth. In Table 7, we see that purified wild-type aconitase exhibited an average of 2670 units of activity per mg of aconitase. Therefore, this method has a purification factor of approximately 18-fold for wild-type aconitase.

3 Discussion

The data presented in this chapter lead us to two important conclusions. First, expression of aconitase with an N-terminal decahistidine tag, while convenient fopurification purposes, is detrimental to enzyme activity. This point has profound implications for previous results concerning aconitase interactions with RNA garnered with the His_{10}-Acn protein, an issue I will consider in the overall Conclusions and Perspectives (see below). In addition, these data demonstrate that aconitase can be purified to near homogeneity using classical techniques with the help of modern, automated FPLC technology.

Despite the advances I made in aconitase purification using this new method, there were pitfalls to my approach. First, the amount of aconitase obtained from each purification scheme was in large part determined by the Superose 12 column bottleneck step; a 500 ml culture equivalent was the maximum input that was adequately separated by this column. This issue could be circumvented by using a larger Superose 12 column, which was not available to me but could be obtained for future studies. Alternatively, a

larger preparation could be split into 500 ml culture equivalents for Superose 12 and MonoQ column analysis and then combined for the final Superdex 200 step. These changes would increase the amount of aconitase obtained from a single purification, a factor that would provide more analysis of each individual preparation before it is exhausted.

A second issue with my purification scheme was the low level of endogenous expression of aconitase in the wild-type and KBP22 (*citB2 citZ340*) strains. In comparison to the level of R741E aconitase purified from strain KBP81 (*citB7*) that *B. subtilis* is capable of producing much higher levels of aconitase protein if the proper regulatory mechanisms are perturbed. Using the knowledge gained in Chapter 1 of this thesis, it is possible that perturbation of the aconitase:*citZ* interaction through *citZ* could result in overexpression of aconitase in the wild-type strain. However, an easier approach for moderate derepression of *citB* expression in the wild-type (and *citB2 citZ340*) strains would be introduction of a *ccpC* mutation, which would derepress aconitase expression by approximately two-fold.

A final issue with this purification was the presence of a shoulder in the aconitase peak during the final gel filtration step in wild-type and C450S preparations (Figure 53). Analysis of the relevant fractions by denaturing SDS-PAGE revealed that this shoulder is comprised of aconitase. It is possible that the aconitase in the shoulder fractions elutes at a slightly different position than the main peak because of a difference in conformation. For example, the main peak may represent the cluster-containing enzymatic form of aconitase, while the shoulder may consist of aconitase in the RNA-binding apoprotein form. To investigate this further, the fractions could be analyzed separately to determine if any possess differences in specific activity. In addition, the fractions could be analyzed by nondenaturing PAGE to look for differences in mobility. It is important to note that I did not include the shoulder fractions in my final aconitase preparation. By eliminating these fractions, I may have inadvertantly removed one conformation (likely the RNA-

binding form) of the protein. However, the ability of aconitase to transition from enzymatic form to RNA-binding form makes this less of a concern. In Chapter 2, I discussed the inclusion of an iron chelator, dipyridyl, in my filter binding assay buffers; this ensured that the protein was converted to the RNA-binding form *in vitro*.

Overall, the new aconitase purification protocol I describe in this chapter has the potential to open interesting new avenues of research. In particular, if adapted to produce large quantities of aconitase, the crystal structure of *B. subtilis* aconitase could be determined. Furthermore, as this protocol purifies aconitase directly from *B. subtilis*, it could be adapted to allow for the purification of aconitase in complex with RNA. For example, eliminating the ammonium sulfate purification step (which disrupts protein:nucleic acid complexes) and instead optimizing the protocol to include gel filtration as the first step could allow for detection of aconitase:RNA complexes using RT-PCR followed by deep sequencing after elution from the anion-exchange column. Beyond this, the same type of purification scheme could be altered to detect potential protein-protein interactions between aconitase and other TCA cycle enzymes, as has been tentatively shown by other groups (Barnes *et al.,* 1986, Meyer *et al.,* 2011).

Conclusions and Perspectives

1 Overall findings

This thesis has established new results concerning the role of aconitase as a regulator of the Krebs cycle in *B. subtilis*. In addition, the role of CcpC as an activator of *citB* expression was elucidated. Beyond this, the role of aconitase in the regulation of sporulation was explored, and a purification scheme for the preparation of aconitase, expressed endogenously and without tags in *B. subtilis*, was devised. In all, the results obtained here have provided new insight into the role of aconitase in the physiology of *B. subtilis*. In addition, the limits of our understanding of that role have been challenged. Below, I explore some of these new perspectives.

2 What is the real state of knowledge about aconitase as an RNA-binding protein?

Since the late 1990s, our laboratory has explored the RNA-binding function of aconitase *in vivo*. An initial study by Alen *et al.* established that purified aconitase could bind to RNA *in vitro* (1999). In recent years, Serio *et al.* demonstrated that a mutant of aconitase defective in RNA-binding had a phenotype *in vivo* (2006a). However, the conclusions from these two papers are complicated by my results, especially in the case of the more recent study. The *in vitro* aconitase:*gerE* interaction described by Serio *et al.* was elucidated using the His_{10}-Acn protein (2006a). However, I found that the expression of the His_{10}-*citB*$^{+}$ construct *in vivo* resulted in the overexpression of a *citB-lacZ* fusion. Since the His_{10}-*citB*$^{+}$ strain is a glutamate prototroph, this result suggests that the tag may perturb aconitase RNA-binding activity. Confusingly, the His_{10}-Acn binds to a described RNA target, *fliT*, with 10-fold greater affinity than the untagged Acn protein. One possible explanation for this discrepancy in results is that the tag may increase nonspecific binding *in vitro* (perhaps through the interaction of positively charged histidine residues with negatively charged RNA) but alter RNA-binding to specific targets *in vivo*. In any case, we must question the aconitase:*gerE* interaction

described previously. Although the *citB5* mutation has an effect on *gerE* mRNA levels *in vivo*, we do not know whether or not this stems from a direct aconitase:*gerE* interaction.

Contributing to this question of RNA-binding specificity are some of my own results. The results in Chapter 1 suggest a role for aconitase in the regulation of citrate synthase expression. However, I was unable to show that binding of aconitase to *citZ* is specific: no negative control RNA was found. Therefore, in my hands, aconitase binds with varying but similar affinity to every RNA tested. We do have evidence that the C450S and R741E mutants of aconitase cannot bind to the *citZ* or *fliT* RNAs. Therefore, we know the binding requires specificity from the protein end, but what about specificity for an RNA target? Could aconitase be a non-specific RNA-binding protein? A well-characterized example of a non-specific nucleic acid binding protein is found in single stranded DNA binding (SSB) protein, which coats single-stranded DNA to prevent premature annealing of DNA strands during replication (Lohman *et al.,* 1994). In addition, a study on a viral nucleocapsid protein by Herschlag *et al.* suggests that non-specific RNA-binding proteins could act as chaperones for the maintenance of proper RNA folding (1994). However, given the microarray results generated by Serio (2005), a truly non-specific role for aconitase RNA-binding seems unlikely. Changes in gene expression produced by the *citB5* or *citB* null mutations were not transcriptome-wide, and one might expect that removal of a non-specific RNA-binding protein would have a global effect. Instead, it seems more likely that *B. subtilis* aconitase does not exhibit specificity *in vitro* due to the reaction conditions used. Although yeast tRNA has been used in reactions in the past, it contains exogenous RNA and is not the best choice for a nonspecific competitor. A better choice for a nonspecific competitor would be total *B. subtilis* RNA, as in effect it acts as the nonspecific competitor within the cell.

While we have ample evidence that *B. subtilis* aconitase interacts with several RNAs *in vitro*, we have no solid biochemical evidence that these interactions are specific. It is possible that any *in vitro* interaction would be non-specific because of improper

conditions. However, this does not preclude the possibility of specificity of binding *in vivo*.

3 How do my results increase our understanding of the *citB5* strain?

My results pertaining to the *citB7* mutant and corresponding Acn_{R741E} protein have shed new light on the results Serio *et al.* obtained with the *citB5* mutant strain (2006a). The *citB5* mutant was originally described in terms of a defect in heat-resistant spore formation that was seen when assayed at an early (T_7) time point. However, this defect disappeared at later time points (post 24-hours), suggesting that there is a delay in the progression of spore formation but not a true block. This delay was attributed, in part, to a delay in the appearance of *gerE* transcript due to the reduced affinity of the Acn_{citB5} protein for *gerE* (Serio *et al.,* 2006a). The interaction of Acn_{citB5} and Acn_{wt} with *gerE* was tested in a gel shift experiment using C-terminally His_6 tagged proteins, and the mutant protein exhibited 4.5-fold less affinity for the RNA than wild-type (Serio *et al.,* 2006a). My results impact this conclusion in two major ways.

First, there is a discrepancy between the data concerning *citB-lacZ* expression and aconitase protein levels in the *citB5* mutant. The *citB5* mutant, like the *citB7* strain, accumulates citrate within the culture fluid of growing cells (Serio 2005). In addition, both strains overexpress *citB-lacZ* in a CcpC-dependent manner; my own results and previously obtained data (A. Serio, unpublished data) confirm this. Both the *citB5* and *citB7* strains exhibit high levels of aconitase enzyme activity *in vivo* (Serio *et al.*, 2006a, and Figure 18). In the *citB7* strain, I attribute this to the high levels of aconitase protein present in the cell (Figure 16). Confusingly, a comparison of aconitase protein levels in the *citB5* strain compared to wild-type revealed no differences in expression levels (Serio 2005). However, this result was obtained using an alkaline phosphatase-conjugated secondary antibody, which I have determined is not sensitive enough to detect differences in aconitase protein levels *in vivo*. Given the similarities between the *citB5* and *citB7* mutants, and the known issues with the antibody, it seems likely that the

aconitase protein levels were underestimated in the *citB5* strain. Furthermore, we can now reevaluate the previous hypothesis for the high aconitase activity in the *citB5* strain, that the Acn_{citB5} protein had a higher enzyme activity than the Acn_{wt} (Serio *et al.,* 2006a). This now seems unlikely, given our knowledge that the purified Acn_{R741E} protein has reduced aconitase enzyme activity. The *citB5* strain has five point mutations, one of which is the R741E substitution. Therefore, I hypothesize that the Acn_{citB5} strain, like Acn_{R741E}, has reduced aconitase enzyme activity compared to wild-type. In addition, I postulate that the high levels of aconitase enzyme activity in *citB5* cell extracts are due to the overexpression of *citB* promoter in high citrate, resulting in high levels of aconitase protein within the cell.

Given these considerations, I believe that the defect in RNA-binding affinity seen for Acn_{citB5} protein *in vitro* was underestimated. When aconitase was purified from wild-type and *citB5* mutant strains, a C-terminal His_6 tag was utilized (Serio *et al.,* 2006a). This tag produced partially pure proteins, and thus a simple calculation of protein concentration was not possible. Instead, a quantitative immunoblot was used to determine relative amounts of aconitase in each preparation. As described above, an AP-conjugated secondary antibody was used to accomplish this quantitation. It is therefore likely that the quantitation was not accurate, and given that the *citB5* strain likely overexpresses Acn, I hypothesize that the concentration of purified Acn_{citB5} was underestimated. Moreover, this would mean the concentration of Acn_{citB5} protein in the *gerE* binding experiments was underestimated. Therefore, the defect in Acn_{citB5}:*gerE* binding was likely greater than the 4.5-fold value calculated previously (Serio *et al.,* 2006a), bringing the Acn_{citB5} defect more in line with the data I generated for the Acn_{R741E} protein.

4 Final perspectives and future directions

The work presented here has elucidated a dual role of aconitase in the regulation of the TCA branch enzymes. In addition, the CcpC regulatory protein, which was initially

characterized as a repressor, is now known to both repress and activate expression of *citB*. There are multiple ways in which we can further explore these phenomena.

In our model for CcpC-dependent regulation of *citB*, CcpC binds to and represses *citB* transcription in the absence of citrate. However, in the presence of citrate, CcpC activates expression of *citB*. Despite the evidence in favor of this model, direct evidence of the switch between these two CcpC regulatory modes due to citrate concentration has not been demonstrated at a molecular level. To do this, one can imagine an *in vitro* transcription experiment that utilizes *B. subtilis* RNA polymerase, CcpC, and *citB* template DNA. Transcription of *citB* would then be monitored in the presence of different concentrations of citrate. However, this experiment is not technically feasible because citrate inhibits *B. subtilis* RNA polymerase *in vitro*. Perhaps, if conditions could be found to circumvent this issue, the proposed experiment could be performed. Alternatively, a direct interaction between CcpC and *B. subtilis* RNA polymerase in the presence of citrate could be detected by a pull-down assay, a result which would support our model that CcpC activates *citB* expression. In addition, the expected conformational change in CcpC that is induced by citrate could be explored using limited proteolysis or by taking a different approach: the crystal structure of CcpC could be solved with and without citrate to determine the conformational change that occurs when citrate binds.

In addition, although aconitase is a bifunctional protein, there is little evidence to support the presence of two functional forms of aconitase in wild-type cells. It would be interesting to examine the relative pools of enzymatic and RNA-binding forms to determine if either predominates. Campanella *et al.* used nondenaturing PAGE analysis followed by immunoblot to discriminate between the different forms of IRP1 (2004); this approach could be adapted for *B. subtilis* aconitase. In addition, it is reasonable to expect that the proportion of aconitase in the RNA-binding conformation would have an effect on any aconitase-dependent regulation. If more of the total aconitase in the cell were present as an enzyme, there would be fewer molecules of the RNA-binding form present

to bind to RNA, and vice versa. Therefore, it would be important to determine if the ratio between the enzymatic and RNA-binding forms is static or if it changes in different conditions.

Finally, it would be interesting to determine if our model for *B. subtilis* aconitase-dependent regulation of Krebs cycle gene expression also holds true for bacteria with clinical significance. As mentioned in the Introduction, the Gram-positive pathogens *Staphylococcus aureus* and *Streptococcus mutans* possess genes encoding aconitase, citrate synthase and isocitrate dehydrogenase. In *S. aureus*, these genes are arranged similarly as in *B. subtilis*: the *citB* and *citZ-citC* operons are separated on the chromosome. In *S. mutans*, the three genes are found in a single operon. It would be worthwhile to investigate the possibility of aconitase-dependent regulation of citrate synthase in these organisms. Furthermore, recent work has indicated a role for aconitase in *S. aureus* virulence. As discussed above, deletion of *S. aureus* aconitase resulted in increased survival in stationary phase compared to wild-type (Somerville *et al.,* 2002). In addition, this same study found that aconitase mutants exhibited reduced levels of virulence factors compared to wild-type (Somerville *et al.,* 2002). The mechanism of this regulation is unknown, but it is feasible that aconitase may be acting directly to regulate virulence in *S. aureus*. The construction and characterization of an RNA-binding mutant of aconitase in *S. aureus* would provide a method to test this hypothesis.

References

Alén, C., and A. L. Sonenshein. 1999. *Bacillus subtilis* aconitase is an RNA-binding protein. Proc Natl Acad Sci U S A **96:**10412-10417.

Anagnostopoulos, C., and J. Spizizen. 1961. Requirements for transformation in *Bacillus subtilis*. J Bacteriol **81:**741-746.

Baichoo, N., T. Wang, R. Ye, and J. D. Helmann. 2002. Global analysis of the *Bacillus subtilis* Fur regulon and the iron starvation stimulon. Mol Microbiol **45:**1613-1629.

Banerjee, S., A. K. Nandyala, P. Raviprasad, N. Ahmed, and S. E. Hasnain. 2007. Iron-Dependent RNA-Binding Activity of *Mycobacterium tuberculosis* Aconitase. J Bacteriol **189:**4046-4052.

Barnes, S. J., and P. D. J. Weitzman. 1986. Organization of citric acid cycle enzymes into a multienzyme cluster. FEBS Lett **201:**267-270.

Beinert, H. 2000. Iron-sulfur proteins: ancient structures, still full of surprises. J Biol Inorg Chem **5:**2-15.

Beinert, H., M. C. Kennedy, and C. D. Stout. 1996. Aconitase as Iron-Sulfur Protein, Enzyme, and Iron-Regulatory Protein. Chem Rev **96:**2335-2373.

Belitsky, B. 2002. Biosynthesis of Amino Acids of the Glutamate and Aspartate Families, Alanine, and Polyamines. *In* A. L. Sonenshein, J. A. Hoch, and R. Losick (ed.), *Bacillus subtilis* and Its Closest Relatives: from Genes to Cells. ASM Press, Washington, D.C.

Belitsky, B., and A. L. Sonenshein. 1998. Role and Regulation of *Bacillus subtilis* Glutamate Dehydrogenase Genes. J Bacteriol **180:**6298-6305.

Belitsky, B. R., and A. L. Sonenshein. 2008. Genetic and biochemical analysis of CodY-binding sites in Bacillus subtilis. J Bacteriol **190:**1224-36.

Blank, L., J. Green, and J. R. Guest. 2002. AcnC of *Escherichia coli* is a 2-methylcitrate dehydratase (PrpD) that can use citrate and isocitrate as substrates. Microbiol **148:**133-146.

Blencke, H.-M., I. Reif, F. M. Commichau, C. Detsch, I. Wacker, H. Ludwig, and J. Stülke. 2006. Regulation of *citB* expression in *Bacillus subtilis*: integration of multiple metabolic signals in the citrate pool and by the general nitrogen regulatory system. Arch Microbiol **185:**136-46.

Bott, M. 2007. Offering surprises: TCA cycle regulation in *Corynebacterium glutamicum*. Trends Microbiol **15:**417-425.

Breusch, F. 1937. Z physiol Chem **250:**262.

Bryan, E. M., B. W. Beall, and C. P. Moran, Jr. 1996. A sigma E dependent operon subject to catabolite repression during sporulation in *Bacillus subtilis*. J Bacteriol **178:**4778-4786.

Bsat, N., and J. D. Helmann. 1999. Interaction of Bacillus subtilis Fur (ferric uptake repressor) with the dhb operator in vitro and in vivo. J Bacteriol **181:**4299-307.

Buchanan, J., and C. Anfinsen. 1949. Partial Purification of Aconitase. J Biol Chem **180:**47.

Burbulys, D., K. A. Trach, and J. A. Hoch. 1991. Initiation of Sporulation in *B. subtilis* Is Controlled by a Multicomponent Phosphorelay. Cell **64:**545-552.

Burkholder, P. R., and N. H. Giles, Jr. 1947. Induced Biochemical Mutations in *Bacillus subtilis*. Am J Bot **34:**345-348.

Bylund, J. E., M. A. Haines, P. J. Piggot, and M. L. Higgins. 1993. Axial filament formation in *Bacillus subtilis*: induction of nucleoids of increasing length after addition of chloramphenicol to exponential-phase cultures approaching stationary phase. J Bacteriol **175:**1886-1890.

Campanella, A., S. Levi, G. Cairo, G. Biasiotto, and P. Arosio. 2004. Blotting Analysis of Native IRP1: A Novel Approach to Distinguish the Different Forms of IRP1 in Cells and Tissues. Biochemistry **43:**195-204.

Campo, N., and D. Z. Rudner. 2006. A branched pathway governing the activation of a developmental transcription factor by regulated intramembrane proteolysis. Mol Cell **23:**25-35.

Chary, V. K., M. Meloni, D. W. Hilbert, and P. J. Piggot. 2005. Control of the Expression and Compartmentalization of σ^G activity during sporulation of *Bacillus subtilis* by Regulators of σ^F and σ^E. J Bacteriol **187:**6832-6840.

Chatterjee, I., P. Becker, M. Grundmeier, M. Bischoff, G. A. Somerville, G. Peters, B. Sinha, N. Harraghy, R. A. Proctor, and M. Herrmann. 2005. Staphylococcus aureus ClpC is required for stress resistance, aconitase activity, growth recovery, and death. J Bacteriol **187:**4488-96.

Chatterjee, I., S. Schmitt, C. F. Batzilla, S. Engelmann, A. Keller, M. W. Ring, R. Kautenburger, W. Ziebuhr, M. Hecker, K. T. Preissner, M. Bischoff, R. A. Proctor, H. P. Beck, H. P. Lenhof, G. A. Somerville, and M. Herrmann. 2009. Staphylococcus aureus ClpC ATPase is a late growth phase effector of metabolism and persistence. Proteomics **9:**1152-76.

Chen, L., and J. D. Helmann. 1994. The *Bacillus subtilis* σD-Dependent Operon Encoding the Flagellar Proteins FliD, FliS, and FliT. J Bacteriol **176:**3093-3101.

Chevance, F., and K. Hughes. 2008. Coordinating assembly of a bacterial macromolecular machine. Nat Rev Microbiol **6:**455-65.

Chia, J.-S., Y.-Y. Lee, P.-T. Huang, and J.-Y. Chen. 2001. Identification of Stress-Responsive Genes in *Streptococcus mutans* by Differential Display Reverse Transcription-PCR. Infect Immun **69:**2493-2501.

Cohn, F. 1872. Untersuchungen über Bacterien. Beitr Biol Pflanzen **1:**127-224.

Condon, C., C. Squires, and C. L. Squires. 1995. Control of rRNA Transcription in *Escherichia coli*. Microbiol Rev **59:**623-645.

Corfe, B. M., R. L. Sammons, D. A. Smith, and C. Mauël. 1994. The *gerB* region of the *Bacillus subtilis* 168 chromosome encodes a homologue of the *gerA* spore germination operon. Microbiol **140:**471-478.

Cozzone, A. J. 1998. Regulation of acetate metabolism by protein phosphorylation in enteric bacteria. Annu Rev Microbiol **52:**127-164.

Craig, J. E., M. J. Ford, D. C. Blaydon, and A. L. Sonenshein. 1997. A null mutation in the *Bacillus subtilis* aconitase gene causes a block in Spo0A-phosphate-dependent gene expression. J Bacteriol **179:**7351-9.

Cunningham, L., M. J. Gruer, and J. R. Guest. 1997. Transcriptional regulation of the aconitase genes (*acnA* and *acnB*) of *Escherichia coli*. Microbiol **143:**3795-3805.

Cutting, S. 2011. *Bacillus* probiotics. Food Microbiology **28:**214-220.

Cutting, S., and J. Mandelstam. 1986. The Nucleotide Sequence and the Transcription During Sporulation of the *gerE* Gene of *Bacillus subtilis*. J Gen Microbiol **132:**3013-3024.

Deuel, T. F., and S. Prusiner. 1974. Regulation of Glutamine Synthetase from *Bacillus subtilis* by Divalent Cations, Feedback Inhibitors, and L-Glutamine. J Biol Chem **249:**257-264.

Deutscher, J. 2008. The mechanisms of carbon catabolite repression in bacteria. Curr Opin Microbiol **11:**87-93.

Dineen, S. S., A. C. Villapakkam, J. T. Nordman, and A. L. Sonenshein. 2007. Repression of Clostridium difficile toxin gene expression by CodY. Mol Microbiol **66:**206-19.

Dingman, D. W., and A. L. Sonenshein. 1987. Purification of aconitase from *Bacillus subtilis* and correlation of its N-terminal amino acid sequence with the sequence of the *citB* gene. J Bacteriol **169:**3062-7.

Ducros, V. M.-A., J. A. Brannigan, R. J. Lewis, and A. J. Wilkinson. 1998. *Bacillus subtilis* regulatory protein GerE. Acta Crystallog **54:**1453-1455.

Ducros, V. M.-A., R. J. Lewis, C. S. Verma, E. J. Dodson, G. Leonard, J. P. Turkenburg, G. N. Murshudov, A. J. Wilkinson, and J. A. Brannigan. 2001. Crystal Structure of GerE, the Ultimate Transcriptional Regulator of Spore Formation in *Bacillus subtilis*. J Mol Biol **306:**759-771.

Duncan, L., S. Alper, and R. Losick. 1996. SpoIIAA governs the release of the cell-type specific transcription factor σ^F from its anti-σ factor SpoIIAB. J Mol Biol **260:**147-164.

Duncan, L., and R. Losick. 1993. SpoIIAB is an anti-σ factor that binds to and inhibits transcription by regulatory protein $\sigma^F$from *Bacillus subtilis*. Proc Natl Acad Sci U S A **90:**2325-2329.

Ehrenberg, C. G. 1835. Physikalische Abhandlungen der Koeniglichen Akademie der Wissenschaften zu Berlin aus den Jahren 1833-1835.

Eichenberger, P., M. Fujita, S. T. Jensen, E. M. Conlon, D. Z. Rudner, S. T. Wang, C. Ferguson, K. Haga, T. Sato, J. S. Liu, and R. Losick. 2004. The Program of Gene Transcription for a Single Differentiating Cell Type during Sporulation in *Bacillus subtilis*. PLoS Biol **2:**e328.

Ellman, G. 1959. Tissue Sulfhydryl Groups. Arch Biochem Biophys **82:**70-77.

Emery-Goodman, A., H. Hirling, L. Scarpellino, B. Henderson, and L. C. Kühn. 1993. Iron regulatory factor expressed from recombinant baculovirus: conversion between the RNA-binding apoprotein and Fe-S cluster containing aconitase. Nucleic Acids Res **21:**1457-1461.

Fisher, S. H. 1999. Regulation of nitrogen metabolism in *Bacillus subtilis*: vive la différence! Mol Microbiol **32:**223-232.

Fisher, S. H., and B. Magasanik. 1984. 2-Ketoglutarate and the Regulation of Aconitase and Histidase Formation in *Bacillus subtilis*. J Bacteriol **158:**379-382.

Flechtner, V. R., and R. S. Hanson. 1969. Coarse and fine control of citrate synthase from *Bacillus subtilis*. Biochim Biophys Acta **184:**252-262.

Fortnagel, P., and E. Freese. 1968. Analysis of Sporulation Mutants II. Mutants Blocked in the Citric Acid Cycle. J Bacteriol **95:**1431-1438.

Fouet, A., and A. L. Sonenshein. 1990. A target for carbon source-dependent negative regulation of the *citB* promoter of Bacillus subtilis. J Bacteriol **172:**835-44.

Fredrick, K., and J. D. Helmann. 1996. FlgM Is a Primary Regulator of σD Activity, and Its Absence Restores Motility to a *sinR* Mutant. J Bacteriol **178:**7010-7013.

Fujita, Y. 2009. Carbon Catabolite Control of the Metabolic Network in *Bacillus subtilis*. Biosci Biotechnol Biochem **73:**245-259.

Fürbaß, R., M. Gocht, P. Zuber, and M. A. Marahiel. 1991. Interaction of AbrB, a transcriptional regulator from *Bacillus subtilis* with the promoters of the transition state-activated genes *tycA* and *spoVG*. Mol Gen Genet **225:**347-354.

Gálvez, S., and P. Gadal. 1995. On the function of the NADP-dependent isocitrate dehydrogenase isoenzymes in living organisms. Plant Science **105:**1-14.

Gao, W., S. Dai, Q. Liu, Y. Xu, Y. Bai, and M. Qiao. 2010. Effect of site-directed mutagenesis of *citB* on the expression and activity of *Bacillus subtilis* aconitase. Mikrobiologiia **79:**774-778.

Ghosh, S., B. Setlow, P. G. Wahome, A. E. Cowan, M. Plomp, A. J. Malkin, and P. Setlow. 2008. Characterization of Spores of *Bacillus subtilis* That Lack Most Coat Layers. J Bacteriol **190:**6741-6748.

Goossen, B., and M. W. Hentze. 1992. Position Is the Critical Determinat for Function of Iron-Responsive Elements as Translational Regulators. Mol Cell Biol **12:**1959-1966.

Görke, B., and J. Stülke. 2008. Carbon catabolite repression in bacteria: many ways to make the most out of nutrients. Nat Rev Microbiol **6:**613-624.

Gosset, G., Z. Zhang, S. Nayyar, W. A. Cuevas, and M. H. Saier, Jr. 2004. Transcriptome Analysis of Crp-Dependent Catabolite Control of Gene Expression in *Escherichia coli*. J Bacteriol **186:**3516-3524.

Green, J., J. C. Crack, A. J. Thomson, and N. E. LeBrun. 2009. Bacterial sensors of oxygen. Curr Opin Microbiol **12:**145-151.

Gruer, M. J., P. J. Artymiuk, and J. R. Guest. 1997. The aconitase family: three structural variations on a common theme. Trends Biochem Sci **22:**3-6.

Gunsalus, R. P., and S.-J. Park. 1994. Aerobic-anaerobic gene regulation in *Escherichia coli*: control by the ArcAB and Fnr regulons. Res Microbiol **145:**437-450.

Haile, D. J. 1999. Regulation of genes of iron metabolism by the iron-response proteins. Am J Med Sci **318:**230-240.

Haile, D. J., T. A. Rouault, J. B. Harford, M. C. Kennedy, G. A. Blondin, H. Beinert, and R. D. Klausner. 1992. Cellular regulation of the iron-responsive element binding protein: disassembly of the cubane iron-sulfer clustur results in high-affinity RNA binding. Proc Natl Acad Sci U S A **89:**11735-11739.

Haldenwang, W. G. 1995. The Sigma Factors of *Bacillus subtilis*. Microbiol Rev **59:**1-30.

Hanson, R. S., J. Blicharska, M. Arnaud, and J. Szulmajster. 1964. Observations on the regulation of the synthesis of the tricarboxylic acid cycle enzymes in *Bacillus subtilis*, Marburg. Biochem Biophys Res Commun **17:**690-695.

Hanson, R. S., and D. P. Cox. 1967. Effect of Different Nutritional Conditions on the Synthesis of Tricarboxylic Acid Cycle Enzymes. J Bacteriol **93:**1777-1787.

Henkin, T. M., F. J. Grundy, W. L. Nicholson, and G. H. Chambliss. 1991. Catabolite repression of alpha-amylase gene expression in *Bacillus subtilis* involves a *trans*-acting gene product homologous to the *Eschericia coli lacI* and *galR* repressors. Mol Microbiol **5:**575-584.

Henson, C. P., and W. W. Cleland. 1967. Purification and Kinetic Studies of Beef Liver Cytoplasmic Aconitase. J Biol Chem **242:**3833-3838.

Herschlag, D., M. Khosla, Z. Tsuchihashi, and R. L. Karpel. 1994. An RNA chaperone activity of non-specific RNA binding proteins in hammerhead ribozyme catalysis. Embo J **13:**2913-2924.

Hilbert, D., and P. J. Piggot. 2004. Compartmentalization of Gene Expression during *Bacillus subtilis* Spore Formation. Microbiol Mol Biol Rev **68:**234-262.

Hirling, H., B. Henderson, and L. C. Kühn. 1994. Mutational analysis of the [4Fe-4S] cluster converting iron regulatory factor from its RNA-binding form to cytoplasmic aconitase. Embo J **13:**453-461.

Ichikawa, H., R. Halberg, and L. Kroos. 1999. Negative regulation by the *Bacillus subtilis* GerE protein. J Biol Chem **274:**8322-8327.

Imlay, J. A. 2006. Iron-sulphur clusters and the problem with oxygen. Mol Microbiol **59:**1073-1082.

Iuchi, S., and E. C. C. Lin. 1988. *arcA* (*dye*), a global regulatory gene in *Escherichia coli* mediating repression of enzymes in aerobic pathways. Proc Natl Acad Sci U S A **85:**1888-1892.

Jin, S., P. Levin, K. Matsuno, A. D. Grossman, and A. L. Sonenshein. 1997. Deletion of the *Bacillus subtilis* Isocitrate Dehydrogenase Gene Causes a Block at Stage I of Sporulation. J Bacteriol **179:**4725-32.

Jin, S., and A. L. Sonenshein. 1996. Characterization of the major citrate synthase of Bacillus subtilis. J Bacteriol **178:**3658-60.

Jin, S., and A. L. Sonenshein. 1994a. Identification of two distinct *Bacillus subtilis* citrate synthase genes. J Bacteriol **176:**4669-79.

Jin, S., and A. L. Sonenshein. 1994b. Transcriptional regulation of *Bacillus subtilis* citrate synthase genes. J Bacteriol **176:**4680-90.

Jourlin-Castelli, C., N. Mani, M. M. Nakano, and A. L. Sonenshein. 2000. CcpC, a novel regulator of the LysR family required for glucose repression of the *citB* gene in *Bacillus subtilis*. J Mol Biol **295:**865-78.

Kaldy, P., E. Menotti, R. Moret, and L. C. Kühn. 1999. Identification of RNA-binding surfaces in iron regulatory protein-1. Embo J **18:**6073-6083.

Kellner, E. M., A. Decatur, and C. P. Moran, Jr. 1996. Two-stage regulation of an anti-sigma factor determines developmental fate during bacterial endospore formation. Mol Microbiol **21:**913-924.

Kennedy, M. C., M. H. Emptage, J.-L. Dreyer, and H. Beinert. 1983. The Role of Iron in the Activation-Inactivation of Aconitase. J Biol Chem **258:**11098-11105.

Kennedy, M. C., L. Mende-Mueller, G. A. Blondin, and H. Beinert. 1992. Purification and characterization of cytosolic aconitase from beef liver and its relationship to the iron-responsive element binding protein. Proc Natl Acad Sci U S A **89:**11730-11734.

Kennedy, S., R. Rauner, and O. Gawron. 1972. On pig heart aconitase. Biochem Biophys Res Commun **47:**740-745.

Kim, H. J., C. Jourlin-Castelli, S. I. Kim, and A. L. Sonenshein. 2002a. Regulation of the bacillus subtilis *ccpC* gene by CcpA and CcpC. Mol Microbiol **43:**399-410.

Kim, H. J., S. I. Kim, M. Ratnayake-Lecamwasam, K. Tachikawa, A. L. Sonenshein, and M. Strauch. 2003. Complex regulation of the *Bacillus subtilis* aconitase gene. J Bacteriol **185:**1672-80.

Kim, H. J., A. Roux, and A. L. Sonenshein. 2002b. Direct and indirect roles of CcpA in regulation of *Bacillus subtilis* Krebs cycle genes. Mol Microbiol **45:**179-90.

Kim, S. I., C. Jourlin-Castelli, S. R. Wellington, and A. L. Sonenshein. 2003. Mechanism of repression by *Bacillus subtilis* CcpC, a LysR family regulator. J Mol Biol **334:**609-24.

Koeller, D. M., J. L. Casey, M. W. Hentze, E. M. Gerhardt, L.-N. L. Chan, R. D. Klausner, and J. B. Harford. 1989. A cytosolic protein binds to structural elements within the iron regulatory region of the transferrin receptor mRNA. Proc Natl Acad Sci U S A **86:**3574-3578.

Koziol, U., L. Hannibal, M. C. Rodríguez, E. Fabiano, M. L. Kahn, and F. Noya. 2009. Deletion of Citrate Synthase Restores Growth of *Sinorhizobium meliloti* 1021 Aconitase Mutants. J Bacteriol **191:**7581-7586.

Krug, A., V. Wendisch, and M. Bott. 2005. Identification of AcnR, a TetR-type repressor of the aconitase gene *acn* in *Corynebacterium glutamicum*. J Biol Chem **280:**585-595.

Kuwana, R., H. Ikejiri, S. Yamamura, H. Takamatsu, and K. Watabe. 2004. Functional relationship between SpoVIF and GerE in gene regulation during sporulation of *Bacillus subtilis*. Microbiol **150:**163-170.

Lauble, H., M. C. Kennedy, and H. Beinert. 1994. Crystal structures of Aconitase with *Trans*-aconitate and Nitrocitrate Bound. J Mol Biol **237:**437-451.

Lemos, J. A., and R. A. Burne. 2008. A model of efficiency: stress tolerance by *Streptococcus mutans*. Microbiol **154:**3247-3255.

Levdikov, V. M., E. Blagova, P. Joseph, A. L. Sonenshein, and A. J. Wilkinson. 2006. The structure of CodY, a GTP- and isoleucine-responsive regulator of stationary phase and virulence in gram-positive bacteria. J Biol Chem **281:**11366-73.

Lewis, M. 2005. The *lac* repressor. Comptes Rendus Biologies **328:**521-548.

Lloyd, S. J., H. Lauble, G. S. Prasad, and C. D. Stout. 1999. The mechanism of aconitase: 1.8 Å resolution crystal structure of the S642A:citrate complex Protein Sci **8:**2655-2662.

Lohman, T. M., and M. E. Ferrari. 1994. *Escherichia coli* single-stranded DNA-binding protein: Multiple DNA-Binding Modes and Cooperativities. Ann Rev Biochem **63:**527-570.

Lynch, A. S., and E. C. C. Lin. 1996. Transcriptional Control Mediated by the ArcA Two-Component Response Regulator Protein of *Escherichia coli*: Characterization of DNA Binding at Target Promoters. J Bacteriol **178:**6238-6249.

Majerczyk, C. D., M. R. Sadykov, T. T. Luong, C. Lee, G. A. Somerville, and A. L. Sonenshein. 2008. Staphylococcus aureus CodY negatively regulates virulence gene expression. J Bacteriol **190:**2257-65.

Martius, C., and F. Knoop. 1937. Hoppe-Seyler's Zeitschrift **246:**1.

Matsuno, K., T. Blais, A. W. Serio, T. Conway, T. M. Henkin, and A. L. Sonenshein. 1999. Metabolic imbalance and sporulation in an isocitrate dehydrogenase mutant of *Bacillus subtilis*. J Bacteriol **181:**3382-3391.

Merriam-Webster. 2011. Merriam-Webster.com.

Meyer, F., J. Gerwig, E. Hammer, C. Herzberg, F. M. Commichau, U. Völker, and J. Stülke. 2011. Physical interactions between tricarboxylic acid cycle enzymes in *Bacillus subtilis*: evidence for a metabolon. Metab Eng **13:**18-27.

Miller, J. 1972. Experiments in molecular genetics. Cold Spring Harbor Laboratory, Cold Spring Harbor, NY.

Moir, A. 1981. Germination Properties of a Spore Coat-Defective Mutant of *Bacillus subtilis*. J Bacteriol **146:**1106-1116.

Moir, A., E. Lafferty, and D. A. Smith. 1979. Genetic Analysis of Spore Germination Mutants of *Bacillus subtilis* 168: the Correlation of Phenotype with Map Location. J Gen Microbiol **111:**165-180.

Monod, J. 1942. Recherches sur la Croissance des Cultures Bactériennes. Hermann et Cie, Paris.

Mueller, J., G. Bukusoglu, and A. L. Sonenshein. 1992. Transcriptional regulation of *Bacillus subtilis* glucose starvation-inducible genes: control of *gsiA* by the ComP-ComA signal transduction system. J Bacteriol **174:**4361-73.

Nakano, M. M., and P. Zuber. 1998. Anaerobic growth of a "strict aerobe" (*Bacillus subtilis*). Annu Rev Microbiol **52:**165-190.

Ohne, M. 1974. Regulation of Aconitase Synthesis in *Bacillus subtilis*: Induction, Feedback Repression, and Catabolite Repression. J Bacteriol **117:**1295-1305.

Owen, O. E., S. C. Kalhan, and R. W. Hanson. 2002. The Key Role of Anaplerosis and Cataplerosis for Citric Acid Cycle Function. J Biol Chem **277:**30409-30412.

Philpott, C., D. J. Haile, T. A. Rouault, and R. D. Klausner. 1993. Modification of a free Fe-S cluster cysteine residue in the active iron-responsive element-binding protein prevents RNA binding. J Biol Chem **268:**17655-17658.

Philpott, C., R. D. Klausner, and T. A. Rouault. 1994. The bifunctional iron-responsive element binding protein/cytosolic aconitase: The role of active-site residues in ligand binding and regulation. Proc Natl Acad Sci U S A **91:**7321-7325.

Priest, F. G. 1993. Systematics and Ecology of *Bacillus*. *In* A. L. Sonenshein, J. A. Hoch, and R. Losick (ed.), *Bacillus subtilis* and Other Gram-Positive Bacteria. American Society of Microbiology, Washington, DC.

Ratnayake-Lecamwasam, M., P. Serror, K. W. Wong, and A. L. Sonenshein. 2001. Bacillus subtilis CodY represses early-stationary-phase genes by sensing GTP levels. Genes Dev **15:**1093-103.

Remington, S. 1992. Mechanisms of citrate synthase and related enzymes (triose phosphate isomerase and mandelate racemase). Curr Opin Struct Biol **2:**730-735.

Resnekov, O., and R. Losick. 1998. Negative regulation of the proteolytic activation of a developmental transcription factor in Bacillus subtilis. Proc Natl Acad Sci U S A **95:**3162-3167.

Riddles, P., R. Blakeley, and B. Zerner. 1983. Reassessment of Ellman's Reagent. Methods in Enzymology **91:**49-60.

Rosenkrantz, M. S., D. W. Dingman, and A. L. Sonenshein. 1985. *Bacillus subtilis citB* Gene Is Regulated Synergistically by Glucose and Glutamine. J Bacteriol **164:**155-64.

Rudner, D. Z., and R. Losick. 2002. A sporulation membrane protein tethers the pro-sigmaK processing enzyme to its inhibitor and dictates its subcellular localization. Genes Dev **16:**1007-1018.

Schmalisch, M., E. Maiques, L. Nikolov, A. H. Camp, B. Chevreux, A. Muffler, S. Rodriguez, J. Perkins, and R. Losick. 2010. Small Genes under Sporulation Control in the *Bacillus subtilis* genome. J Bacteriol **192:**5402-5412.

Scholze, H. 1983. Studies on aconitase species from *Saccharomyces cerevisiae*, porcine and bovine heart, obtained by a modified isolation method. Biochim Biophys Acta **746:**133-137.

Schumacher, M. A., G. Seidel, W. Hillen, and R. Brennan. 2007. Structural mechanism for the fine-tuning of CcpA function by the small molecule effectors glucose 6-phosphate and fructose 1,6-bisphosphate. J Mol Biol **368:**1042-50.

Serio, A. W. 2005. The Role of Aconitase, A Bi-Functional Protein, in Iron Regulation and Sporulation in *Bacillus subtilis*. PhD Thesis. Tufts University, Boston.

Serio, A. W., K. B. Pechter, and A. L. Sonenshein. 2006a. *Bacillus subtilis* aconitase is required for efficient late-sporulation gene expression. J Bacteriol **188:**6396-405.

Serio, A. W., and A. L. Sonenshein. 2006b. Expression of yeast mitochondrial aconitase in *Bacillus subtilis*. J Bacteriol **188:**6406-10.

Serrano, M., L. Côrte, J. Opdyke, C. P. Moran, Jr, and A. O. Henriques. 2003. Expression of *spoIIIJ* in the Prespore Is Sufficient for Activation of σ^G and for Sporulation in *Bacillus subtilis*. J Bacteriol **185:**3905-3917.

Serrano, M., A. Neves, C. M. Soares, C. P. Moran, Jr, and A. O. Henriques. 2004. Role of the Anti-Sigma Factor SpoIIAB in Regulation of σ^G during *Bacillus subtilis* Sporulation J Bacteriol **186:**4000-4013.

Setlow, P. 2003. Spore germination. Curr Opin Microbiol **6:**550-6.

Shalel-Levanon, S., K. Y. San, and G. N. Bennett. 2005. Effect of oxygen, and ArcA and FNR regulators on the expression of genes related to the electron transfer chain and the TCA cycle in Escherichia coli. Metab Eng **7:**364-74.

Shivers, R. P., and A. L. Sonenshein. 2004. Activation of the Bacillus subtilis global regulator CodY by direct interaction with branched-chain amino acids. Mol Microbiol **53:**599-611.

Slack, F. J., P. Serror, E. Joyce, and A. L. Sonenshein. 1995. A gene required for nutritional repression of the Bacillus subtilis dipeptide permease operon. Mol Microbiol **15:**689-702.

Soh, J.-R., D.-H. Shin, D. Y. Kwon, and Y.-S. Cha. 2008. Effect of Cheonggukjang supplementation upon hepatic acyl-CoA synthase, carnitine palmitoyltransferase I, acyl-CoA oxidase and uncoupling protein 2 mRNA levels in C57BL/6J mice fed with high fat diet. Genes Nutr **2:**365-369.

Somerville, G. A., M. S. Chaussee, C. I. Morgan, J. R. Fitzgerald, D. W. Dorward, L. J. Reitzer, and J. M. Musser. 2002. Staphylococcus aureus aconitase inactivation unexpectedly inhibits post-exponential-phase growth and enhances stationary-phase survival. Infect Immun **70:**6373-82.

Sonenshein, A. L. 2007. Control of key metabolic intersections in *Bacillus subtilis*. Nat Rev Microbiol **5:**917-27.

Sonenshein, A. L. 2002. The Krebs Citric Acid Cycle, p. 151-162. *In* A. L. Sonenshein, J. A. Hoch, and R. Losick (ed.), *Bacillus subtilis* and its Closest Relatives: from Genes to Cells. ASM Press, Washington, D.C.

Spizizen, J. 1958. Transformation of Biochemically Defecient Strains of *Bacillus subtilis* by Deoxyribonucleate. Proc Natl Acad Sci U S A **44:**1072-1078.

Srere, P., H. Brazil, and L. Gonen. 1963. The Citrate Condensing Enzyme of Pigeon Breast Muscle and Moth Flight Muscle. Acta Chemica Scandinavica **17:**S129-S134.

Srivatsan, A., Y. Han, J. Peng, A. Tehranchi, R. Gibbs, J. Wang, and R. Chen. 2008. High-Precision, Whole-Genome Sequencing of Laboratory Strains Facilitates Genetic Studies. PloS Genetics **4:**e1000139.

Steil, L., M. Serrano, A. O. Henriques, and U. Völker. 2005. Genome-wide analysis of temporally regulated and compartment-specific gene expression in *Bacillus subtilis*. Microbiol **151:**399-420.

Strauch, M., and J. A. Hoch. 1993. Transition-state regulators: sentinels of *Bacillus subtilis* post-exponential gene expression. Mol Microbiol **7:**337-342.

Strauch, M., V. Webb, G. Spiegelman, and J. A. Hoch. 1990. The Spo0A protein of *Bacillus subtilis* is a repressor of the *abrB* gene. Proc Natl Acad Sci U S A **87:**1801-1805.

Tang, Y., and J. R. Guest. 1999. Direct evidence for mRNA binding and post-transcriptional regulation by *Escherichia coli* aconitases. Microbiol **145:**3069-3079.

Tang, Y., J. R. Guest, P. J. Artymiuk, and J. Green. 2005. Switching aconitase B between catalytic and regulatory modes involves iron-dependent dimer formation. Mol Microbiol **56:**1149-1158.

Tang, Y., J. R. Guest, P. J. Artymiuk, R. C. Read, and J. Green. 2004. Post-transcriptional regulation of bacterial motility by aconitase proteins. Mol Microbiol **51:**1817-1826.

Tang, Y., M. A. Quail, P. J. Artymiuk, J. R. Guest, and J. Green. 2002. *Escherichia coli* aconitases and oxidative stress: post-transcriptional regulation of *sodA* expression. Microbiol **148:**1027-1037.

Tang, Y.-W., and C. W. Stratton. 2010. *Staphyloccus aureus*: An Old Pathogen with New Weapons. Clin Lab Med **30:**179-208.

Voet, D., and J. G. Voet. 2004. Biochemistry, 3rd ed, vol. 1. John Wiley & Sons, Inc.

von Wachenfeldt, C., and L. Hederstedt. 2002. Respiratory Cytochromes, Other Heme Proteins, and Heme Biosynthesis, p. 163-179. *In* A. L. Sonenshein, J. A. Hoch, and R. Losick (ed.), *Bacillus subtilis* and its Closest Relatives: from Genes to Cells. ASM Press, Washington, D.C.

Walden, W. E., A. I. Selezneva, J. Dupuy, A. Volbeda, J. C. Fontecilla-Camps, E. C. Theil, and K. Volz. 2006. Structure of Dual Function Iron Regulatory Protein I Complexed with Ferritin IRE-RNA. Science **314:**1903-1908.

Weitzman, P. D. J. 1981. Unity and diversity in some bacterial citrate acid-cycle enzymes. Adv Microb Physiol **22:**185-244.

Wiegand, G., and S. Remington. 1986. Citrate Synthase: Structure, Control, and Mechanism. Ann Rev Biophys Biophys Chem **15:**97-117.

Wray, L. V., Jr., J. M. Zalieckas, and S. H. Fisher. 2001. *Bacillus subtilis* Glutamine Synthetase Controls Gene Expression through a Protein-Protein Interaction with Transcription Factor TnrA. Cell **107:**427-435.

Wright, J. A., P. Maeba, and B. D. Sanwal. 1967. Allosteric regulation of the activity of citrate synthase of *Escherichia coli* by α-ketoglutarate. Biochem Biophys Res Commun **29:**34-38.

Yokoseki, T., T. Iino, and K. Kutsukake. 1996. Negative Regulation by FliD, FliS, and FliT of the Export of the Flagellum-Specific Anti-Sigma Factor, FlgM, in *Salmonella typhimurium*. J Bacteriol **178:**899-901.

Yokoseki, T., K. Kutsukake, K. Ohnishi, and T. Iino. 1995. Functional analysis of the flagellar genes in the *fliD* operon of *Salmonella typhimurium*. Microbiol **141:**1715-22.

Zheng, L., R. Halberg, S. Roels, H. Ichikawa, L. Kroos, and R. Losick. 1992. Sporulation Regulatory Protein GerE from *Bacillus subtilis* Binds to and Can Activate or Repress Transcription from Promoters for Mother-cell-specific Genes. J Mol Biol **226:**1037-1050.

Zheng, L., and R. Losick. 1990. Cascade Regulation of Spore Coat Gene Expression in *Bacillus subtilis*. J Mol Biol **212:**645-660.

Ziegler, D. R., Z. Prágai, S. Rodriguez, B. Chevreux, A. Muffler, T. Albert, R. Bai, M. Wyss, and J. B. Perkins. 2008. The Origins of 168, W23, and Other *Bacillus subtilis* Legacy Strains. J Bacteriol **190:**6983-6995.

Zucker, M. 2003. Mfold web server for nucleic acid folding and hybridization prediction. Nucleic Acids Res **31:**3406-15.

Zumbrennen, K. B., M. L. Wallander, S. J. Romney, and E. A. Leibold. 2009. Cysteine Oxidation Regulates the RNA-binding Activity of Iron Regulatory Protein 2. Mol Cell Biol **29:**2219-2229.